

A Multifaceted Approach to Covert Attention Brain-Computer Interfaces

THÈSE N° 9052 (2018)

PRÉSENTÉE LE 14 DÉCEMBRE 2018

À LA FACULTÉ DES SCIENCES ET TECHNIQUES DE L'INGÉNIEUR
CHAIRE FONDATION DEFITECH EN INTERFACE DE CERVEAU-MACHINE
PROGRAMME DOCTORAL EN NEUROSCIENCES

ÉCOLE POLYTECHNIQUE FÉDÉRALE DE LAUSANNE

POUR L'OBTENTION DU GRADE DE DOCTEUR ÈS SCIENCES

PAR

Christoph SCHNEIDER

acceptée sur proposition du jury:

Prof. D. N. A. Van De Ville, président du jury
Prof. J. D. R. Millán-Ruiz, directeur de thèse
Prof. C. Michel, rapporteur
Prof. B. Blankertz, rapporteur
Prof. D. Ghezzi, rapporteur



ÉCOLE POLYTECHNIQUE
FÉDÉRALE DE LAUSANNE

Suisse
2018

Experience is merely the name men gave to their mistakes.
— Oscar Wilde, *The Picture of Dorian Gray*

To my grandparents

Acknowledgments

As much as a thesis is usually referred to as the work of one person, nothing could be further from the truth. The journey of my PhD, which is coming to an end with this thesis, would not have been possible without the help of many people, and would have certainly be less enjoyable without many more.

First, I want to thank my supervisor, Professor José del Rocío Millán, who has given me the opportunity to work in this absolutely fascinating field of science. I am also very grateful for the freedom I was granted in my research work which enabled me to pursue my very own scientific interests. This resulted in me being lost at times and failing at others, but in the end it has allowed me to grow into an independent researcher, even if there is still so much more to learn.

Then, I want to thank the proofreaders of this thesis, Anahita, Luca, Marija, Michael and Simis, for all the hours they have put in to read and improve my manuscript.

Further I want to thank all the people in our lab with whom I had the honor to work. Thank you for your open ears and great advice, for making time to discuss with me, and for cheering me up when things were rough. I specifically want to thank you, Simis, for being there for me from the first day of my PhD until the last one, for your guidance, patience and calm words. I want to thank Michael for our long coffees and discussions about the fascinating intricacies of human cognition and science in general. And I want to thank Luca T. for always being there when I had questions and to urge me to put my ideas and results into writing, even when I wasn't satisfied with what I got. And thank you to the NIRS-heros team, Coralie, Blanca and Ali for the debates and encouragements.

I also want to express my gratitude to the great times I could spend with all my colleagues outside the scope of work. Thank you to Luca R. for being my workout buddy and motivator, Arnaud for teaching me how to correctly pump iron, Tiffany for her steady encouragements and always believing in me, Marija for her never-ending cheerfulness at lunch, Zahra and Sareh for teaching me the beauty of the Persian language and Pierluca for patiently answering all my Italian questions. I will never forget the road trip through the south-western USA with Michael, Sareh and Tiffany, skiing with Kyuwaha and Ruslan, ski touring with sleepover in a hut with Michael, Stéphanie and Kyuwaha, hiking (and nearly getting lost) with Dong and Ping-Keng, and traveling Austria with Tiffany. Thank you for those precious memories.

Finally, I wanted to say an enormous thank you to my parents Walter and Irmtraud, my siblings Martin, Johannes, Cornelia, Franziska, Marianne, Katharina and Michael, my grandmothers Theresia and Hedwig, my close friends, especially Ewald, Philipp and Beat, and my girlfriend

Acknowledgments

Anahita. Thank you for carrying me through the bad times and for enjoying the good times with me. Thank you for your love, your encouragement and your friendship.

Lausanne, 28 September 2018

C. S.

Abstract

Over the last years, brain-computer interfaces (BCIs) have shown their value for assistive technology and neurorehabilitation. Recently, a BCI-approach for the rehabilitation of hemispatial neglect has been proposed on the basis of covert visuospatial attention (CVSA). CVSA is an internal action which can be described as shifting one's attention to the visual periphery without moving the actual point of gaze. Such attention shifts induce a lateralization in parietooccipital blood flow and oscillations in the so-called alpha band (8-14 Hz), which can be detected via electroencephalography (EEG), magnetoencephalography (MEG) or functional magnetic resonance imaging (fMRI). Previous studies have proven the technical feasibility of using CVSA as a control signal for BCIs, but unfortunately, these BCIs could not provide every subject with sufficient control. The aim of this thesis was to investigate the possibility of amplifying the weak lateralization patterns in the alpha band — the main reason behind insufficient CVSA BCI performance.

To this end, I have explored three different approaches that could lead to better performing and more inclusive CVSA BCI systems. The first approach illuminated the changes in the behavior and brain patterns by closing the loop between subject and system with continuous real-time feedback at the instructed locus of attention. I could observe that even short (20 minutes) stretches of real-time feedback have an effect on behavioral correlates of attention, even when the changes observed in the EEG remained less conclusive. The second approach attempted to complement the information extracted from the EEG signal with another sensing modality that could provide additional information about the state of CVSA. For this reason, I firstly combined functional near-infrared spectroscopy (fNIRS) with EEG measurements. The results showed that, while the EEG was able to pick up the expected lateralization in the alpha band, the fNIRS was not able to reliably image changes in blood circulation in the parietooccipital cortex. Secondly, I successfully combined data from the EEG with measures of pupil size changes, induced by a high illumination contrast between the covertly attended target regions, which resulted in an improved BCI decoding performance. The third approach examined the option of using noninvasive electrical brain stimulation to boost the power of the alpha band oscillations and therefore render the lateralization pattern in the alpha band more visible compared to the background activity. However, I could not observe any impact of the stimulation on the ongoing alpha band power, and thus results of the subsequent effect on the lateralization remain inconclusive.

Overall, these studies helped to further understand CVSA and lay out a useful basis for further exploration of the connection between behavior and alpha power oscillations in CVSA tasks,

Acknowledgments

as well as for potential directions to improve CVSA-based BCIs.

Keywords: brain-computer interface, covert visuospatial attention, electroencephalography, functional near-infrared spectroscopy, pupillometry, transcranial alternating current stimulation, alpha oscillations

Zusammenfassung

In den letzten Jahren haben Gehirn-Computer Schnittstellen (BCI) mehr und mehr ihren Wert für Unterstützungstechnologie und Neurorehabilitation gezeigt. Erst kürzlich wurde ein BCI-Ansatz auf der Basis von verdeckter visuell-räumlicher Aufmerksamkeit (CVSA) für die Rehabilitation von visuellem Neglect vorgeschlagen. CVSA ist ein rein internes Phänomen und beschreibt die Verschiebung des Aufmerksamkeitszentrums weg vom fixierten Punkt in die visuelle Peripherie ohne dabei die Augen zu bewegen. Solche Aufmerksamkeitsverschiebungen veranlassen eine Lateralisation in der Durchblutung des parietooccipitalen Kortex, als auch in Oszillationen im Frequenzbereich der Alpha-Wellen (8-14 Hz). Dies kann durch Elektroenzephalografie (EEG), Magnetoenzephalografie (MEG) oder funktioneller Magnetresonanztomografie (fMRT) gemessen werden. Vorangegangene Studien haben die technische Machbarkeit aufgezeigt, CVSA als Steuersignal für BCIs heranzuziehen, aber leider waren diese Systeme nicht von allen Versuchspersonen beherrschbar. Das Hauptziel dieser Dissertation war es, zu untersuchen, wie schwache Lateralisationsmuster in der Alpha-Frequenz, welche der Hauptgrund für unzureichende Kontrolle über ein CVSA BCI sind, zu verstärken.

Zu diesem Zweck habe ich drei verschiedene Ansätze erforscht, zu besseren und genaueren CVSA BCIs zu gelangen, welche mehr Menschen offen stehen. Der erste Ansatz beleuchtete die Veränderungen im Verhalten und der Gehirnwellen wenn das BCI system "geschlossen" wird, d.h. wenn kontinuierlich eine Echtzeitrückmeldung vom Computer an den Benutzer erfolgt. Dabei konnte ich in Erfahrung bringen, dass sogar kurze Perioden (20 Minuten) mit Echtzeitrückmeldung einen signifikanten Effekt auf die Verhaltensgestützte Messung haben, auch wenn im EEG keine Veränderungen erkennbar sind. Im zweiten Ansatz habe ich versucht, das EEG um eine weitere Aufnahmemodalität zu ergänzen, um mehr, und vor allem komplementäre Information über den Zustand der CVSA zu erhalten. Aus diesem Grund habe ich zuerst funktionelle Nahinfrarotspektroskopie (fNIRS) mit dem EEG kombiniert, aber die Resultate zeigten, dass während das EEG die erwartete Lateralisation in der Alpha-Frequenz aufzeichnen konnte, das fNIRS keine aussagekräftigen Daten lieferte. Danach habe ich das EEG mit Pupillometrie kombiniert. Zwei verschieden helle Seiten am Versuchsbildschirm lösten dabei eine Verengung oder Erweiterung der Pupille aus, je nachdem welcher Seite mehr Aufmerksamkeit geschenkt wurde. Die Fusion beider Methoden konnte dabei die einzeln erreichte Leistung übertreffen. Der dritte Ansatz untersuchte die Option, nichtinvasive elektrische Gehirnstimulation zur Verstärkung der körpereigenen Signale einzusetzen. Eine Erhöhung der Frequenzstärke im Alpha-Bereich könnte nämlich helfen, die Lateralisation, welche die Verschiebungen in der CVSA begleitet, besser von der restlichen Gehirnaktivität zu abzuheben.

Acknowledgments

Allerdings konnte ich keinen Effekt der elektrischen Hirnstimulation erkennen, und dadurch die Frage, ob eine Verstärkung der Alpha-Frequenz auch eine bessere Erkennbarkeit von CVSA im EEG mit sich bringt, nicht ausreichend beantworten.

Im Großen und Ganzen haben diese Studien dazu beigetragen CVSA etwas besser zu verstehen. Weiters haben sie eine brauchbare Basis für die fortschreitende Erforschung der Beziehung zwischen Verhalten und den Verteilung der Alpha-Wellen im Gehirn während andauernder CVSA gelegt. Und schlussendlich, haben sie auch mögliche Richtungen aufgezeigt, wie das ursprünglich angestrebte Ziel — die Erkennungsrate von CVSA Signalen zu verbessern — erreichbar wäre.

Schlagwörter: Gehirn-Computer Schnittstelle (BCI), verdeckte visuell-räumliche Aufmerksamkeit (CVSA), Elektroenzephalogramm (EEG), funktionelle Nahinfrarotspektroskopie (fNIRS), Pupillometrie, transkranielle Wechselstromstimulation (tACS), Alpha-Wellen

Contents

Acknowledgments	v
Abstract (English/Français/Deutsch)	vii
List of figures	xiii
List of tables	xvi
1 Introduction	1
1.1 Brain-computer interfaces	2
1.2 Brain imaging technologies for BCI	2
1.3 Mental commands for EEG-based BCIs	5
1.3.1 Evoked signals	6
1.3.2 Endogenous signals	7
1.4 Covert visuospatial attention	8
1.5 Covert visuospatial attention BCIs	11
1.6 Choice of BCI and limitations	13
1.7 Thesis aims and outline	14
2 Real-time feedback	17
2.1 Introduction	18
2.2 Materials and Methods	19
2.2.1 Participants	19
2.2.2 Experimental protocol	19
Offline paradigm	20
Real-time feedback paradigm	20
2.2.3 Data acquisition and processing	20
Behavior	22
Preprocessing	22
Alpha lateralization	23
Closed-loop feedback	23
Post-hoc classification	24
2.2.4 Reporting	25
2.3 Results	25

Contents

2.3.1	Behavioral correlates of attention	25
2.3.2	Neurophysiological correlates of attention	26
2.3.3	Single trial classification	30
2.4	Discussion	30
2.4.1	Closed-loop feedback for CVSA	31
2.4.2	Alpha-band lateralization	32
2.4.3	Single trial classification	33
2.5	Conclusion	34
3	Multimodal sensing	35
3.1	Introduction	36
3.2	Functional near-infrared spectroscopy	38
3.2.1	Introduction	38
3.2.2	Materials and Methods	41
	Participants	41
	Material	42
	Experimental protocols	43
	Data processing	45
3.2.3	Results	49
	Experiment 1	49
	Experiment 2	54
	Experiment 3	57
3.2.4	Discussion	57
3.3	Pupillometry	59
3.3.1	Introduction	59
3.3.2	Materials and Methods	60
	Visual display	60
	Data analysis	60
	Classifier fusion	61
3.3.3	Results	62
3.3.4	Discussion	64
3.4	Conclusion	65
4	Brain stimulation	69
4.1	Introduction	70
4.2	Materials and Methods	71
4.2.1	Participants	71
4.2.2	Experimental setup	71
4.2.3	Session structure	71
	Resting state	72
	CVSA task	72
	Transcranial alternating current stimulation	74
4.2.4	Questionnaire	75

4.2.5	Data processing	75
	EEG preprocessing	75
	Individual alpha frequency	75
	Alpha lateralization index	76
	Discriminative analysis	76
4.3	Results	76
	4.3.1 Effect of tACS on alpha power	76
	4.3.2 Effect of tACS on alpha-power lateralization during CVSA	77
	4.3.3 Changes in classification accuracy	78
	4.3.4 Behavioral effect	78
	4.3.5 Comparison with no-stimulation condition	79
4.4	Discussion	79
	4.4.1 tACS parameter choices	80
	4.4.2 Simulation of the electric field	84
	4.4.3 Choice of control condition	86
	4.4.4 Role of enhanced alpha power in CVSA	86
4.5	Conclusion	86
5	Discussion and conclusion	87
	5.0.1 Contributions	87
	5.0.2 Proposed future work	88
	5.0.3 Conclusion	90
	Bibliography	91
	Curriculum Vitae	115

List of Figures

1.1	Components of a BCI system	3
1.2	Temporal and spatial resolution of different brain imaging modalities	6
1.3	Visual scanning patterns of neglect patients	10
1.4	Retinotopic organization of α -power during CVSA	11
1.5	Thesis outline	14
2.1	Experimental design and visual feedback	21
2.2	Behavioral results	27
2.3	Electrophysiological results	28
2.4	Correlation of electrophysiological and behavioral results	29
2.5	Correlation with the α -LI and classification results	31
3.1	Basics of functional near-infrared spectroscopy (fNIRS)	39
3.2	Coverage of existing literature	41
3.3	Cap setups for EEG and fNIRS	44
3.4	Experimental setup and subject placement	45
3.5	Visual protocol with temporal scheme for CVSA task.	45
3.6	Visual protocol with temporal scheme for rotating checkerboard pinwheel.	46
3.7	Distribution of reaction time in dependence of the trial duration.	49
3.8	Topoplot correlation EOG with EEG	50
3.9	Time series R^2 -value topoplots, left minus right trials, for EEG	51
3.10	EEG lateralization topoplots with respect to slow and fast reaction times	51
3.11	Sensitivity map of the used fNIRS setup	52
3.12	Grand average topoplot of HbO activation in experiment 1	53
3.13	Time series R^2 -value topoplots, left minus right trials, for fNIRS	54
3.14	EEG lateralization topoplots for 16-channel montage	55
3.15	Grand average topoplot of HbO activation difference in experiment 2	56
3.16	Evoked response in fNIRS signal to passive visual stimulation.	57
3.17	Experimental setup for multimodal EEG and pupillometry BCI	61
3.18	Pupil size during CVSA — pilot data	62
3.19	Grand average pupil size during CVSA	63
3.20	Unimodal and multimodal classification accuracies	63
3.21	Multimodal feature space of posterior probabilities	64

List of Figures

4.1	Experimental design, visual protocol, stimulation setup	73
4.2	Alpha power changes as a result of tACS in the α - or β -band	77
4.3	PSDs pre and post stimulation for single subjects	78
4.4	Mean α -lateralization index span pre and post tACS	79
4.5	Individual α -power lateralization index over time and topographical lateralization patterns	80
4.6	Classification accuracy pre and post tACS	83
4.7	Behavioral changes due to tACS	83
4.8	Comparison of tACS-induced effects for α , β and no stimulation.	84
4.9	Simulations of the tACS-generated electric field (literature comparison)	85

List of Tables

2.1	Subject pairings	19
3.1	Classification accuracies experiment 1	55
3.2	Classification accuracies experiment 2	56
4.1	List of tACS stimulation parameters and setup (literature comparison).	82

Acronyms

α -LI α -power lateralization index.

ADL activities of daily living.

ANOVA analysis of variances.

BCI brain-computer interface.

BOLD blood oxygen level dependent.

CVA canonical variate analysis.

CVSA covert visuospatial attention.

DPF differential pathlength factor.

ECoG electrocorticography.

EEG electroencephalography.

EOG electrooculogram.

ERD event-related desynchronization.

ERP event related potential.

ErrP error-related potential.

ET eye tracker.

fMRI functional magnetic resonance imaging.

fNIRS functional near-infrared spectroscopy.

FPR false positive rate.

HbO oxygenated hemoglobin.

HbR reduced hemoglobin.

HbT total hemoglobin.

Acronyms

HD high definition.

IAB individual alpha band.

IAF individual alpha frequency.

IE interaction effect.

ITR information transfer rate.

LDA linear discriminant analysis.

LED light emitting diode.

LFP local field potential.

MEA micro-electrode array.

MEG magnetoencephalography.

MI motor imagery.

MRCP motor-related cortical potential.

PET positron emission tomography.

PLR pupillary light response.

PSD power spectral density.

RF random forest.

RT reaction time.

SEM standard error of the mean.

SSVEP steady state visually evoked potential.

tACS transcranial alternating current stimulation.

TMS transcranial magnetic stimulation.

VE validity effect.

VEP visually evoked potential.

1 Introduction

“Want to play hangman? asks Theophile, and I ache to tell him that I have enough on my plate playing quadriplegic. But my communication system disqualifies repartee: the keenest rapier grows dull and falls flat when it takes several minutes to thrust it home. By the time you strike, even you no longer understand what had seemed so witty before you started to dictate it, letter by letter. So the rule is to avoid impulsive sallies. It deprives conversation of its sparkle, all those gems you bat back and forth like a ball — and I count this forced lack of humor one of the great drawbacks of my condition.” — Jean-Dominique Bauby, *The Diving Bell and the Butterfly*

This quote above is from a book that Jean-Dominique Bauby has written while being in a locked-in state after a massive stroke and it showcases his frustration with the slow means of communication — depriving it of many of its most pleasant forms. His medical condition left him only in control of one of his eyelids and communication was bound to a caregiver spelling the letters of the alphabet and him twitching his eyelid at the letter of choice.

Locked-in patients, whose mind and memories are fully intact but their body completely paralyzed, are the archetype of people for whom we research and develop brain-computer interfaces (BCIs). These systems provide a direct link from brain activity to a computer, that could serve in a variety of actions: communication, controlling light, entertainment and positioning in the bed or wheelchair. Growing from this use as a replacement for lost body functions, BCIs have also proved their merits in neurological rehabilitation by coupling standard rehabilitation with the brain activity.

Even though the current state of the art is remarkably advanced to the technology Jean-Dominique Bauby had at his disposal, this technology does not work for everybody and is often — if it works — not accurate enough. For this reason, my thesis revolves around improving the decoding of one of the mental commands that can be used to build such BCIs: shifts in visual attention to one or the other side of the visual field, called covert visuospatial attention (CVSA).

In the following, I start with a brief introduction into the components of a BCI. Next, I move on

to which brain imaging technologies have been used for BCI and discuss their individual advantages and disadvantages. Then, I will speak about the different electroencephalography (EEG)-based brain signals that have been exploited for BCIs. Further, I introduce covert visuospatial attention (CVSA) and its use in BCI before explaining my choice of BCI components. In the end I motivate the work in this thesis and give a brief overview of the conducted experiments.

1.1 Brain-computer interfaces

A BCI is a system designed to allow interaction between the brain — the seat of our consciousness and intentions — with the outside world, bypassing the motor pathways we usually rely on when communicating with our environment; be it in speech, writing, or with gestures and mimics (Wolpaw et al., 2002).

A BCI system needs multiple components to work hand in hand, some of which are user-dependent and some machine dependent (see Figure 1.1 for a graphical representation). First, we need the human to produce a mental command, i.e. a clearly defined thought, by engaging in a mental task, e.g. thinking of a specific movement (Curran and Stokes, 2003). As a next step, these brain signals must be acquired with a suitable brain imaging technology. In this thesis I mainly used the EEG, but there exist many more options (Min et al., 2010). Further, the acquired signal has to be preprocessed, i.e. cleaned from artifacts and noise to ensure the highest possible quality. Then we have to extract the specific features (or patterns) that are modulated by the mental command (Nicolas-Alonso and Gomez-Gil, 2012). These could be for example the amplitude in the EEG signal or the voxels that show increased blood flow in the functional magnetic resonance imaging (fMRI). Thereafter the extracted features need to be classified (matched) to one of the mental commands, e.g. imaginary left vs. right hand movement (Lotte et al., 2007). Once the mental command is decoded, it can be sent to the application interface, which transforms it into a pre-coded action. In the applications depicted in Figure 1.1 (b) this would mean that the computer game avatar jumps, or a letter is selected, or that the hand closes and grasps an object. With the application changing its state based on the decoded commands, the user gets feedback of how his mental command has been interpreted by the BCI. Given enough time, this allows the user to learn how to use the BCI, not unlike learning how to use a new tool (Perdikis et al., 2018).

1.2 Brain imaging technologies for BCI

In theory, every brain imaging modality which is able to pick up signals that can be voluntarily modulated by a person is a possible candidate for building a BCI. With this in mind, it is not surprising that many different modalities have been explored for the use of BCI, everyone with its own set of advantages and disadvantages.

In fact, the different methods can be divided into two distinct groups, based on the physiological

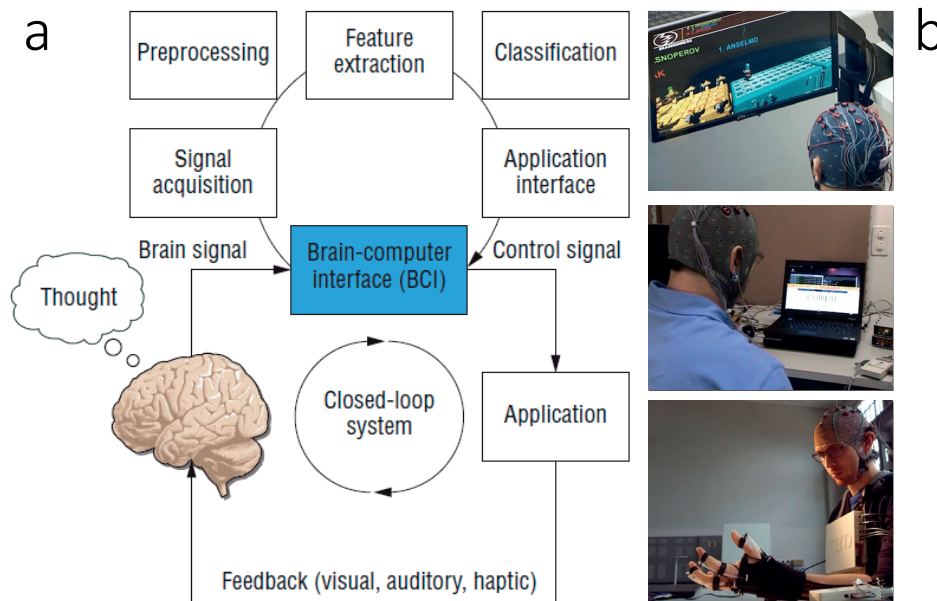


Figure 1.1 – Components and applications of BCIs. (a) Main components for a closed-loop BCI. The upper loop depicts the steps taken on the machine side of the BCI whereas the lower loop shows the implication of the user. (b) Three different applications for a BCI: a computer game (top), a spelling device (middle) and an exoskeleton for restoring grasp (bottom). Figure adapted from (Nijholt and Tan, 2008)

mechanism they are exploiting. The first group of brain imaging devices is based on cerebral hemodynamics: the more active a certain brain region is, the more need for oxygen and nutrients, and thus the higher the blood volume, as controlled by vasoconstriction and -dilation down to the capillary level (Jespersen and Østergaard, 2012). A common limitation of hemodynamics-based brain imaging devices is therefore a poor temporal resolution, resulting from the long delay (5-10 s) between the neuronal activity and the corresponding peak blood flow (Lindquist et al., 2009).

Positron emission tomography (PET) images blood flow via the concentration of a radioactive marker that has to be injected into the bloodstream before the measurement. This already rules the PET out for the continued use in a BCI, since regular radioactive injections would pose a serious health risk.

The fMRI, on the other hand, does not suffer from this disadvantage, since it measures blood oxygenation levels with magnetic fields. fMRI scanners offer noninvasive whole-brain imaging (cortical and subcortical structures) with an ever increasing spatial resolution (less than 1 mm^3) thanks to the development of more and more powerful scanners (e.g. 7 Tesla). On the downside, they are expensive, large and non-portable, and require the subject to lie still inside a constrained tube. Additionally, fMRI-scanners also have a high cost of maintenance due to their requirement of liquid helium cooling. Over the years, fMRI has proven to be a viable

Chapter 1. Introduction

modality for BCI (Weiskopf et al., 2004a; Yoo et al., 2004; Weiskopf et al., 2007) but it continues to be used more in the realm of basic neurofeedback studies (Weiskopf et al., 2004b; Shibata et al., 2011; Sitaram et al., 2017). This makes sense when considering that the therapeutic effect of neurofeedback should carry on after a session, while being enclosed in an fMRI-tube is quite bothersome for assistive BCI applications as compared to a cap that has to be worn.

The third wide-spread device for monitoring blood circulation is the functional near-infrared spectroscopy (fNIRS), which uses the absorption properties of hemoglobin for near-infrared light to extract relative changes in blood oxygenation (see Chapter 3.2 for details). fNIRS devices are comparably cheap, mobile (can be integrated into a cap with wireless data link) and robust to body motion, as long as the light emitters and detectors do not move in place. On the downside, the fNIRS allows only to image the outer layer of the cortex, and has a more crude spatial resolution of approximately one cm, even though new multiprobe systems try to remedy this by combining information from multiple light paths. Another factor is that hair absorbs a large amount of the near-infrared light, and so, recording brain activity below thick hair requires a long and very careful setup. fNIRS enjoyed a surge in experimental BCIs from the 2010's on (Tai and Chau, 2009; Bauernfeind et al., 2011; Naseer et al., 2014; Weyand et al., 2015; Shin et al., 2016).

The second group of brain imaging technologies is based on the electric and electromagnetic fields generated by the activity of single neurons or whole populations of them. Single-cell spiking (axonal firing) and local field potentials (LFPs) can be recorded with implanted micro-electrode arrays (MEAs), the best known representative being the Utah-array (Maynard et al., 1997). These electrode arrays have a very high temporal resolution and signal-to-noise ratio and allow to map very complex commands to the recorded firing rates, e.g. freely moving a robot arm (Hochberg et al., 2012), typing on a virtual keyboard (Jarosiewicz et al., 2015) or restoring reaching and grasping functions with electrical muscle stimulation (Ajiboye et al., 2017). The downsides of this technology are ethical and medical concerns, since the electrode array has to be placed via open brain surgery which comes with an infection risk. Further, the pins are placed directly into the upper cortical layer, and thus are hurting the neuronal tissue and provoke scar formation (Polikov et al., 2005; McConnell et al., 2009). Finally, they also only allow a limited brain coverage.

A slightly less invasive recording technique is electrocorticography (ECoG), where arrays of flat metal electrodes embedded in a polymer layer, are placed either directly on the cortical surface (subdural ECoG) or on top of the dura mater (epidural ECoG). Historically, ECoG was developed to exactly localize epileptogenic zones (the starting point of seizures) prior to surgical removal (Reif et al., 2016). But many studies have shown the merits of ECoG as a sensing modality for BCI (Leuthardt et al., 2004; Leuthardt et al., 2006; Schalk et al., 2008). The recorded oscillatory activity of neuron populations is hardly attenuated by the tissue in between, which allows a high signal-to-noise ratio while the surgical placement of the electrodes is already done minimally invasive. Intense efforts have been undertaken in the last years to push for the implantation of ECoG solely for the purpose of BCI and current systems

are designed to remain inside the skull for life (Mestais et al., 2015; Romanelli et al., 2018).

The noninvasive pendant to the ECoG, and the father of all BCI modalities, has been the EEG (Farwell and Donchin, 1988; Wolpaw et al., 1991). The technology behind the EEG is rather simple and the first human EEG recordings of Hans Berger had taken place already more than 90 years ago (Collura, 1993). But the simple amplification of the potential difference between two metal electrodes has been improved up to today's standards, where we are able to record up to 256 channels simultaneously, with less noise due to active preamplification inside the electrodes themselves and can receive the signals wirelessly, making the subject truly mobile. Thus the EEG remains one of the most affordable brain imaging technologies, and offers a very good temporal resolution while at the same time being noninvasive. Being a noninvasive technique, it also can be used without ethical and medical concerns. The downsides of the EEG are the limitation to image mainly cortical structures, the low spatial resolution and low signal-to-noise ratio, as well as the high susceptibility for electrical artifacts generated by eye movements or muscle activation of e.g. the tongue or neck (Muthukumaraswamy, 2013).

Lastly, also magnetoencephalography (MEG) can be used for BCI applications (Mellinger et al., 2007; Bahramisharif et al., 2010; Horschig et al., 2015). The MEG measures the magnetic fields generated by neuronal activity noninvasively. The big advantage over the EEG is the high spatial resolution (2-3 mm) and the opportunity to image deeper brain regions, both possible because, differently than the electric fields, the magnetic fields are not attenuated by the tissue they are passing through. On the downside, traditional MEG devices were expensive, immobile, required liquid helium cooling and a magnetically shielded room. Very recently though, Boto et al. (2018) developed a new technology that allows for a head-mounted (and thus mobile) MEG, albeit some magnetic shielding is still necessary at this point.

Figure 1.2 shows an overview over the temporal and spatial resolution of each of the discussed brain-imaging modalities. For the research presented in this thesis I decided to use the EEG as my main recording device. The noninvasiveness allows for the inclusion of healthy subjects and larger patient populations, it allows a high temporal precision and enough spatial resolution to pick up the desired signals (see Section 1.4), and all that for a relatively low cost.

1.3 Mental commands for EEG-based BCIs

As mentioned before, a BCI is a system that uses a brain imaging modality — here the EEG — to decode voluntary changes in brain activity. Over time, multiple different mechanisms have been found that lead to stable and reproducible modulations, large enough to be picked up by the EEG. Such modulations can be either a voluntary response to an external stimulus (evoked signals) or the result of a self-initiated mental task (endogenous signals).

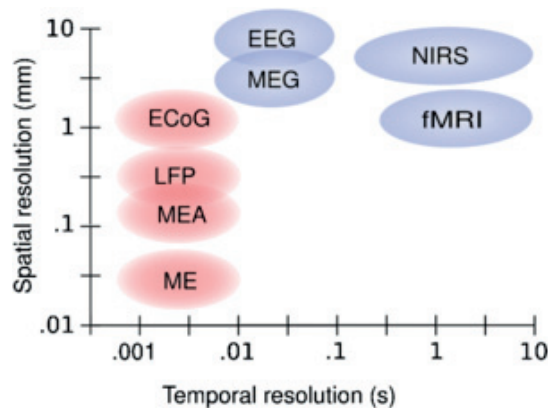


Figure 1.2 – Temporal and spatial resolution of different brain imaging modalities. Micro-electrodes (ME) are not described independently from microelectrode arrays (MEA) in the text, but operate under the same principles. Both can record single-neuron spiking activity as well as LFPs. While the spatial resolution of the PET is on the same range as the one of the fNIRS, the temporal resolution on the scale of tens of seconds, would place it to the right of the graph. Invasive methods are depicted in red, noninvasive methods in blue. Picture taken from (Van Gerven et al., 2009)

1.3.1 Evoked signals

Sensory, perceptual or cognitive processes produce specific wave forms in the EEG in response to different external stimuli. Such neuronal correlates to external events are subsumed under the title of event related potentials (ERPs) and are defined as a well defined amplitude change in the cortical electrical signal which is generated in response to sensory, cognitive or motor events (Woodman, 2010). Different external events lead thereby to ERPs in different brain areas.

Visually evoked potentials (VEPs) are waveforms in the occipital cortex (over the visual areas) that comes as a response to a visual stimulus, mostly rapid luminosity changes (Curtis, 1940). Since this response is involuntary and cannot be modulated, an extension of that phenomenon is used for BCI, the steady state visually evoked potential (SSVEP). For recording SSVEPs, a flickering light of a stable frequency is attended to by the subject, which induces a rhythmic train of VEPs at this exact frequency (Müller-Putz et al., 2005; Wang et al., 2006). When placing multiple flickering lights — each with its own, unique flicker frequency — in the visual field, the VEP-frequency recorded in the EEG will be the one of the attended target. This means, that attention (covert or overt) to the target stimulus can be decoded and used for controlling a BCI (Kelly et al., 2004; Ordikhani-Seyedlar et al., 2014). The SSVEP is a very robust and large signal, and allows high information transfer rates (ITRs) (Chen et al., 2015). However, the flickering lights are very arduous for the eyes and are thus usually not suitable for long continuous applications.

Error-related potentials (ErrPs) are observed after self-generated or observed errors over

frontocentral brain areas (Falkenstein et al., 2000). BCIs based only on ErrPs have been presented by Ferrez and del R. Millán (2008), Chavarriaga et al. (2014) and Iturrate et al. (2015). A more natural inclusion of ErrPs into the BCI framework is to use the generated potential as a correction mechanism, e.g. undoing the last choice taken by the BCI classifier (Schalk et al., 2000; Schmidt et al., 2012; Spüler et al., 2012)

A third type of ERP is the so-called P300 signal, named after the prominent positive peak forming around 300 ms after the external stimulus (Donchin and Smith, 1970). This potential is the largest over centroparietal areas and is elicited by the occurrence of a wanted, but rare event — the *oddball* (Fabiani et al., 1987; Farwell and Donchin, 1988; Polich and Kok, 1995). Such oddball paradigms have been widely used in BCI, for example for spellers (Cuntai et al., 2004; Krusienski et al., 2008), robotic arms (Palankar et al., 2009) and telepresence robots (Escolano et al., 2010). P300-based BCI are the one of the most successful ones to date with a high ITR and very reliable detection of the intended command (Müller-Putz et al., 2005; Müller-Putz and Pfurtscheller, 2008; Guger et al., 2009).

A common downside of evoked potentials as input signal for a BCI is the dependency on external stimulation: either flickering lights, oddball stimuli or generated errors. The continuous sensory input necessary to use such type of BCIs can grow tiring very quickly — independent of the sensory pathways used — and thus decrease concentration. A further disadvantage is the high variability in amplitude of the evoked potential, so that current implementations always average over several occurrences to get a stable classification. And finally, it is hard to design a self-paced BCI paradigm with evoked signals, since they are elicited automatically as a response to the stimulus, and as such, the user cannot decide freely when to start or stop sending a command.

1.3.2 Endogenous signals

Endogenous signals, on the other hand, theoretically allow a completely self-paced use of the BCI since the patterns are generated by engaging in a mental task. Arguably the best explored and most widely used mental task is motor imagery (MI), the kinesthetic imagination of a movement (Decety and Ingvar, 1990). The usual MI tasks are the imagination of opening and closing the hand, lifting or wiggling the feet and swallowing or moving the tongue (Pfurtscheller et al., 2006). The imagined movement leads to a decrease in oscillatory α - and β -band power over the corresponding areas in the motor cortex, called an event-related desynchronization (ERD) (Pfurtscheller and Lopes Da Silva, 1999). MI has been widely used in a vast collection of BCI applications like spellers (Perdikis et al., 2014), wheelchairs (Carlson and Millán, 2013), drones (LaFleur et al., 2013) exoskeletons (Randazzo et al., 2018) and computer games (Perdikis et al., 2018). Further, MI BCIs enable successes in neurorehabilitation when coupled with robotic devices or functional electrical stimulation (Ang et al., 2011; Ang et al., 2015; Biasiucci et al., 2018).

Contrary to the oscillatory activity modulated with MI, motor-related cortical potentials

Chapter 1. Introduction

(MRCPs) are negative potential changes related to a voluntary movement onset, hence their other name *Bereitschaftspotential* (readiness potential in English), as it appears when a participant is prepared to execute a movement (Kornhuber and Deecke, 1965). This allows the conscious act of preparing (to execute) a movement to function as a command for BCI control (Gu et al., 2009; Garipelli et al., 2013; Xu et al., 2014; Jiang et al., 2015).

An interesting research field concerns music (Schaefer et al., 2011a; Schaefer et al., 2011b) or speech imagery (DaSalla et al., 2009; Brigham and Kumar, 2010; Wang et al., 2013), which generates signals mostly over the temporal cortices. Specifically speech imagery would be the perfect match for a BCI speller, if thought words could be directly decoded and communicated by the computer. Even though promising steps have been taken in the right direction, it is still a long way until reaching this overarching goal (Leuthardt et al., 2011; Martin et al., 2016).

Finally, also the visual cortices can generate endogenous signals by shifting visuospatial attention, as described in detail in the next section. A comprehensive review of the different BCI systems published can be found in Hwang et al. (2013).

1.4 Covert visuospatial attention

As humans, we are mainly visual animals, relying heavily on our eyesight for movements and spatial orientation. CVSA is defined as the direction of attention to a locus in the visual field that is different from the point of gaze. In laymen terms, this is often referred to as looking at something "out of the corner of one's eyes". We naturally rely on this function — even though most of the time unconsciously — for deciding on the locus of the next visual fixation (Posner, 1980; Findlay, 1997; Eimer et al., 2006; Van der Stigchel and Theeuwes, 2007), planning arm movement trajectories (Baldauf and Deubel, 2010; Hesse and Deubel, 2011) and keeping track of more than one object of interest in the visual field (Mangun and Buck, 1998).

Posner (1980) was the first one to show that shifting the visual attention covertly to a target area decreases the reaction time to events in this region, while simultaneously increasing the reaction time for events in other, non-attended areas. This showed that attention is a limited resource that cannot cover the entire visual field equally. Thereby it is still debated if CVSA is an independent cognitive mechanism or closely related to the planning of motor actions, like eye saccades or hand reaching. The latter reasoning is denominated the "premotor theory of attention" and was publicized by Rizzolatti et al. (1987). It quickly gained a large following due to its simplicity, the fact that CVSA experiments indeed required a motor response after the attention shift, and lastly it also provides an explanation to the natural role of CVSA. Nevertheless, also this theory has been challenged, especially with the rise of neuroimaging technologies that found — all shared networks aside — differences between the structures activated in attention shifts and saccades (Crawford and Muller, 1992; Corbetta et al., 1998).

Covert shifts of attention can be either elicited by external stimuli or by a voluntary internal process. This has been studied with two types of visual cues, preceding the appearance of

a target stimulus: direct and symbolic cues. Direct cues appear at the same location as the target stimulus, and involuntarily draw attention to this area (Corbetta and Shulman, 2002). They have the greatest effect on reaction times if the time difference between the cue and the target appearance is around 100 ms (Müller and Findlay, 1988; Adam et al., 2000). Shorter time intervals do not allow for a sufficient shift in CVSA while for longer intervals (above 200 ms) the directed attention is again withdrawn from the cued location (Müller and Rabbitt, 1989). Symbolic cues, on the other hand, are usually presented centrally (or even in another sensory modality, like sound) and hold information about the location of the upcoming target in a form that needs cognitive decoding, e.g. an arrow, a shape, a color or the spoken words *left* or *right*. The attention shifts after symbolic cues appear significantly later than with direct cues and they reach their maximum effectiveness from around 300 ms onwards (Müller and Findlay, 1988; Müller and Rabbitt, 1989). This can be contributed to the fact that symbolic cues first need to be interpreted before the attention shift can be initiated (Corbetta and Shulman, 2002). Additionally, these voluntary covert shifts of attention can last for a much longer time (Posner et al., 1987; Thut et al., 2006).

Lesion studies on people who displayed symptoms of inability to covertly direct their attention after trauma or stroke allowed first insights of the implication of specific brain areas in an *visual attention network* (Posner et al., 1987; Mesulam, 1999; Corbetta et al., 2005). A lead symptom in many of the affected patients is the so-called hemispatial neglect syndrome, a condition in which awareness of stimuli is reduced on one side of the visual field (Parton et al., 2004). In extreme cases, this can lead to a complete disregard of anything on that side, may it be visual information, sound or their own body (Marshall and Halligan, 1988; Corbetta et al., 2005; Corbetta and Shulman, 2011; Schindler and Bartels, 2013). Even though the remaining visual field is comparable to patients with hemianopsia, visual neglect is a more devastating condition as patients are in most cases not aware of their deficit, and thus do not move their head to bring things into their visual field. Affected individuals therefore often need continuous care because they are susceptible to falls, wheelchair collisions, and do not groom or dress their neglected body half (Appelros et al., 2002). Karnath and Rorden (2012) point out the connection of certain stroke-affected brain areas with different cardinal symptoms of spatial neglect: the perisylvian network (superior/middle temporal, inferior parietal, ventrolateral frontal cortices) with egocentric spatial neglect, the posterior (and potentially inferior) parietal cortex with allocentric spatial neglect and the temporo-parietal junction with symptoms of extinction (see also De Schotten et al. (2011)). Schindler and Bartels (2013) showed that the brain regions correlating with covert visual attention are also the ones active in egocentric spatial representation tasks. This demonstrates the complexity of the *visual attention network* (Corbetta and Shulman, 2011), and foreshadows the problems encountered when rehabilitation is attempted. At the moment, a variety of therapy methods are in use. Behavioral therapies, like *scanning*, target mostly building helpful habits for reading, eating and other activities of daily living (ADL), while *prism adaptation* and *smooth pursuit eye movement* try to shift the center of optical representation in the brain (Kerkhoff et al., 2013; Kerkhoff et al., 2014; Rossetti et al., 1998). For an extensive review of current therapies for

Chapter 1. Introduction

hemispatial neglect see Yang et al. (2013) or Klinke et al. (2015). Unfortunately, the results of current therapies are not consistent and the need to find new methodological interventions is urgent.

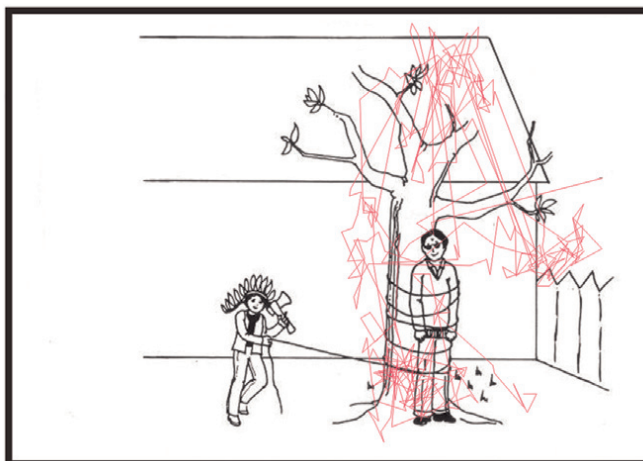


Figure 1.3 – Visual scanning patterns of neglect patient. Exemplary visual scanning path (in red) of a patient with hemispatial neglect syndrome, when instructed to attentively study the picture in detail. It is obvious that the left half of the picture was neglected. Figure adapted from (Karnath, 2015)

Based on these lesion studies, noninvasive brain imaging advanced our understanding of the components of the *visual attention network*, be it using PET (Corbetta et al., 1993; Nobre et al., 1997) or fMRI (Kastner et al., 1999; Beauchamp et al., 2001). But shifts in attention, either overt or covert, do not only produce hemodynamic correlates. Worden et al. (2000) were the first to report an increase in the power of α -oscillations in the hemisphere opposite to the attended side. Further, they already reported an α -power distribution that fits the retinotopic organization of the visual cortex, with lowest powers observed over the cortical area which corresponded to the locus of attention (Figure 1.4). This discovery was corroborated and refined in many studies to come (Sauseng et al., 2005; Kelly et al., 2006; Thut et al., 2006; Rihs et al., 2007; Bahramisharif et al., 2010). Since α -oscillations are believed to play a crucial role in the suppression of sensory input to many different cortical areas (Kerlin et al., 2010; Romei et al., 2010; Banerjee et al., 2011; Ciavarro et al., 2013), the observed shift in occipital α -power during CVSA is less the product of increased sensitivity of neurons corresponding to the attended area but rather the active suppression of stimuli from other areas (Jensen and Mazaheri, 2010; Foxe and Snyder, 2011).

The retinotopic layout of the CVSA-induced α -patterns allows — at least in theory — the decoding of the exact attended point in the visual field. This, of course, made CVSA an interesting mental task to explore for the use in BCIs, especially since the internal attention shifts do not depend on any motor functionality and thus could also be deployed by completely locked-in patients. In the following section I give a brief overview of CVSA BCIs based on the EEG.

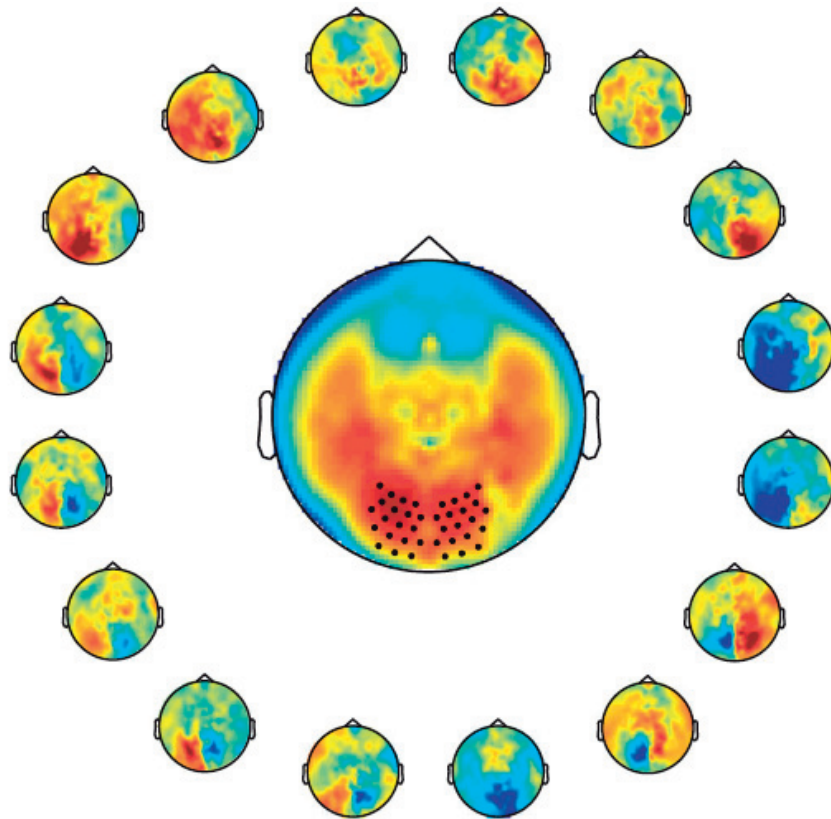


Figure 1.4 – Retinotopic organization of α -power during CVSA. The center head shows that the overall average distribution of α -band power is concentrated over the parietooccipital areas. The small heads show the α -power distribution during spatial attention to targets at 16 different locations on a 2D screen. The head location with respect to the center reflects the location of the target with respect to the central fixation point. The inversion of the parietooccipital α -pattern between left and right side covert attention is clearly visible (increases in red, decreases in blue). Figure adapted from (Bahramisharif et al., 2010)

1.5 Covert visuospatial attention BCIs

The first uses of CVSA in the realm of BCI was the discovery that SSVEP BCIs also work if the flickering stimulus is only attended covertly, which opened up this type of systems for people with gaze fixation problems (Kelly et al., 2005), albeit the decoding accuracy dropped about 20% compared with overt attention to the flicker stimuli (Kelly et al., 2004). Later, Brunner et al. (2010) and Treder and Blankertz (2010) have shown that the widely-used P300 spellers depend heavily on the eye fixation on the target letter. This finding entailed further research on how to optimize spellers that work when the target letters are attended covertly only. They showed that covert attention to the target creates a sufficiently large P300 potential when the letters are regrouped the center in a circular or hexagonal fashion (Liu et al., 2011; Treder et al., 2011b; Aloise et al., 2012; Schaeff et al., 2012). Liparas et al. (2014) have ultimately also

Chapter 1. Introduction

created a BCI that could decode the side of a covertly attended stimulus from the shape of the resulting VEP.

Even though BCIs based on evoked potentials display very high classification accuracies, they are still inherently limited by their dependence on external stimuli. This downside might be outweighed by the good performance for short tasks like spelling a text message, but it does not allow for the same effortless and natural integration as do endogenous control signals. For this reason, decoding the locus of covert attention from the topographical pattern of the occipital α -power was a logical step forward. The first ones to report decoding of covert attention from α -power were Van Gerven and Jensen (2009) using MEG. Following, proof-of-principle BCIs have been developed also with EEG signals (Treder et al., 2011a; Tonin et al., 2012; Roijendijk et al., 2013). Usually, the time of continuous covert attention to the target was chosen on the scale of a couple of seconds, but Gunduz et al. (2012) and Belyusar et al. (2013) showed that it is possible to decode α -power lateralization on a timescale of a few hundred milliseconds in ECoG and EEG respectively. Shortly thereafter, online BCIs had been developed using fMRI (Andersson et al., 2012; Andersson et al., 2013a), EEG (Treder et al., 2011b; Tonin et al., 2013) and MEG (Horschig et al., 2015; Okazaki et al., 2015).

The dominant visual protocol in these studies used a central fixation and two target areas to the left and the right. A symbolic cue in the center indicates the side that the target will appear on, and for the most part, the actual target appearance is linked to either a reaction time or visual discrimination task. Nevertheless, there were protocols operating with four (Van Gerven and Jensen, 2009; Andersson et al., 2012) and six different target positions (Treder et al., 2011b; Treder et al., 2011a). A good review covering visual attention based BCIs in further detail can be found in Astrand et al. (2014).

Aside from the use as an assistive technology (e.g. spellers, exoskeletons, electric stimulation), there have been first attempts made explore the effect of real-time feedback of an CVSA-based BCI for rehabilitation in spatial neglect. While for post-stroke motor rehabilitation the role of BCIs is fairly well defined as the facilitation of motor learning through direct feedback on cortical activity, the matter is distinctly more difficult for hemineglect. Kinsbourne (1987) established the model of spatial attention as a balance of constant hemispheric rivalry which can be disrupted in the event of a stroke. Further evidence for this theory came from observed correlation between spatial orientation bias and an imbalance in the activation of the dorsal parietal cortex (Corbetta et al., 2005) as well as in α -power in the anatomically unaffected occipital cortex (Newman et al., 2013). For that reason, this interhemispheric imbalance stands in the focus of current rehabilitation research. Transcranial magnetic stimulation (TMS) of parietal and occipital areas has proven to affect visuospatial attention (Thut, 2014) and to alleviate symptoms of unilateral neglect (Cazzoli et al., 2012). Further, Robineau et al. (2014) recently reported successful hemispheric rebalancing through fMRI neurofeedback on occipital (α -) activity while Tonin et al. (2017) showed similar results after EEG-based closed-loop BCI training.

1.6 Choice of BCI and limitations

MI-based BCIs have already demonstrated their value in motor rehabilitation after cerebral lesions (Ang et al., 2015; Pichiorri et al., 2015; Biasiucci et al., 2018). Since, as mentioned before, the current state of rehabilitation for patients with hemispatial neglect syndrome is not satisfactory, there is the hope that BCI-aided rehabilitation can alleviate this condition. This was my main motivation for the research work in this thesis. Taking into account the advantages and disadvantages of the different possibilities for the BCI components, I decided to concentrate my efforts on EEG-based CVSA BCI. In the following I want to explain my choices by distilling the important points of the previous sections that covered the state of the art.

Starting with the brain imaging modality, I decided to mainly use the EEG, complemented by the fNIRS (see Section 3.2). Even though the EEG does not present the same spatial resolution as implanted electrodes or the newest generations of fMRI scanners, it has the large advantage of being lightweight, wireless and mobile. Although patients with restraining disabilities would (and do) agree to the implantation of electrodes, a noninvasive brain imaging modality is more versatile, practically risk-free and can thus be also perfectly integrating in hospital- or home-based rehabilitation, where the goal is to reach functional independence (i.e. getting rid of technologies such as the BCI).

Also my decision to not rely on evoked potentials of any kind, can be justified from both, an assistive and rehabilitative use case. As already mentioned, protocols for evoked potentials need to constantly present stimuli in a sensory modality, mostly in the visual domain, and this gets exhausting very soon. Further, endogenous signals can be trained and thus the use of the BCI becomes a more natural interaction. When considering rehabilitation, the role of a BCI is to restore the action-feedback loop that is disrupted in these patients. For motor rehabilitation this means that motor-related commands are linked to functional electrical stimulation that contracts the muscles and therefore produced sensory feedback to the motor areas. In the case of hemispatial neglect, the idea is to present visual stimulation at times when the covert attention is (relatively) good. Also for this, the endogenous shift in α -oscillations is the preferred candidate.

A major drawback of using CVSA as a mental command for BCIs is that the decoding accuracy does not reach the levels that can be obtained with evoked potentials, or even other endogenous signals like MI (Ahn and Jun, 2015). Especially in rehabilitation, we want to make sure that the brain patterns get decoded correctly, not to erroneously enforce undesired neuronal activity. Further, BCI users get discouraged if the system error rate is too high, i.e. when they feel that the BCI chooses commands randomly and not based on their input. From a purely statistical viewpoint, a performance above the 95% confidence interval of a random classifier can be interpreted as information transfer. While this boundary lies at around 60% in a two-class BCI (dependent on the number of trials), participants usually only report the feeling of being in control when they achieve accuracies of around 70% in a binary task (Kübler et al., 2004;

Fard and Grosse-Wentrup, 2014). The fact that the reported mean accuracies in two-class BCIs using covert attention lie around 70% (Van Gerven and Jensen, 2009; Tonin et al., 2012; Tonin et al., 2013; Horschig et al., 2015) means that about half of the BCI users did or would not feel in control. So, before we can dedicate our time and energy to explore the most beneficial BCI paradigms and setups for the rehabilitation of spatial neglect, we first need to improve on the current decoding accuracies.

1.7 Thesis aims and outline

The main aim of this thesis was to raise the binary classification performance in CVSA BCIs to achieve a more reliable command interpretation and to enable people who are not in control with the current systems to use such a BCI. Since the state of the literature did not favor a specific direction to achieve this goal, I decided to investigate three complementary approaches: (i) giving real-time feedback to allow the subjects to adapt and improve the patterns generated by their mental commands, (ii) combining the EEG with a complementary sensing modality to get richer information about the brain state and (iii) using noninvasive brain stimulation to increase the α -lateralization patterns during CVSA (Figure 1.5).

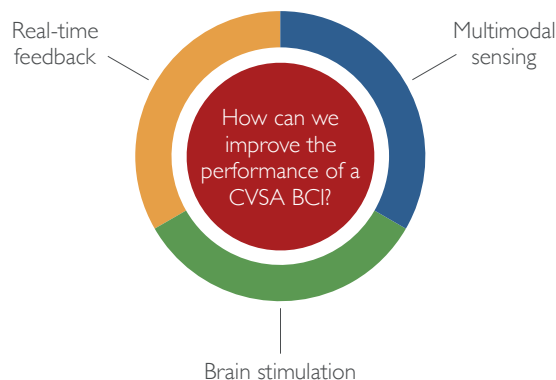


Figure 1.5 – Thesis chapters outline. The question of how to improve classification performance for CVSA BCIs was approached in three different ways, each described in a chapter of this thesis.

Chapter 2 (Real-time feedback) The goal of this study was to investigate the impact of continuous real-time feedback on the behavioral and BCI performance. I hypothesized that closing the loop between user and machine will allow for an adaptation of the user-generated brain activity to maximize the outcome, as presented with the feedback. To this end I designed and conducted the first blinded crossover EEG study which compared real-time feedback on the occipital α -power lateralization with sham feedback. I report on this process and on the subsequent behavioral, electrophysiological and BCI results, which showed significant

positive effects of the real-time feedback on the behavior but not on the α -power lateralization.

Chapter 3 (Multimodal sensing) Compared to Chapter 2, where the increase in classification performance is an effect on the user side, in this chapter we illuminate the addition of other sensing modalities to the EEG in order to allow for better decoding accuracies. This puts the weight of enhanced performance on the machine side of the system. In the first part I assess the combination of EEG with fNIRS, report the challenges in the integration of the two modalities and the final negative outcomes which led to cease this approach. The second part discusses the fusion of EEG and pupillometry data into a hybrid BCI, the necessary adaptations in the visual protocol and the promising results that showed an increase in mean and maximal classification accuracy as well as in the number of subjects above chance level.

Chapter 4 (Brain stimulation) The idea of this chapter was to use noninvasive brain stimulation to enhance the neural substrate that is modulated by CVSA, and thus allow for better classification. I developed and conducted a double-blinded crossover study testing the effects of transcranial alternating current stimulation (tACS) in the individual α - or β -band on the baseline α -oscillations and the subsequent modulations during CVSA. I describe the design and implementation of this study and discuss possible reasons why the stimulation did not lead to substantial differences between the two groups, nor compared with a *no stimulation* condition that was added in an additional experiment.

Chapter 5 (Discussion and conclusion) In the end, I summarize the findings of this thesis, highlight their contribution to the current state-of-the-art and discuss ideas to expand the presented research in the future.

2 Real-time feedback

Visual attention can be spatially oriented, even in the absence of saccadic eye-movements, to facilitate the processing of incoming visual information. One behavioral proxy for this so-called covert visuospatial attention (CVSA) mechanism is the validity effect (VE): the reduction in reaction time (RT) to visual stimuli after valid spatial cues, compared to the increase in RT to stimuli after invalid cues. At the electrophysiological level, one correlate of CVSA is the lateralization in the occipital α -band oscillations, resulting from α -power increases ipsilateral and decreases contralateral to the attended hemifield. While this α -band lateralization has been considerably studied using electroencephalography (EEG) or magnetoencephalography (MEG), little is known about whether it can be trained to improve CVSA behaviorally. In this cross-over sham-controlled study we used continuous real-time feedback of the occipital α -lateralization to modulate behavioral and electrophysiological markers of covert attention. Fourteen subjects performed a cued CVSA task, involving fast responses to covertly attended stimuli. During real-time feedback runs, trials extended in time if subjects reached states of high α -lateralization. Crucially, the ongoing α -lateralization was fed back to the subject by changing the color of the attended stimulus. We hypothesized that this ability to self-monitor lapses in CVSA and thus being able to refocus attention accordingly would lead to improved CVSA performance during subsequent testing. We probed the effect of the intervention by evaluating the pre-post changes in the VE and the α -lateralization. Behaviorally, results showed a significant interaction between feedback (experimental – sham) and time (pre – post) for the validity effect, with an increase in performance only for the experimental condition. We did not observe significant pre-post changes in the α -lateralization, but a negative correlation between the feedback-driven changes in behavior and electrophysiology. Our findings suggest that real-time feedback on the α -lateralization is a promising tool to enhance the level of covert visuospatial attention. This opens up the exploration of applications of the proposed training method for the rehabilitation of hemispatial neglect and other attentional disorders.

Partial results of this chapter have been submitted in Schneider, C., Pereira, M., Tonin, L., Millán, JdR., 2018. Real-time EEG feedback on alpha power lateralization leads to behavioral improvements in a covert attention task. *NeuroImage*

2.1 Introduction

We can enhance our sensitivity to an upcoming visual stimulus by paying attention to its location in our visual field, even when the location is not foveated (Posner, 1980; Desimone and Duncan, 1995; Thut et al., 2006). This state, when the focus of visual attention is different from the point of gaze, is referred to as CVSA (Posner, 1980). Such shifts of attention are accompanied by modulations in the power of occipital cortical oscillations, primarily in the α -band between 8 and 14 Hz (Sauseng et al., 2005). The spatial pattern of α -oscillations produced by the visual attention follows the retinotopic organization of the visual cortex (Engel et al., 1997; Kelly et al., 2006; Rihs et al., 2007). During CVSA α -oscillations desynchronize in the hemisphere contralateral to the attended hemifield and synchronize in the opposite hemisphere (Sauseng et al., 2005; Thut et al., 2006; Foxe and Snyder, 2011). These modulations have been used to command a brain-computer interface (BCI) by attending to one or the other hemifield (Treder et al., 2011b; Tonin et al., 2013; Horschig et al., 2015).

At the behavioral level, researchers showed that α -power lateralization is indicative of the perception of faint visual stimuli (Van Dijk et al., 2008) and that it varies in accordance with the RT (Thut et al., 2006). However, increased sensitivity at the attended location means in turn a decreased sensitivity for other areas. This can be studied with invalid cueing, where a stimulus appears at a location different from what was indicated by a spatial cue (Posner, 1980; Vossel et al., 2006). In such invalid trials, subjects react slower and are less accurate on discrimination tasks, not only compared with valid cues, but also compared to no cue at all (Rizzolatti et al., 1987; Gitelman et al., 1999; Sauseng et al., 2005). This so-called VE is also referred to as the cost of reorienting attention (Rizzolatti et al., 1987; Corbetta et al., 2000), supporting the theory that α -oscillations are a suppression mechanism, reducing the weight of stimuli in unattended areas (Jensen and Mazaheri, 2010; Foxe and Snyder, 2011).

There is evidence that neurophysiological processes of visual attention can be experimentally modulated with noninvasive brain stimulation (Bestmann et al., 2007; Thut and Miniussi, 2009; Romei et al., 2010). Alternatively, neurofeedback has shown its potential for endogenous modulation of brain correlates of covert attention: Scharnowski et al. (2012) and De Bettencourt et al. (2015) have modulated visual discrimination performance and stimulus perception by training with real-time functional magnetic resonance imaging (fMRI) feedback, while Okazaki et al. (2015) used feedback based on MEG. However, to the best of our knowledge, no study has yet attempted to modulate RT using real-time feedback.

Therefore, we set out to study whether continuous closed-loop feedback based on the occipital α -power lateralization in a CVSA task has the potential to (i) modulate CVSA – as indexed by the VE based on the RTs – and (ii) amplify the lateralization in the α -band. Additionally, since an amplified α -power lateralization means that attention shifts to the left and right hemifield produce more contrasting brain patterns, we also expect to (iii) see improvement in the single-trial classification accuracy.

2.2 Materials and Methods

2.2.1 Participants

Fourteen healthy subjects, age 23 ± 1.52 years, with normal or corrected to normal vision took part in the study. All gave informed written consent and received course credits for their participation. The study was covered by the ethical protocol N° PB_2017-00295 of the ethical commissions of the cantons of Vaud and Geneva, Switzerland and confirmed with the standards of the Declaration of Helsinki (World Medical Association, 2013).

2.2.2 Experimental protocol

The study involved recordings on three different days — 51.5 ± 17.7 (minimum 16) and 12.7 ± 6.5 (minimum 7) days apart, to limit carry-over effects to following sessions. One recording session lasted approximately 90 minutes, including the technical setup. Time on task was less than 40 minutes per session, with breaks after each run (every 9-10 minutes).

On the first recording day subjects practiced for one run to familiarize with the task. Then they performed four offline runs (no feedback) to calibrate their individual decoder for the real-time feedback (Figure 2.1A). On day two and three the α -power lateralization index (α -LI) feedback was administered in a single-blinded crossover design. Subjects were paired based on their mean α -LI and their mean RT during day one while keeping the resulting groups balanced (Table 2.1). Then one member of each pair was randomly assigned to either receive real or sham α -LI feedback on day two and then switched the feedback group on day three. Therefore, both days had the same run structure: they started and ended with one offline run, while the real-time feedback was given during two middle runs.

	reaction times		α -LI span	
	Group A	Group B	Group A	Group B
Pair 1	463 ms	392 ms	0.090	0.108
Pair 2	440 ms	410 ms	2.590	0.988
Pair 3	468 ms	423 ms	0.359	1.380
Pair 4	403 ms	452 ms	0.176	0.248
Pair 5	378 ms	428 ms	0.076	0.294
Pair 6	342 ms	425 ms	0.009	0.284
Pair 7	398 ms	374 ms	-0.054	0.061
Average	413 ms	415 ms	0.464	0.480

Table 2.1 – Table of subject pairs and groups. Subjects were paired with respect to reaction times and their α -power lateralization index, with each partner receiving the real-time feedback (RT FB) either on day two or three. Both groups are well balanced in terms of both variables. The gray entries indicate the subject which was removed from all post-hoc analysis due to excess artifacts.

Offline paradigm

Each trial started with the presentation of a gray central fixation point at 0.5° visual angle and subjects were instructed to neither move nor blink until the trial was over. After one to two seconds (random duration), a cue – corresponding to the task to perform – was presented for 100 ms: half a circle (line width 0.1° , radius 2°) to the left or to the right indicated the side to attend to, a full circle around the fixation point indicated a central fixation trial (no covert attention shift). This was followed by the sustained attention phase – one to five seconds – where subjects were instructed to covertly attend to the target placeholder indicated by the cue. Target placeholders were circles with an inscribed cross (line width 0.2° , radius 2° , centered at 12° extremity from the center point and at a downward angle of 30° from the horizontal midline; Figure 2.1B). To be consistent with the real-time feedback runs where color represented the decoded α -LI (see below), the color of both target placeholders varied randomly between isoluminant red and green (L^*a^*b color space (CIELAB), L and b constant, a varied between -80 and 80). A trial ended when the inscribed cross disappeared in the to-attend target (valid cue) or on the opposite side (invalid cue). Subjects were instructed to react to the trial end as fast as possible with a button press using the right index finger. The inter-trial interval was 2-3 seconds long.

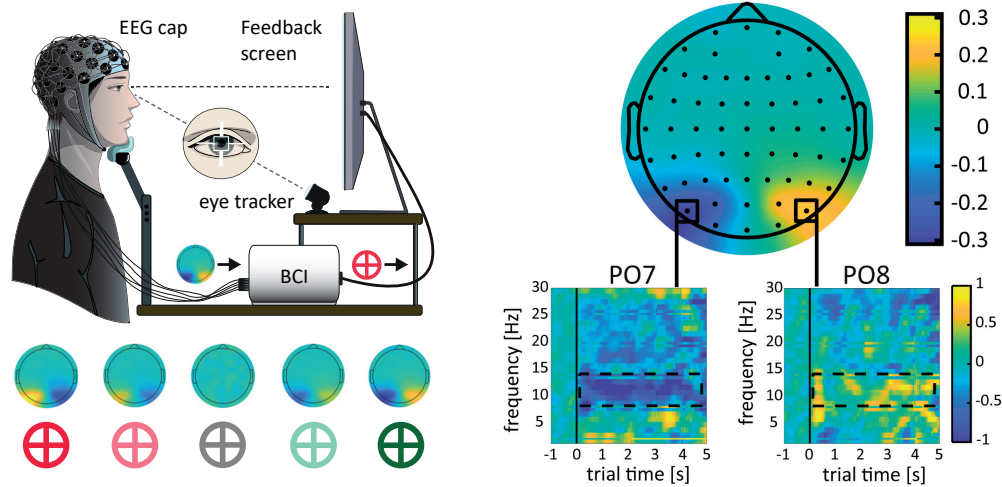
Real-time feedback paradigm

The feedback runs differed from the offline runs in the following:

To engage subjects more in the task, the online protocol was presented in the framework of a game which rewarded longer trials (dependent on their real-time α -LI performance) and fast reaction times with points. Every second of the achieved trial duration gave one point; the result was counted full for a RT of 200 ms, decreased linearly, and reached zero points for a RT of 500 ms and above. The min. and max. duration of the sustained attention period was between 2 and 20 seconds. For subjects in the experimental condition, the color of the cued target placeholder reflected their instantaneous α -LI (see Section 2.2.3) with red indicating incorrect lateralization, gray no lateralization and green correct lateralization. The trial ending times were determined from a real-time stochastic process which allowed (on average) longer trials for a correct α -LI and shorter trials for an incorrect α -LI. In the case of the sham condition, subjects were presented with the replay of the feedback session of their match regarding the α -LI and RTs from day one. In both feedback conditions, the inter-trial interval was stretched to 4-5 seconds to allow for more rest due to the longer trial times.

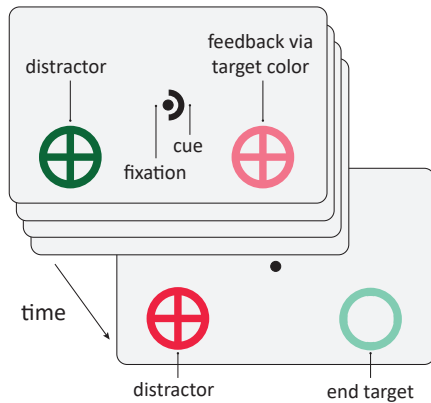
2.2.3 Data acquisition and processing

Subjects sat in a dark, shielded room, with their head in a headrest that was fixed 50 cm in front of a 24" LCD monitor. The EEG was recorded with an active 64 channel HIamp EEG amplifier (g.tec, Schiedlberg, Austria) at 512 Hz and referenced to the linked ears. The electrodes were

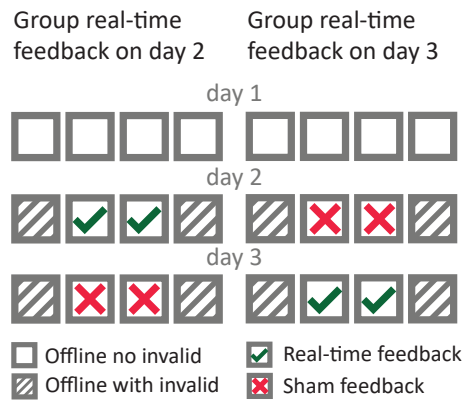


(a) Closed-loop BCI setup for the real-time feedback.

(b) Topological α -band activation and frequency-time spectrum.



(c) Screen display for the CVSA task.



(d) Run sequence during the three recording days.

Figure 2.1 – Experimental design and visual feedback. (a) Experimental setup for the real-time feedback. The instantaneous α -LI was extracted in real-time from the subjects' EEG activity and then mapped to the target color on screen. The used color ranged from a saturated red for a strong but incorrect lateralization, over gray for no lateralization to a saturated green for correct lateralization. Below the setup is an exemplary mapping of the EEG lateralization for a right-side trial. (b) Grand average of the α -LI on the first day. The head topology plot of the average difference between right and left sided trials shows the highest hemispheric activation at electrode sites PO7 and PO8. The time-frequency plots below confirm the corresponding α -band lateralization in the selected frequency band (dashed box) after the cue (vertical line, trial time = 0).

Chapter 2. Real-time feedback

Figure 2.1 – Figure caption, continued. (c) Visual display at the time of the cue presentation (foreground) and at the end of the sustained attention phase (background). Subjects were instructed to fixate the center point throughout the trial and shift their attention towards the cued side. At the end of each trial, when the inscribed cross disappeared at the cued (valid trial) or uncued side (invalid trial), subjects responded as fast as possible with a button press. Distractor and target placeholder were changing colors throughout the sustained attention phase, but only in the online runs of the experimental condition this feedback was informative of the subject's brain activity (see Panel 2.1a for the mapping of the feedback color). Note that the symbol sizes are not to scale. (d) Graphic representation of the runs in each recording day. The first day consisted of four offline runs without invalid cues. On the basis of these four runs, a decoder was built for each subject that was used for giving feedback on the α -LI in the online runs. Day two and three started and ended both with offline runs containing catch trials (i.e. invalid cues). The subjects in the experimental condition received real-time feedback on their α -LI while subjects in the sham condition received non-informative feedback.

positioned according to the international 10-20 system with the ground electrode on FCz. Eye movements and blinks were recorded with an eyeLink 1000 Plus optical eye tracker (ET) (SR research, Ottawa, Canada) at 500 Hz. All software for recording and real-time processing as well as for the on-screen display was written inhouse. The recording setup is displayed visually in Figure 2.1D. Following data processing and analysis was done in MATLAB Release 2017b (The MathWorks, Inc., Natick, Massachusetts, United States). The topographical plots were produced with the FieldTrip toolbox (Oostenveld et al., 2011).

Behavior

We chose the validity effect as our behavioral outcome measure, which was defined by Posner (1980) as the difference in RTs between invalid and valid cue trials. The VE measures the cost of reorienting visuospatial attention, which is directly linked to the attentional commitment to the cued target location (Posner, 1980; Corbetta et al., 2000; Vossel et al., 2006). We discarded all trials with RTs shorter than 200 ms or longer than 1 s, or if the subjects pressed the button before the end of the trial. To stay comparable to the electrophysiological results, we also discarded trials that contained EEG or ET artifacts.

Preprocessing

After visual inspection, we replaced EEG channels with abnormal signal-to-noise ratio by an interpolation of good channels in a 50 mm radius. Then we removed trials with EEG signal artifacts, eye blinks or a gaze deviation of more than 2° visual angle from the central fixation (Roijendijk et al., 2013; Horschig et al., 2015). For reasons of consistency, we also discarded trials that were flagged as RT artifacts. On average, $9.5 \pm 3.9\%$ of the trials were excluded due to artifacts. We needed to remove one subject entirely from the analysis due to an excessive amount of blinks and saccades (more than 50% of all trials affected).

Alpha lateralization

We computed the power spectral density (PSD) on sliding windows of one second with an overlap of 62.5 ms (Tonin et al., 2012; Horschig et al., 2015). This resulted in a time resolution of the PSD features of 16 Hz. Figure 2.1C shows the grand average α -power modulation for right-side trials minus left-side trials on day one. We see that the α -band lateralization was restricted to the parietooccipital areas with PO7-PO8 as the electrode pair with the highest difference. The spectra for PO7 and PO8 further showcase that subjects indeed modulated the selected α -band (Figure 2.1C, bottom). This is consistent with the frequency band and electrode locations used in similar studies (Thut et al., 2006; Rihs et al., 2009; Okazaki et al., 2015).

Thus, we defined the α -power lateralization index (α -LI) as the difference of electrodes PO8-PO7 in the α -band (8-14 Hz):

$$\alpha\text{-LI} = \alpha(\text{PO8}) - \alpha(\text{PO7}) \quad (2.1)$$

The resulting α -LI is negative when the left visual hemifield is attended and positive when the right visual hemifield is attended (Thut et al., 2006). Lastly, we subtracted the trial baseline α -LI ([-1,0] s before the cue) from all α -LI values during the trial.

Since we provided real-time feedback on the α -LI, we also chose it as our electrophysiological outcome measure. For analysis purposes we therefore constructed an offset-independent measure of the amplitude of the α -band modulation: the α -LI span. It is defined as the average difference between the mean α -LI for right and left trials throughout a run and is as such not influenced by a non-zero α -LI during rest. Thus, the α -LI span can be increased by a growing difference in α -power between left and right CVSA as well as by being in a high lateralization state for a longer time on average.

Closed-loop feedback

For the closed-loop feedback we mapped the α -LI to the red-green color range (Figure 2.1D), using the data gathered on day one. Ensuring a balanced distribution between left and right cue trials, we pooled all α -LI samples of day one for a given subject and fitted a normal distribution $\mathcal{N}(\mu, \sigma^2)$ to the resulting histogram. We assumed the mean μ to represent no CVSA to any given side, and $\pm 2\sigma$ being inside the individual modulable range of the α -LI.

During the closed-loop feedback phase, the transformation of the α -power lateralization index α -LI for every timepoint t to a color value was the following:

1. Subtract the baseline α -LI (last second before cue)
2. Given the noisiness of the EEG we exponentially smoothed the α -LI to create a less

volatile feature $\alpha\text{-LI}_t^s$:

$$\alpha\text{-LI}_0^s = 0 \quad (2.2)$$

$$\alpha\text{-LI}_t^s = 0.9 \cdot \alpha\text{-LI}_{t-1}^s + 0.1 \cdot \alpha\text{-LI}_t \quad (2.3)$$

3. Taking the mean μ and standard deviation σ of the Normal distribution fitted on day one, we linearly mapped the interval $\mu \pm 2\sigma$ to the interval $[-1, 1]$, which corresponded to [red, green]. Therefore, for every time point t , the color value C was defined as

$$C_t = \frac{\phi \cdot \alpha\text{-LI}_t^s - \mu}{2\sigma} \quad (2.4)$$

In order to always let green represent the desired modulation direction, we flipped the $\alpha\text{-LI}$ by multiplying with ϕ , depending on the direction of the cue:

$$\phi(\text{cue}) = \begin{cases} -1 & \text{if cue = left} \\ 1 & \text{if cue = right} \end{cases} \quad (2.5)$$

Any value exceeding the interval $[-1,1]$ after the transformation was clipped.

We used a stochastic process to elongate trials when subjects showed strong, correct lateralization. We chose to do so to maximize the time people spent in states of correct and high α -lateralization. We decided on a stochastic over a deterministic process in order to ensure readiness for the button press at all times during the trial, independent of the color shown. The color value $C \in [-1, 1]$ was linearly mapped to a cutoff value $\kappa \in [0.006, 0]$. In every update cycle, a uniformly distributed random number $x \in [0, 1]$ was drawn and the trial ended if $x < \kappa$ or it reached 20 s. The specific range of κ was chosen so that a random $\alpha\text{-LI}$ signal would result in an average trial duration of 10 seconds.

Post-hoc classification

Besides the effect of the real-time feedback on the electrophysiological and behavioral measures, we were also interested in whether the intervention could improve the control of a BCI. To this use, we trained a machine learning algorithm (classifier) on parts of the available data, so that it learns the specific patterns for each attended side for any given subject. The learned rule is then applied to new data of the same subject and a binary decision (left or right) is taken. The percentage of agreement with the ground truth, i.e. the side indicated by the cue, yields the *single trial classification accuracy*.

We trained linear discriminant analysis (LDA) classifiers on three different types of features: the baselined $\alpha\text{-LI}$ used in the real-time feedback ($\mathcal{C}_{\alpha\text{-LI}}$), the non-baselined $\alpha\text{-LI}$ ($\mathcal{C}_{\text{N-}\alpha\text{-LI}}$), and a *channels \times frequency bands* array containing the PSDs of the electrodes located in the parieto-occipital cortex (P7, P5, P3, P1, Pz, P2, P4, P6, P8, PO7, PO3, POz, PO4, PO8, O1, Oz,

O2) in seven one-Hertz wide bands from 8 Hz to 14 Hz (\mathcal{C}_{MV}). In all three cases we averaged the features over time to get a more stable estimate of the brain activity throughout the trial, yielding one data point for each feature and trial. For the multivariate classifier \mathcal{C}_{MV} we first ranked the features using canonical variate analysis (CVA) (Galán et al., 2007) and limited their number to maximum 10 to prevent overfitting.

We used 10-fold cross validation to train and test the LDA classifiers. The feature selection step was performed in each training fold and the same features selected for testing. This process was repeated 100 times with randomly assembled folds to consolidate the accuracy estimations in face of the low number of data points. The chance level was computed as the upper bound of the 95% confidence interval of a binomial distribution with an expectation value 0.5 for 80 trials per run.

2.2.4 Reporting

Any results reported follow the following notations: The term grand average refers to the average across the individual subject averages across trials. Means and standard deviations are noted in the format $a \pm b$. Error bars depicted in plots are the standard error of the mean (SEM) across subjects, unless stated otherwise. The significance threshold for statistical tests is set at $p = .05$. For all correlations we report the empirical Pearson correlation coefficient r , the coefficient of determination r^2 and we calculated the p-value through a permutation test with 10,000 repetitions.

2.3 Results

2.3.1 Behavioral correlates of attention

First, we tested whether our real-time feedback intervention produced the hypothesized increase in the behavioral outcome measure (VE). For this, we performed a two-way repeated measures analysis of variances (ANOVA) with the within-subject factors *time* (pre/post) and *feedback* (experimental/sham). We found a significant interaction ($F(1, 12) = 5.54, p = .036$) with an effect size of $\eta_p = .316, 95\% \text{ CI} = [.033, .658]$. The VE increased 40 ± 45 ms for the experimental condition while it increased only 9 ± 52 ms after the sham feedback (Figure 2.2a). In the sham condition, 7 subjects increased and 6 subjects decreased their VE whereas in the experimental condition 10 out of 13 subjects increased their VE (Figure 2.2b).

We did not find simple effects, neither of *feedback* ($F(1, 12) = 0.20, p = .664$) nor of *time* ($F(1, 12) = 4.03, p = .068$). Post-hoc paired t-tests (FDR-corrected for multiple comparisons) revealed a difference in validity effect pre and post intervention for the experimental condition ($t(12) = -3.11, p = .036$), but not for the sham condition ($t(12) = -0.56, p = .586$). The effect size of the significant pre-post difference in the BCI feedback group was $\eta_p = .446, 95\% \text{ CI} = [.014, .745]$. There was no significant difference ($t(12) = -0.85, p = .547$) between the feedback

Chapter 2. Real-time feedback

groups before the intervention and a non-significant trend in the post-intervention comparison ($t(12) = 2.05, p = .126$).

We then decomposed the VE into valid and invalid RTs to find whether one was driving the observed effect. On average, RTs to peripheral targets after invalid cues were 141 ± 66 ms longer than for correctly cued peripheral trials. In the experimental condition the RTs in validly cued trials decreased by 2 ± 19 ms while they increased by 14 ± 30 ms for the sham condition. The RTs for invalidly cued trials increased by 39 ± 40 ms for the experimental condition and by 22 ± 50 ms for the sham condition (Figure 2.2c). Repeated measures two-way ANOVAs showed a significant interaction for valid trials ($F(1, 12) = 4.82, p = .049$), but not for invalid trials ($F(1, 12) = 1.42, p = .257$).

In order to see whether habituation to the task influenced the RTs, we looked at the mean RTs after valid and invalid cues on day one and in the pre-intervention runs on day two and three (Figure 2.2d). We observed a significant decrease of mean RTs over days ($F(1.21, 14.52) = 18.78, p < .001$; Greenhouse-Geisser corrected). Therefore, we verified that the order in which the subjects were assigned to the BCI or sham feedback did not confound our results. For this we employed a three-way mixed repeated measures ANOVA to evaluate the effect of the within subject factors of *feedback* and *time* and the between subject factor of *order* (starting with real or sham feedback). We found no three-way interaction $order \times feedback \times time$ ($F(1, 11) = 0.66, p = .433$) and the between-subject effect of *order* was not significant ($F(1, 11) = 0.02, p = .898$). The interaction $time \times feedback$ was still significant ($F(1, 11) = 5.070, p = .046$).

2.3.2 Neurophysiological correlates of attention

Firstly, we wanted to confirm that our real-time feedback intervention allowed subjects to improve their α -LI, as opposed to the sham feedback. Figure 2.3a displays the α -LI during the intervention for left and right sided trials in the experimental and sham condition. We observed a near-significant increase in the average α -LI span over the trial duration for the experimental condition ($F(2.25, 24.80) = 2.89, p = .069$; Greenhouse-Geisser corrected). For the sham condition on the other hand, we did not find a significant α -LI span growth ($F^{GG}(1.44, 17.26) = 0.09, p = .859$; Greenhouse-Geisser corrected).

Our electrophysiological outcome measure of the closed-loop training was the change in the α -LI span between the pre and post intervention offline sessions. We found no interaction effect of the factors $time \times feedback$ in a two-way repeated measures ANOVA ($F(1, 11) = 1.587, p = .232$), nor were the simple effects of *feedback* ($F(1, 12) = 0.046, p = .834$) or *time* ($F(1, 12) = 0.398, p = .540$) significant. The average α -LI span was stable between pre and post intervention sessions ($0.016 \pm 0.396 \frac{\mu V^2}{Hz}$) while it decreased slightly for the sham feedback condition ($(0.141 \pm 0.557 \frac{\mu V^2}{Hz})$) (Figure 2.3b).

We then explored the relationship between the changes observed in the behavioral and electrophysiological outcome measures. To this end, we computed the interaction effect

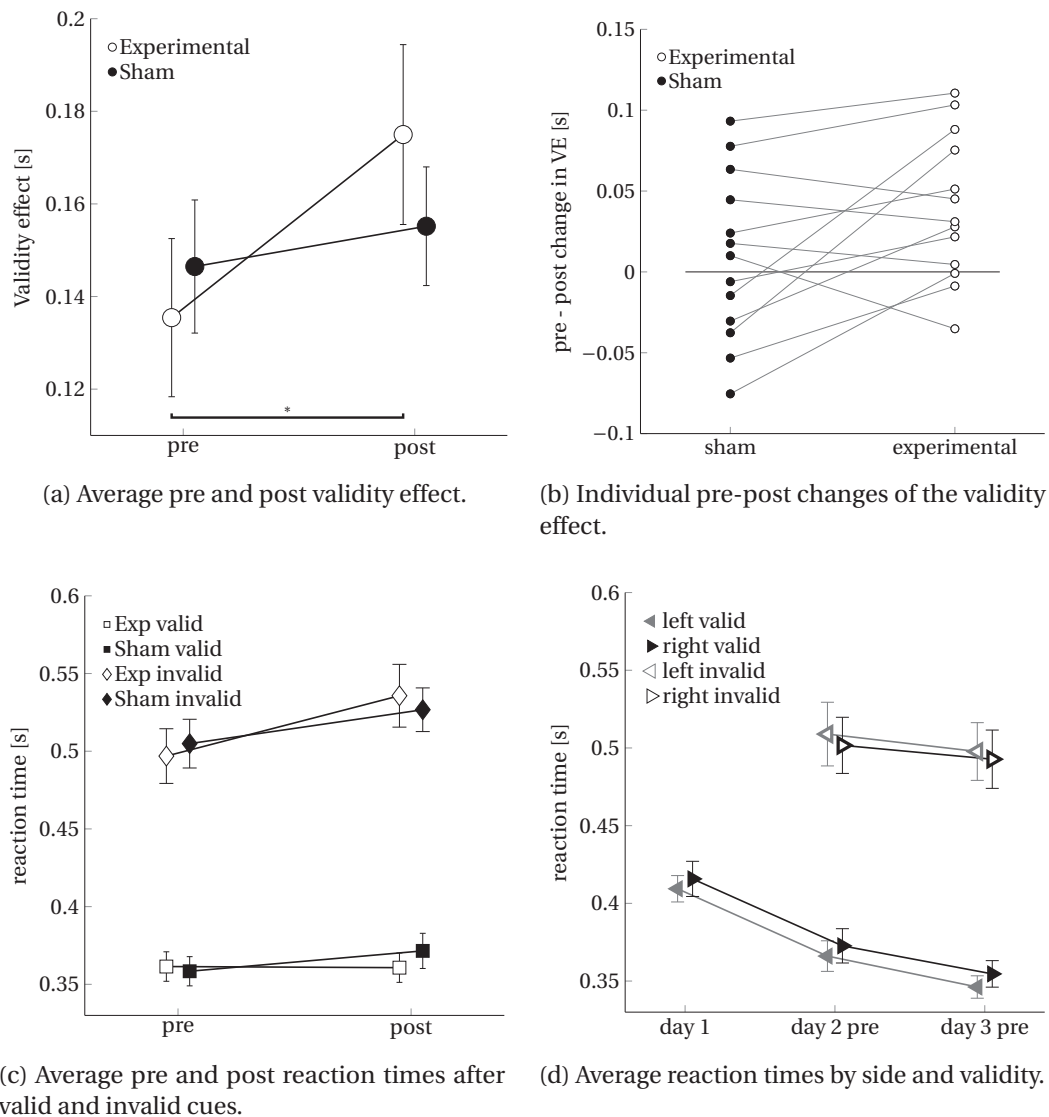


Figure 2.2 – Behavior. (a) Mean validity effect pre and post intervention for the experimental (white circles) and sham group (black circles). Pre-post difference in the experimental group was significant ($p < .05$, FDR corrected). Whiskers represent the SEM across subjects. (b) Pre-post changes in the VE for the sham (black circles on the left) and experimental condition (white circles on the right) for every subject. Solid lines connect data points of the same subject. (c) Average reaction times pre and post intervention for validly cued (squares) and invalidly cued (diamonds) trials for the experimental (white) and the sham (black) group. Whiskers represent the SEM across subjects. (d) Mean reaction times for left (gray left triangles) and right (black right triangles) side trials on recording days 1, 2 and 3. Reaction times to validly cued trials are connected with solid lines, those for invalidly cued trials (catch trials) are connected with dashed lines. Whiskers represent the SEM across subjects.

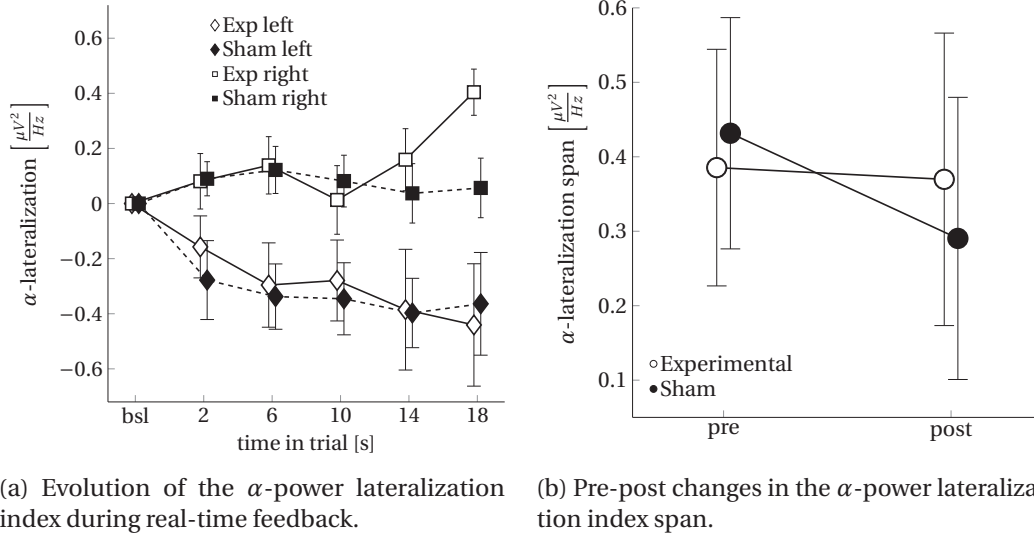


Figure 2.3 – Electrophysiology. (a) Averaged baselined lateralization index for left (diamonds) and right (squares) cued trials during the online training phase in the experimental (white) and sham (black) condition. Data were binned into the baseline period (bsl) and five subsequent 4 s windows centered around 2, 6, 10, 14 and 18 s. Whiskers represent the SEM across subjects. (b) The average pre-post changes of the average α -LI span for the experimental and the sham condition. No significant changes. Whiskers represent the SEM across subjects.

(IE) for the VE and the α -LI for each subject individually:

$$IE_{VE} = \left(VE_{\text{post}}^{\text{BCI}} - VE_{\text{pre}}^{\text{BCI}} \right) - \left(VE_{\text{post}}^{\text{sham}} - VE_{\text{pre}}^{\text{sham}} \right) \quad (2.6)$$

$$IE_{\alpha\text{-LI}} = \left(\alpha\text{-LI}_{\text{post}}^{\text{BCI}} - \alpha\text{-LI}_{\text{pre}}^{\text{BCI}} \right) - \left(\alpha\text{-LI}_{\text{post}}^{\text{sham}} - \alpha\text{-LI}_{\text{pre}}^{\text{sham}} \right) \quad (2.7)$$

First, to test whether differences in α -lateralization could explain the behavioral effect, we correlated the $IE_{\alpha\text{-LI}}$ with the IE_{VE} . We found a significant correlation ($n = 13, r = -.59, r^2 = .43, p = .030$), but – contrary to our expectations – negative. This means that the more subjects increased their α -LI after real feedback compared to sham, the more decreased their CVSA, as indexed by lower VE (Figure 2.4a). Second, we tested whether the amount of changes in α -power lateralization *during* the online training – rather than between pre and post offline sessions – affected the improvement in CVSA. We found no correlation between the IE_{VE} and the amount of lateralization during the training ($n = 13, r = .17, r^2 = .17, p = .569$, Figure 2.4b). Lastly, we examined whether the individual resting-state α -band power (measured on day one) has an influence on the behavioral changes. We found no correlation between them ($n = 13, r = -.43, r^2 = .29, p = .135$, Figure 2.4c). The figure indicates that 3 out of the 13 subjects had a naturally elevated α -power which could be considered an outlier compared to the rest of the subjects α -power ($> 2 \frac{\mu V^2}{\text{Hz}}$). Thus, we recomputed the results without those three subjects to see if any effect was driven by them. The major change was a loss in significance for the correlation between the $IE_{\alpha\text{-LI}}$ and the IE_{VE} ($n = 10, r = -.05, r^2 = .14, p = .90$). The behavioral *time* \times *feedback* interaction became even stronger ($F(1, 9) = 6.77, p = .029$).

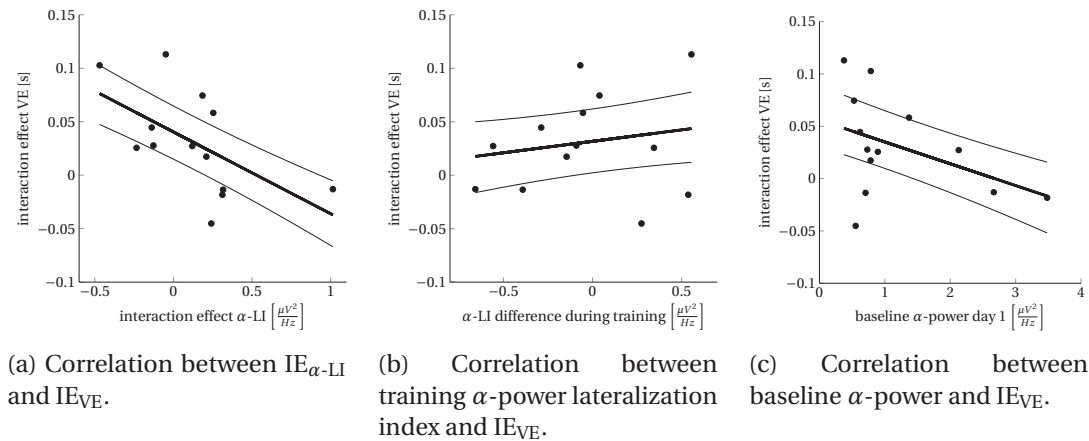


Figure 2.4 – Correlation of electrophysiological and behavioral results. (a) Significant correlation ($n = 13$, $r = -.59$, $r^2 = .43$, $p = .030$) between the interaction effect $IE_{\alpha-LI}$ and IE_{VE} . The thick line indicates the linear fit to the data, the two thin lines display the 95% confidence interval. (b) Non-significant correlation ($n = 13$, $r = .17$, $r^2 = .17$, $p = .576$) between differences (experimental minus sham) in α -LI during the real-time training and the behavioral interaction effect IE_{VE} . The thick line indicates the linear fit to the data, the two thin lines display the 95% confidence interval. (c) Non-significant correlation ($n = 13$, $r = -.43$, $r^2 = .29$, $p = .135$) between the baseline α -power on day one and the behavioral interaction effect IE_{VE} . Three subjects displayed a visibly elevated level of resting state α -power ($> 2 \frac{\mu V^2}{Hz}$) on all recording days. The thick line indicates the linear fit to the data, the two thin lines display the 95% confidence interval.

2.3.3 Single trial classification

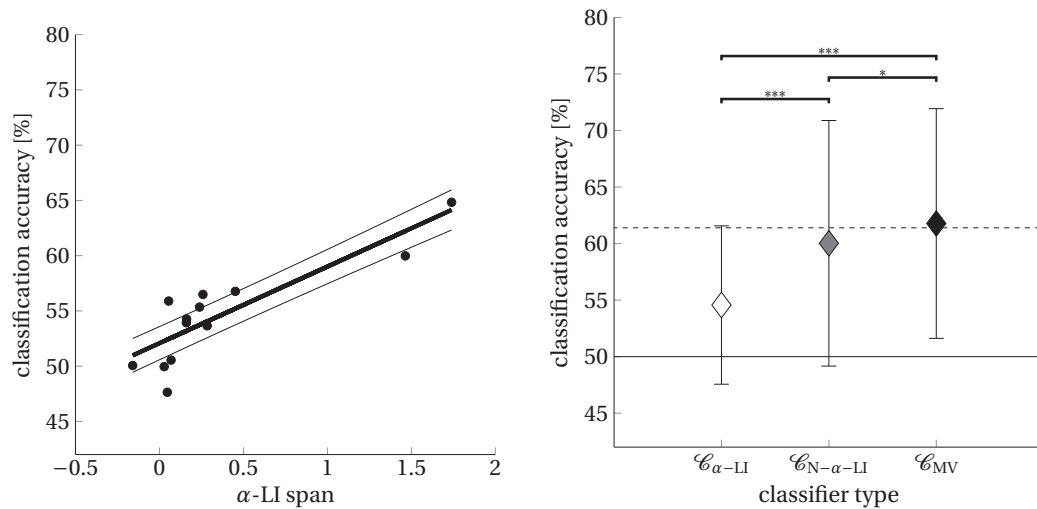
We sought to decode the attended side during the CVSA task in real time by utilizing only brain activity in the α -band. We hypothesized that a larger average modulation of the α -LI would lead to a better separation of the brain patterns of the two classes (left and right side CVSA), and thus allow for higher classification performance. To test this, we computed the post-hoc single trial classification performance on each of the offline runs on day two and three for each subject separately : pre- and post-runs in the experimental and sham condition. We found that the α -LI span correlated strongly ($n = 13, r = .86, r^2 = .78, p < .001$; Figure 2.5a) with the classification performance based on the $\mathcal{C}_{\alpha\text{-LI}}$ (Section 2.2.3). This correlation was still significant when removing the two outliers with high (> 1) α -LI span. We also found similar correlations between the α -LI span and the classification accuracies of $\mathcal{C}_{\text{N-}\alpha\text{-LI}}$ ($n = 13, r = .68, r^2 = .54, p = .01$) and \mathcal{C}_{MV} ($n = 13, r = .60, r^2 = .45, p = 0.03$).

To test if the real-time feedback intervention had an effect on the classification performance, we employed repeated measures ANOVAs for the within subject factors of *feedback* and *time* and the between subject factor of *order*. We did not observe a significant interaction on any level ($F(1, 12) < 1.604, p > .231$) for neither of the three classifiers $\mathcal{C}_{\alpha\text{-LI}}$, $\mathcal{C}_{\text{N-}\alpha\text{-LI}}$ and \mathcal{C}_{MV} . Thus, we averaged the classification performance over all four runs for each individual subject.

We decoded CVSA above chance level ($p < .05$) in a single trial setting using the multivariate classifier \mathcal{C}_{MV} (black diamond in Figure 2.5b). We achieved an average classification accuracy of $61.9\% \pm 10.2\%$ where 7 out of 13 subjects performed significantly above chance level (min. 62.2%, max. 75.8%). Similarly, although on average slightly below chance level, $\mathcal{C}_{\text{N-}\alpha\text{-LI}}$ (gray diamond) yielded an average classification performance of $60.0\% \pm 10.9\%$ with six subjects above chance level (min. 63.8%, max. 76.5%). Classification of the baselined α -LI $\mathcal{C}_{\alpha\text{-LI}}$ (white diamond) performed worst, with an average accuracy of $54.5\% \pm 7.0\%$ and only one subject above chance level (64.8%). In comparison, the accuracy strongly improved from $\mathcal{C}_{\alpha\text{-LI}}$ to $\mathcal{C}_{\text{N-}\alpha\text{-LI}}$ ($t(51) = -4.56, p < .001$), respectively \mathcal{C}_{MV} ($t(51) = -6.23, p < .001$). The difference between $\mathcal{C}_{\text{N-}\alpha\text{-LI}}$ and \mathcal{C}_{MV} was significant ($t(51) = -1.68, p = .049$).

2.4 Discussion

This study reports a behavioral improvement in CVSA indexed by higher VE after providing 20 minutes of EEG-based closed-loop feedback on occipital α -band lateralization. No such improvement was observed when providing the same subjects with feedback that was not linked to their brain activity but to the recorded brain activity of another subject. We thus verify that the improvement in CVSA cannot be explained by behavioral learning per se but was the result of our feedback manipulation. Contrarily to our prediction, however, behavioral improvement did not correlate with the α -lateralization during the training and was negatively related with pre-post increases in lateralization. Finally, we were able to successfully decode the attended side on a single trial level but classification accuracy was unaffected by the feedback intervention.



(a) Correlation between the α -power lateralization index span and the classification performance of $\mathcal{C}_{\alpha\text{-LI}}$. (b) Mean single trial classification performances.

Figure 2.5 – Correlation with the α -LI and average classification results. (a) Significant positive correlation between the α -LI span and the classification accuracy. As expected, the classification performance improves with higher α -power modulation. The thick solid line indicates the linear fit to the data, the two thin solid lines display the 95% confidence interval. (b) Single trial classification results for three different feature spaces: the baselined α -LI ($\mathcal{C}_{\alpha\text{-LI}}$), the non-baselined α -LI ($\mathcal{C}_{\text{N-}\alpha\text{-LI}}$) and a multivariate feature space (\mathcal{C}_{MV}). The difference in classification performance between $\mathcal{C}_{\alpha\text{-LI}}$ and $\mathcal{C}_{\text{N-}\alpha\text{-LI}}$ respectively \mathcal{C}_{MV} was highly significant. $\mathcal{C}_{\text{N-}\alpha\text{-LI}}$ and \mathcal{C}_{MV} are significantly different. The latter is the only one achieving a mean classification performance above the upper bound of the 95% confidence interval (dashed line) of the chance level (solid line). The error bars indicate standard deviations.

2.4.1 Closed-loop feedback for CVSA

The goal of any online feedback intervention is ultimately to change behavioral markers through operand conditioning using a biomarker (Sherlin et al., 2011). Two studies with a real-time feedback approach similar to ours, one using fMRI and the other MEG, have presented somewhat contradictory behavioral changes in the perception threshold of covert stimuli.

Scharnowski et al. (2012) provided subjects with real-time feedback on occipital blood oxygen level dependent (BOLD) activity during a neurofeedback session. Subsequently, they showed improved perception of Gabor patches in the visual field corresponding to the trained area; but only for those subjects that managed to upregulate the BOLD signal (Scharnowski et al., 2012). Unlike this study, our feedback strategy aimed at training subjects to maintain high lateralization *throughout* the task.

In another study Okazaki et al. (2015) successfully trained α -lateralization by linking it to the discriminability of faces. This procedure, however, led to a drop in performance post

intervention in the experimental groups in the untrained hemifield, while no changes were observed in the sham groups (Okazaki et al., 2015). Our study differed on many aspects: Firstly, we linked the lateralization to the probability of the trial ending and thus alerted subjects in case of low lateralization to reorient their attention. Therefore, our design differs from studies that linked attentional brain signals to task difficulty (De Bettencourt et al., 2015; Okazaki et al., 2015). Secondly our outcome measure was RT rather than discrimination performance. Lastly, we used the same task for training and testing, thus maximizing transferability while Okazaki et al. (2015) trained on faces and tested on Gabor patches.

We point out that our study, using EEG, showed behavioral effects after around 20 minutes of closed-loop feedback while fMRI studies like Scharnowski et al. (2012) and Robineau et al. (2014) needed multiple sessions of BOLD feedback to achieve an effect. This suggests that the temporal contiguity of the feedback, which is certainly higher in EEG, plays an important role in the speed of learning (Rahmandad et al., 2009; Sherlin et al., 2011; Sulzer et al., 2013).

In the next section, we discuss how our results – taken together with those of previous neurofeedback and neurostimulation studies – show that α -oscillations have a causal effect on behavior but that this effect could be more complex than previously assumed.

2.4.2 Alpha-band lateralization

The grand average pattern of α -power differences between left- and right-cued trials displayed the typical lateralization introduced by CVSA tasks (Kastner et al., 1999; Worden et al., 2000; Sauseng et al., 2005; Rihs et al., 2007). The sustained lateralization (on average) observed during training suggests that subjects were able to maintain covert attention to the target for up to 20 seconds, which is longer as in any previously reported study (Andersson et al., 2012; Scharnowski et al., 2012; Okazaki et al., 2015).

Even though there is evidence that motor preparation can influence occipital α -power levels (Kajihara et al., 2015), the chosen study design counters possible cross-contamination in the EEG-signal on two levels. First, trial duration was not fixed but was either randomly determined (offline runs) or stochastically jittered (online runs), which diminishes a build-up of expectation with respect to the button press. Secondly, subjects were instructed to only use their right index finger for the reaction time task. This leads to the same activation for either attended side and thus was automatically disregarded when contrasting the two conditions in the averages or the classification.

Interestingly, we could not observe any significant pre-post changes in the α -LI span after the real-time feedback, although the observed effect goes into the right direction: the α -LI span decreased more in the sham condition than in the experimental conditions, but the differences were not significant. This stands in contrast to the study of Okazaki et al. (2015), who showed a significant increase in lateralization index after the feedback training – although only for targets in the left hemifield. A possible explanation could be that the changes that

we observed during the online training were not strong enough to be maintained until post-testing. Another factor could be the low signal-to-noise ratio of the EEG, which requires to average more trials to get to a reliable estimate of the α -LI span. Behavioral measures, on the contrary, are less noisy.

Initially, we assumed a higher lateralization value to be representative of higher CVSA, which should be reflected in a higher VE. Unexpectedly, we found a negative correlation between the changes in the α -LI span and the VE. While this correlation connects well with the increased stimulus perception threshold after neurofeedback training (compared to sham) found by Okazaki et al. (2015), it was lost when excluding three subjects with unusually high baseline α -power. This makes a simple linear relationship between changes in the RTs and the α -LI span unlikely. The stronger interaction effect for the VE when those three subjects were taken out corroborates Hanslmayr et al. (2007), who reported that a high occipital α -power correlated negatively with stimulus perception performance. This is in line with the hypothesis that α -oscillations are a mechanism of inhibition of neuronal firing activity (Jensen and Mazaheri, 2010; Romei et al., 2010). Nevertheless, we also could rule out a correlation between the baseline α -power and the observed behavioral changes. This demonstrates that the relation of occipital α -band power lateralization and RT-based correlates of CVSA is less straightforward as previously thought. Further studies will be needed to throw light on the neural mechanisms that connect the two.

2.4.3 Single trial classification

Oscillatory brain patterns associated with CVSA have been used as an input modality for BCIs: (Van Gerven and Jensen, 2009; Treder et al., 2011b; Tonin et al., 2013). In a post-hoc analysis, we could successfully decode the attended side from modulations in the α -band in 7 out of 13 subjects. Since, although debated, evidence suggests that BCI use is a skill that can be learned, we would expect performance improvements for a longer series of training sessions (Curran and Stokes, 2003; Perdakis et al., 2018).

Compared to the studies of Scharnowski et al. (2012) and Okazaki et al. (2015), who have worked with fMRI- and MEG-based feedback respectively, EEG-based feedback is cost effective and portable. This would allow for an easier application in and outside the clinical environment, e.g. in spatial neglect rehabilitation (Tonin et al., 2017). But one of the challenges in EEG is the tendency for nonstationarities (Lotte et al., 2007; Arvaneh et al., 2013). In order to separate task related changes from the fluctuating "physiological" noise, a pre-cue baseline activity often gets subtracted from the in-task EEG signal (Rihs et al., 2007). Since we were interested in feeding back only the modulation induced by the CVSA task, we opted for baselining our signals. But as observed in the post-hoc single trial classification, better classification could have been achieved without baselining. A possible explanation could be, that the maximally achieved lateralization is independent of the α -LI at the start of the CVSA task. This connects well with Van Dijk et al. (2008), who found that the perception of a visual

stimulus could be predicted by the instantaneous (not purposefully modulated) α -power distribution. This suggests that natural fluctuations of the occipital α -power lateralization are intrinsically modulating the attentional resources and are thus not "physiological" noise that needs to be offset.

Finally, we observed a substantial performance difference between employing a rigid one-size-fits-all classifier ($\mathcal{C}_{\alpha\text{-LI}}$) and a classifier that was trained on features of individually picked electrode locations and frequency subbands (\mathcal{C}_{MV}). The BCI field has a long tradition of using machine learning approaches to individualize correlates of mental tasks (Millán et al., 2002; Lemm et al., 2011). In our case, judging by the increased post-hoc classification performance, it might be argued that subjects could have learned better given a more individualized feedback. However, this would only be true for subjects with above-chance classification performance. In the case of little or no difference in the features between the two classes, such a classifier might actually be trained on "noise" – non-physiological features that stand out randomly from the training data. Hence, selecting features based on the physiologically meaningful group average is a more promising approach for those subjects. Since a pilot study suggested that only half of all subjects reach above-chance classification performance, we therefore opted for giving real-time feedback on a fixed band and electrode locations in our experiment, with the individual mapping of the modulation range as the only free parameter. Future work could investigate the use of multivariate classification approaches within neurophysiological constraints on the weights to further improve CVSA discriminability and eventually behavior.

2.5 Conclusion

Our results show that continuous real-time feedback on the α -LI is able to improve behavioral correlates of CVSA in a healthy population. This is a first important step towards a tool for rehabilitation of the spatial neglect syndrome where visual perception is impaired in one visual hemifield. Further work is still needed to establish a strong link between the behavioral improvements and the observed changes in the electrophysiology, which would allow to specifically and individually target the occipital α -power imbalances observed in these patients. Combined with advanced understanding of the mechanisms of spatial neglect, online feedback could become an efficient add-on training for the rehabilitation of hemineglect patients.

3 Multimodal sensing

Decoding covert visuospatial attention (CVSA) to the left or right visual field with electroencephalography (EEG)-based systems leaves a substantial part of the population without brain-computer interface (BCI) control, i.e. the classification accuracy is not significantly different from chance. One approach that proved useful for improving motor-related BCIs was to combine information of two different brain imaging modalities, all and foremost EEG and functional near-infrared spectroscopy (fNIRS). But also the combination with non-brain-related physiological measures has proven its potential. In this chapter we explored the usefulness of two hybrid BCIs systems — combining EEG with fNIRS or pupillometry — to increase the classification accuracy in a CVSA task. To this end we developed specialized setups and paradigms to simultaneously record EEG and fNIRS or EEG and the pupil size while subjects performed a CVSA task. Then we built and evaluated the unimodal and combined classifiers. Despite contrary reports in literature, we could not find task-related activation in the fNIRS signal. Further investigation showed that even strong visual stimulation with a rotating checkerboard was not picked up by the device. The combination of EEG and pupil size on the other hand, allowed modest increases in the classification accuracy and enabled more subjects to perform above chance level than any of the unimodal classifiers alone. In the case of the more promising combination of EEG with pupil size measurements, we expect that an improved visual protocol would bring further increases in decoding performance. Thus we believe that it holds great potential for further use. Additionally, following reported use of fNIRS on the visual system, we still believe that upgrades in hardware technology could render the fNIRS a valuable modality to complement the EEG in a hybrid CVSA BCI. Our findings suggest that fusion could be meaningful where single modalities fail to exhibit above-chance performances. Even though the achieved benefits in our study were rather small, it is up to the intended application of the hybrid BCI to justify the addition of a more complex setup and data processing stream. Even small gains could be very important if e.g. this allows more people to benefit from BCI-based rehabilitation protocol.

Parts of the results of this chapter have been published in Schneider, C., Millán, JdR., 2016. Comparing EEG and fNIRS for a covert attention BCI. Proceedings of the 6th international BCI meeting, p.96

3.1 Introduction

We have demonstrated in the last chapter that closed-loop feedback on the lateralization pattern of the occipital α -band can enhance behavioral correlates of CVSA, but that the effect on the BCI decoding accuracy was not significant. Especially subjects that displayed classification accuracies not significantly different from random have a hard time making use of the closed-loop feedback (Wolpaw, 2010). Large efforts undertaken in hardware development and a vast battery of machine learning techniques have not been able to sufficiently increase the maximum decoding accuracy achieved with EEG-BCIs. On the one hand this means that EEG-BCIs still suffers from a large inter-session variability, which constrains a prolonged use of the BCI without updating the computer-based classifier, and on the other hand leaves a non-negligible group (15-30%) of people without any considerable BCI control (Dickhaus et al., 2009). For these people, the electrical activity between different intentional commands looks too similar from the viewpoint of the decoding algorithm. This could even be due to differences in individual brain anatomy, which are believed to have an influence on the ability to decode meaningful features from EEG; i.e. if an investigated cortical area is located on a sulcus (good signal) or in a gyrus (no signal) (Kirschstein and Köhling, 2009; Goldenholz et al., 2009).

This naturally leads to the exploration of other brain-imaging modalities to test whether the same or other task-related neural correlates could be observed. Over the years, BCIs have also been built by observing the magnetic field of the brain with magnetoencephalography (MEG) (Lal et al., 2005; Mellinger et al., 2007) or hemodynamic changes in brain tissue with functional magnetic resonance imaging (fMRI) (Weiskopf et al., 2004a) and fNIRS (Coyle et al., 2004; Matthews et al., 2008). But since every imaging modality comes with its own set of disadvantages (no portability and cost for MEG and fMRI, slow signal for fMRI and fNIRS, only cortical imaging possible for fNIRS and EEG), a combination of two imaging modalities allow a fuller picture of the brain activity. In order to achieve this, it only makes sense to investigate imaging modalities which provide information that is complementary – or *orthogonal* when formulated mathematically – to each other.

Literature reveals that different combinations of brain-imaging modalities have been used together to enrich the information gained from the examined brain processes. The most common combination in medical studies, positron emission tomography (PET) + fMRI is not feasible for the use of BCIs due to the necessity to infuse radioactive isotopes into the body prior to a PET scan. Other combinations that have been explored are EEG + fMRI (Ritter and Villringer, 2006; Huster et al., 2012), MEG + fMRI (Dale et al., 2000; Downing et al., 2001) and EEG + fNIRS (Wallois et al., 2012; Fazli et al., 2012). When narrowing down the options for the use in a BCI framework, we want the ability to image simulataneously with both sensing modalities, because otherwise the added information would not be available in a single-trial decoding setup. Current literature provides some proof of principle BCI studies for BCIs that combine EEG and fMRI (Zotев et al., 2014; Zich et al., 2015; Liu et al., 2016) and EEG and fNIRS (Fazli et al., 2012; Blokland et al., 2014; Morioka et al., 2014; Putze et al., 2014; Yin et al.,

2015; Buccino et al., 2016). The obtained results showed that extracting information from two complementary brain imaging modalities has the potential to be beneficial for pattern decoding and classification (Bießmann et al., 2011; Huster et al., 2012; Fazli et al., 2012). This was even explored in rehabilitation settings (Yu et al., 2013), where multimodal BCIs proved useful. Thus, combining different sensing modalities in a BCI bears the potential to minimize the number of people left without control, increase the decoding accuracy, and decrease the false positive rate (FPR), which is essential for feedback-based learning.

Therefore, I wanted to explore the possibility to expand the data space obtainable with the EEG by including other sensing modalities into a hybrid BCI. This additional modalities should in the best case yield orthogonal information on the CVSA process, i.e. information that is not correlated with the EEG data. Additionally, a simultaneous use of both modalities should be possible without one modality introducing artifacts in the other one. Finally, the added modalities should in the best case not take away the advantage of EEG-based BCIs, i.e. modest costs and portability. Especially when targeting a rehabilitation application, the system should be noninvasive, ideally portable for bedside or out-of-hospital use, be set up quickly for each session and be cheap in purchase and maintenance. Given these constraints, I have identified two interesting candidates: fNIRS and pupillometry. In the following two sections I report on the inclusion of each of them with EEG into a CVSA BCI.

Another aspect that comes into play in a hybrid BCI setup is the way how to combine the different information streams. For the proposed BCI setup, there are two principal possibilities of fusing the information: either at the feature level (feature fusion; concatenating the features and therefore expanding the feature space available for classification) or at the classifier level (classifier fusion; classifying the information of each modality separately and then combining the results based on the confidence based in each modality). The applicability of each of the two methodologies is mainly influenced by the temporal resolution of the signals. For example, electric or magnetic fields can change on the millisecond range to reflect the brain's reaction to a stimulus, while the hemodynamic trace of the same reaction takes up to several seconds to reveal itself. In such cases, a simple concatenation of the feature spaces will not allow an improvement in the classification performance simply because the peak signal of the two modalities will not be present at the same time. This could be counteracted by time-warping both signals to a pre-computed template (Wöllmer et al., 2009) or saving the peak activation in the fast modality to match it with the peak activation in the slower modality (Fazli et al., 2012). But these actions are very error-prone and thus mostly avoided and replaced by a fusion of the classifier outputs. In these cases, the output of the fast modality classification can either serve as a prior to the slower modality, or the two decisions are combined after each modality has finished its classification. The question of how to optimally combine two independent input data streams opens up a whole field of machine-learning and optimization algorithms (Bießmann et al., 2011; Dähne et al., 2015). In this thesis I did not dive deeply into this topic and, due to the different temporal dynamics of the signals involved, used classifier fusion on the trial level to achieve combined classification results.

3.2 Functional near-infrared spectroscopy

3.2.1 Introduction

fNIRS is an optical brain imaging technique that works on the principle of near-infrared light being absorbed mainly by hemoglobin (present in red blood cells to transport oxygen). This range in the near-infrared spectrum is called the *optical window*, since most of the body tissues e.g. skin, bones, muscles, etc. are basically transparent under near-infrared light; i.e. these tissues do not absorb light of this wavelength (Jöbsis, 1977). For that reason, the amount of attenuation measured between light source and light detector is mainly dependent on the amount of hemoglobin, and thus blood in the light path. As is the case with the blood oxygen level dependent (BOLD) signal in fMRI, we are interested in how much oxygen is transported to a certain brain region. To this end, a minimum of two wavelengths λ_1, λ_2 is chosen, where the light attenuation of oxygenated and reduced hemoglobin differs substantially between these two wavelengths (Figure 3.1a). This then allows to compute the relative proportion of oxygenated hemoglobin (HbO) and reduced hemoglobin (HbR) in the total hemoglobin concentration (see Section 3.2.2 for details). The change in the total hemoglobin (HbT) is computed as $HbT = HbO + HbR$.

If the tissue imaged is thin enough, e.g. a finger, a light source can be put on one side, and the detector on the other side. In this method, which is called transmission near-infrared spectroscopy, the light will fully traverse all the tissue between the source and the sensor. This is for example used for pulse oximetry or the brain oxygenation measurement for neonates (Jöbsis, 1977). But the penetration depth of the emitted light is not high enough to do the same for bigger volumes, as is for example the adult human head. In order to image cortical blood oxygenation in adults, the fNIRS relies on the backscattering of light: the emitted light will spread and some part of it will resurface due to multiple scattering in the tissue (Ferrari et al., 1985). The flight path of resurfacing photons will on average describe a curved shape that is often referred to as the *banana shape* (Figure 3.1b). This means that the further away from the light source an emitted photon resurfaces, the deeper it penetrated the tissue. This yields a de facto standard distance of approximately 3 cm between source and detector for adult fNIRS brain imaging to ensure the upper cortical layers lie in the flight path of the majority of photons (Strangman et al., 2003; Ferrari and Quaresima, 2012). Even though further distances would theoretically yield even higher penetration depths which could allow to image deeper brain structures, the overall light attenuation is too strong, and no reliable signal can be picked up without increasing the source light intensity above safe levels.

As mentioned before, the fNIRS (usually) measures the relative proportions of oxygenated and reduced hemoglobin in the blood. In this sense, even though the physical principles are very different, the signal we obtain is comparable to the BOLD signal obtained with fMRI. When a cortical region is more active (higher number of neurons firing), the body provides more oxygen to these regions by upregulating the influx of oxygenated blood. This is called the *hemodynamic response* to neural activity (see Ferrari and Quaresima (2012) for details).

3.2. Functional near-infrared spectroscopy

Due to the time needed for the adaptation of the blood flow via relaxations of the vessels and the distribution of the blood in the target tissue, this response has a delay in its build-up and displays overall slower dynamics (Figure 3.1c). Cortical regions that are supplied with higher amounts of oxygenated blood during a task as compared to resting are assumed to be implicated in the neural processes of this task. Therefore complementary neural correlates are imaged with fNIRS than in the EEG, even though some models have been probed which couple certain characteristics of these two modalities (Moosmann et al., 2003).

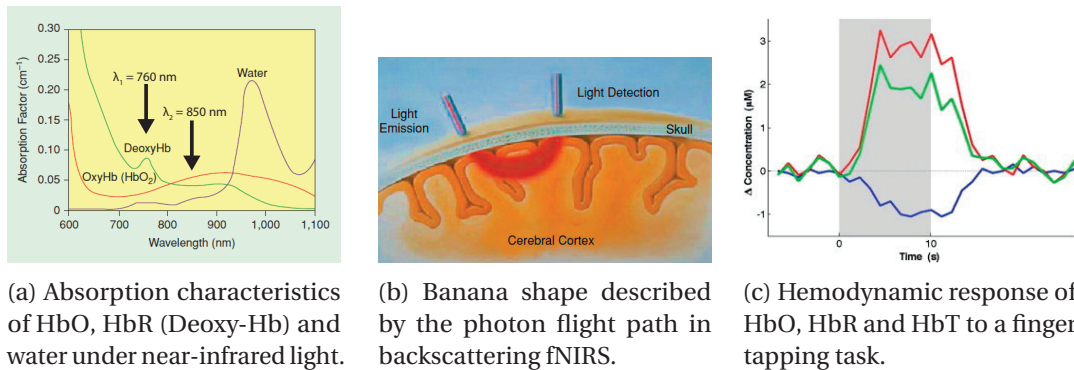


Figure 3.1 – Basics of functional near-infrared spectroscopy (fNIRS). (a) Absorption characteristics in the near-infrared range for HbO, HbR and water. Arrows mark the two different wavelengths of the light emitting diode (LED) lights sources of the device used in the experiment. Figure adapted from (Bunce et al., 2006). (b) *Banana Shape*: Flight path of the photons that are detected from a specific source-detector combination (in red). This constitutes one recording channel of the fNIRS setup. Figure adapted from (Bunce et al., 2006). (c) The average HbO (in red) and HbR (in blue) hemodynamic response to a finger tapping task. The HbT is depicted in green. We see the signal plateauing at around 10 seconds and falling after the end of the task, indicated by the vertical dashed line. Figure adapted from (Funane et al., 2014).

The possibility to image task-related changes in brain oxygenation brought attention to the use of fNIRS as a sensing modality for BCIs. Compared with the fMRI, which has proven its potential for BCIs but suffers from its cost and the necessity of the user lying motionlessly inside the constricted scanner tube, the fNIRS is affordable, small and lightweight, and is very robust even to motion artifacts, as long as the optodes (light sources and detectors) stay well attached to the scalp (Nicolas-Alonso and Gomez-Gil, 2012). Over the years, fNIRS has proven to be able to decode a wide range of brain-activity inducing tasks, starting from upper (Cui et al., 2010; Anwar et al., 2016) and lower limb movement, motor imagery (Coyle et al., 2007; Leff et al., 2011; Fazli et al., 2012), mental arithmetic (Power et al., 2010; Bauernfeind et al., 2011; Shin et al., 2016), music imagery (Power et al., 2010), visual stimuli (Plichta et al., 2007) and emotional responses (Tai and Chau, 2009). See Naseer and Hong (2015) for an extensive list of studies.

This naturally led to studies exploring the use of fNIRS for the use of brain-computer interaction.

The mainly investigated mental commands were motor imagery (Coyle et al., 2007; Leff et al., 2011; Fazli et al., 2012; Koo et al., 2015), mental arithmetic (Power et al., 2010; Bauernfeind et al., 2011; Shin et al., 2016) and even direct intent of choice (Luu and Chau, 2009). The majority of the published fNIRS BCI studies do not include any application, but are instead focused solely on the decoding performance. Few studies have shown applications for communication (Naito et al., 2007; Naseer et al., 2014), neurorehabilitation of the motor system (Rea et al., 2014; Chang et al., 2014) and cognitive neurorehabilitation (Arenth et al., 2007; Mihara et al., 2012; Mihara et al., 2013; Kober et al., 2014). Finally, fNIRS was also viewed as a good candidate to construct so-called passive BCIs. These are systems that detect the user's state of e.g. fatigue or emotion and can allow interaction on this (Zander and Kothe, 2011; Herff et al., 2014; Khan and Hong, 2015).

Given that fNIRS and EEG, while having both proven their worth for the construction of BCI systems, have quite complementary advantages and disadvantages, a combination of the two systems harbors the potential for improved performance. Compared to the EEG, fNIRS has a slightly higher spatial resolution which is not affected by volume conduction, but due to the slow hemodynamic response the temporal resolution is worse. This is further helped by the fact that the electrical potential measured with EEG and the optical imaging with fNIRS do not interact with each other. This means, differently from the combination fMRI and EEG, where the magnetic field artifacts of the fMRI have to be elaborately removed from the EEG signal, both modalities enjoy uninterrupted and undisturbed readings. Another important point is, that EEG electrodes and fNIRS optodes can both be integrated into one cap, allowing for a non-intrusive setup (Fazli et al., 2012). Modern devices with WIFI or Bluetooth communication even allow freely moving subjects (Piper et al., 2014).

Fazli et al. (2012) and Koo et al. (2015) demonstrated the beneficial fusion of EEG and fNIRS signals for decoding sensorimotor rhythms and Putze et al. (2014) reported improved decoding performances in audiovisual tasks. This motivated me to explore the possibility of a multimodal EEG-fNIRS system for a CVSA BCI. Apart from the aforementioned Putze et al. (2014), a few further studies used fNIRS to decode CVSA: Harasawa and Shioiri (2011) showed a stronger increase in the HbO signal coming from the left occipital cortex during a lateralized covert attention task. Moosmann et al. (2003) found a positive correlation between the strength of occipital α -oscillations and HbR. Since occipital α -power gets lateralized by CVSA, I assumed to see this lateralization also in the recorded HbR concentrations. Morioka et al. (2014) were the first (and until now only) group that published on a combined EEG-fNIRS BCI for CVSA. Instead of trying to decode the locus of attention directly from the fNIRS signal, they used the differences in the HbO concentrations between left and right side attention as priors for the corresponding EEG locations. This allowed them to improve the decoding performance significantly by 7.7%.

The principal objective of the study reported here was to develop and evaluate a prototype of a multimodal CVSA-based BCI that could find its use in the long term in the rehabilitation of unilateral spatial neglect (Figure 3.2). Taking into account all the points discussed above, the

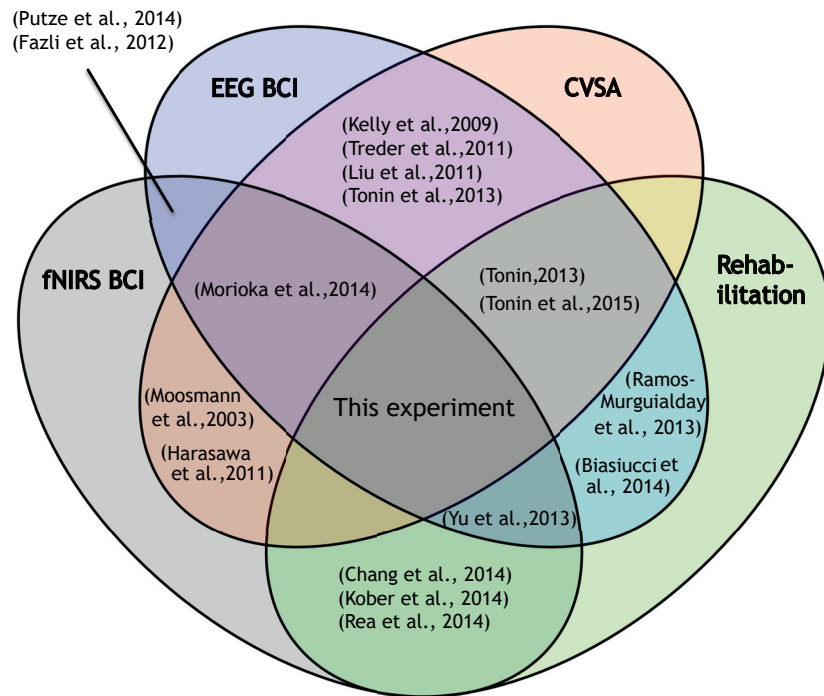


Figure 3.2 – Non-exhaustive overview of published literature covering the areas of the multimodal EEG-fNIRS CVSA BCI.

combination EEG and fNIRS looked like the most promising combination of brain-imaging modalities available, especially when having the portability of the BCI system in mind.

Therefore, I performed three small studies that aimed at quantifying the potential of combining fNIRS with EEG. The first study targeted the feasibility of decoding CVSA from the fNIRS and to compare its BCI performance to the one obtained with EEG. The second study aimed at simultaneously recording fNIRS and EEG and fusing the two sensing modalities for a real-time decoding of CVSA. Due to unexpected activation maps and non-satisfactory classification results from the fNIRS modality, I conducted a third experiment to determine if the used fNIRS system is able to pick up the hemodynamic response of a strong, passive stimulation of the visual cortex.

3.2.2 Materials and Methods

Participants

Taken all three experiments together we recorded data from 13 subjects. Five subjects, all male, aged 33 ± 6 years participated in the first experiment. Five more subjects, one female, four male, age 27.2 ± 2.56 years participated in the second experiment. Three subjects, all male, age 30.3 ± 0.95 years participated in the third experiment. All subjects reported normal

Chapter 3. Multimodal sensing

or corrected to normal vision. All subjects gave their informed consent for their participation in written form. The protocols used were covered by the ethical protocol N° PB_2017-00295, cleared by the ethical commissions of the cantons of Vaud and Geneva, Switzerland, and conformed with the Declaration of Helsinki (World Medical Association, 2013).

Material

fNIRS The fNIRS device used in all three experiments was a NIRScout (NIRx, Berlin, Germany) with a maximum of 16 sources and 24 detectors. This device uses LEDs to emit near-infrared light in the wavelengths of 760 and 850 nm. This specific fNIRS device is able to send out 60 light pulses per second, but since an activation of more than one light source at a time could lead to skewed light detection results, the 60 Hz base rate has to be divided by the number of sources used in the setup. Since we used 13 light sources in the setup (Figure 3.3a), our final sampling rate was around 4.6 Hz. The optode configuration was based on Morioka et al. (2014) and placed the light sources at the positions CPz, CP3, CP4, P1, P2, PPO5h, PPO6h, POz, O1, O2, PO9, Iz, PO10 and the detectors at positions CP1, CP2, CPP5h, CPP6h, Pz, P3, P4, PO3, PO4, PO7, PO8, Oz, I1, I2, according to the international 10-20 system (Figure 3.3a). This arrangement covered the parietooccipital cortex while ensuring an inter-optode distance of 2-4 cm between neighboring sources and detectors, which is in agreement with literature (Ferrari and Quaresima, 2012; Morioka et al., 2014).

To ensure proper coverage and penetration depth of the light paths, we simulated the sensitivity of this specific source-detector montage. The sensitivity of the fNIRS is defined as the magnitude of difference between a change in the actual hemoglobin levels in the imaged brain areas and the recorded signal. To compute the sensitivity index of the fNIRS-setup, Monte Carlo random walk photon scattering computations were performed and mapped to a Colin brain atlas standardized brain using the *AtlasViewer* plugin of the HOMER2 toolbox (Huppert et al., 2009).

We identified 44 usable channels, which were source-detector pairs with less than 5 cm distance on the scalp. For the third experiment, a slightly smaller optode setup has been used with sources at the positions (P1, P2, PPO5h, PPO6h, POz, O1, O2) and detectors at the positions (Pz, P3, P4, PO3, PO4, PO7, PO8, Oz). We decided on this to allow a more evenly distributed grid of optodes, keeping the inter-optode distance as close as possible to the recommended 3 cm while still using standard EEG positions. Additionally, this smaller montage allowed us to raise the recording frequency to 8.6 Hz, which was important since this experiment targeted to image the exact hemodynamic response (including on- and -offset timing) to large visual stimuli.

EEG In experiment one, where fNIRS and EEG were recorded in two different sessions, we registered electroencephalography (EEG) activity from the scalp using a g.Hlamp (g.tec, Graz, Austria) EEG-amplifier with 60 active AgCl-electrodes at standard 10-10 positions (see figure 3.3b for the placement). The sampling frequency was set at 512 Hz and a hardware bandpass

filter between 0.01 and 100 Hz was selected to remove slow drifts in the signal and unused high frequencies. In experiment two, which focused on simultaneous recording of fNIRS and EEG data, we complemented the fNIRS optode setup as described above with sixteen parietooccipital EEG channels at the positions CPP3h, CPP1h, CPP2h, CPP4h, P7, P5, P6, P8, PPO1h, PPO2h, POO1h, POO2h, POO9h, O11h, O12h, POO10h. The amplifier used for this was an actiCHamp (Brain Products, Gilching, Germany), because the same cap connectors could be used for the EEG electrodes and the fNIRS optodes. The sampling frequency was set to 500 Hz.

electrooculogram (EOG) In order to control for eye movements in the covert attention trials of experiments one and two, we additionally recorded the EOG with three channels at 512 Hz, also using the g.HIamp EEG amplifier. The EOG electrodes were placed at the left and right canthi of the eyes, the nasion and the corresponding ground electrode on the right mastoid.

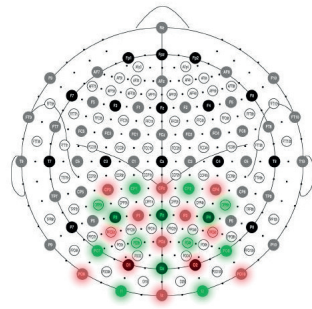
Experimental protocols

Subjects were in all cases seated in a dimly lit, quiet room, 50 cm in front of a 24 inch LCD monitor which contained all visual information throughout the protocol. See Figure 3.4 for a picture of the recording setup.

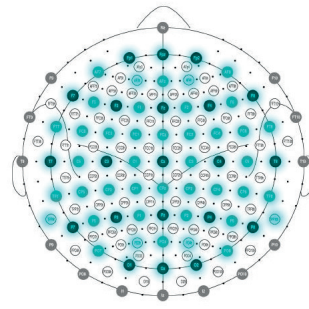
Experiment 1 Each participant was engaged in two recording sessions – one with EEG and one with fNIRS – with the exact same experimental protocol. Every session consisted of four runs of 20 trials, 10 left and 10 right. This yielded 40 trials per condition (left/right) and session.

The experimental protocol followed the general structure of CVSA protocols described in literature (Tonin et al., 2013; Horschig et al., 2015; Morioka et al., 2014). Each trial began with an acoustic beep and a 2 second fixation period, followed by a 100 ms central cue. The cue differed for the three classes: angled left arrow for left CVSA, angled right arrow for right CVSA, and a green dot for center fixation, with the varying cues presented in a pseudorandom order. The following attention period was randomly chosen between 6 and 10 seconds. The long duration compared to previous reports for EEG-BCI was chosen due to the hemodynamic response peaking only at around 6-7 seconds (Moosmann et al., 2003; Bunce et al., 2006; Morioka et al., 2014). Each attention period ended with the appearance of a yellow dot at the indicated location (target) and was followed by a button press (reaction time task) of the participant. Then a 10 second rest period ended the trial which should allow the hemodynamic response to settle back down (Moosmann et al., 2003; Bunce et al., 2006; Morioka et al., 2014). The temporal structure and screen display of the protocol is depicted visually in Figure 3.5.

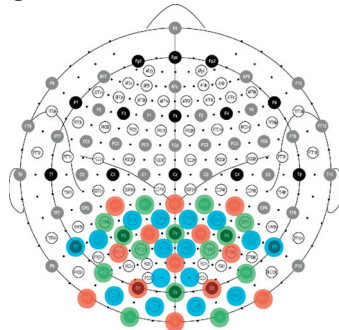
Experiment 2 Since in this experiment fNIRS was recorded simultaneously with EEG, each subject participated in one recording session only. Apart from this, nothing changed with respect to the visual protocol and timings from experiment one.



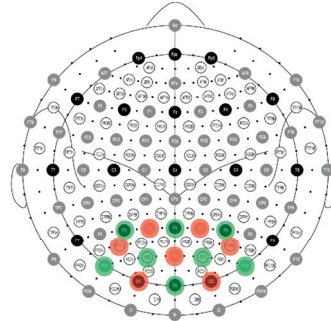
(a) fNIRS optode positions used in experiment one. Source positions are colored red and detector positions green.



(b) EEG electrode positions used in the first experiment are marked in blue.



(c) Joint fNIRS and EEG setup used in experiment two. fNIRS source and detector positions are marked red and green respectively, EEG channels are marked in blue.



(d) fNIRS optode positions used in experiment three. Source positions are marked red and detector positions green.

Figure 3.3 – Channel layout for the EEG and fNIRS for the studies one to three. In study one, fNIRS (3.3a) and EEG (3.3b) were recorded separately. In study two, a combined fNIRS and EEG setup was defined (3.3c). In the last study, a refined fNIRS-only setup was used (3.3d). Images adapted from Oostenveld and Praamstra (2001).

Experiment 3 Due to inconclusive results in experiments 1 and 2, we wanted to test our recording setup in a situation with strong activation of the visual cortex. Therefore fNIRS data was recorded while subjects were passively visually stimulated with a rotating checkerboard pinwheel (Ward et al., 2015; Zaidi et al., 2015). Two subsequent runs with ten trials each were recorded in one session, one with a pinwheel size of 80% of the screen height, the other one with 98% of the screen height. Each trial started with one second of fixation on a uniform gray background. Then a checkerboard pinwheel was displayed for five seconds, rotating at a speed of one full rotation every two seconds. The direction of rotation was randomly chosen and changed every 2 ± 0.5 seconds. This was then followed by 16 seconds of rest before the next trial started. A schematic screen display and temporal arrangement is displayed in Figure 3.6.

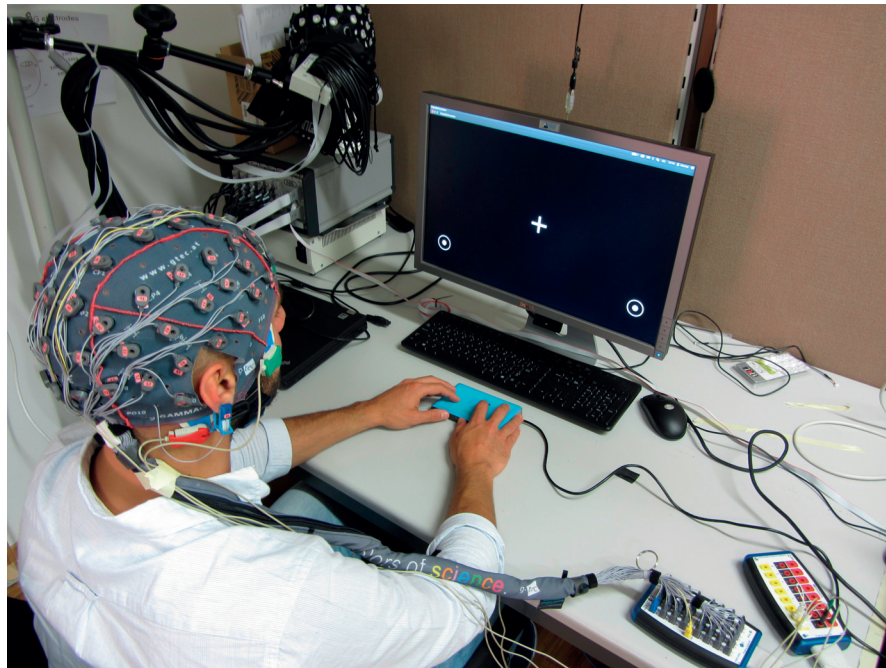


Figure 3.4 – Experimental setup and subject placement for the EEG-recording. The subject was shifting the covert attention to the target on the side indicated by the cue. After the target changed color, the subject was responding with a button press (blue pad). The fNIRS and joint fNIRS-EEG recordings were done in the same way.

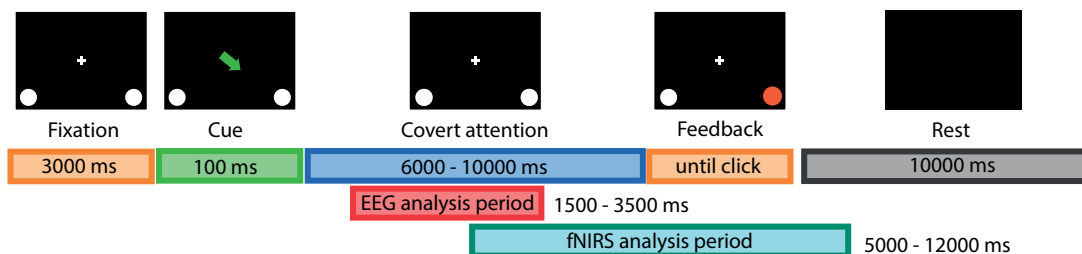


Figure 3.5 – Visual protocol with temporal scheme for CVSA task for experiments one and two. Please note that for better visibility, the symbols on the screen are displayed proportionally larger than in reality and the yellow target is printed in red. The time windows for analysis of the EEG and fNIRS signals are the ones used in experiment two.

Data processing

All data was analyzed with MATLAB R2017b (The MathWorks, Inc., Natick, Massachusetts, USA). The topographical plots were produced with the FieldTrip toolbox (Oostenveld et al., 2011). fNIRS data was extracted and preprocessed in the HOMER2 toolbox (Huppert et al., 2009).

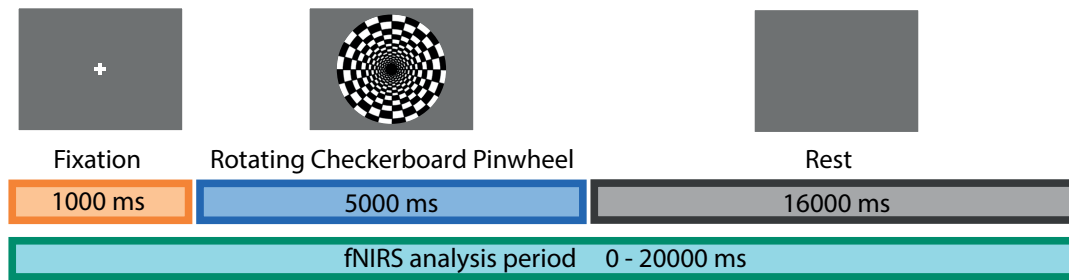


Figure 3.6 – Visual protocol with temporal scheme for the rotating checkerboard pinwheel of experiment three.

EOG From the raw EOG a horizontal signal was computed by taking the difference between the two channels at the canthi of the eyes. The vertical signal was then obtained by taking the difference between the channel at the nasion and the mean of the two horizontal electrodes. The resulting signal was then downsampled to 256 Hz and bandpass filtered between 0.01 and 7 Hz with a 4th order Butterworth filter (Schlögl et al., 2007). A trial-based automated heuristic blink detection algorithm was implemented to discriminate blinks from saccades and other EOG artifacts. To ensure covert attention towards the targets at the left and right screen side, only trials without horizontal eye movements were kept for further analysis. Trials without blinks, on the other hand, could not be fully avoided due to their long duration.

EEG EEG data was downsampled to 256 Hz, the offset removed (only necessary for the amplifier used in experiment two), and abnormally noisy channels detected and interpolated automatically. The EEG was then bandpass filtered between 1 and 45 Hz with a 4th order Butterworth filter. For every trial the log-power spectral density (PSD) was calculated on a 0.5 second sliding window with a 112 sample overlap, yielding a PSD time resolution of 16 Hz. As individual features, one-Hertz frequency bands spanning the α -oscillatory activity (8-14 Hz) were extracted from the PSDs.

In the first experiment, I modeled the classification approach of Tonin et al. (2012) with separate classifiers for subwindows in the trail. To this end, every epoch was split into 11 consecutive half-second windows from 0.5 to 6 seconds. The time frame 0.5-6 seconds was bounded by the length of the PSD-window on the lower end and the minimal trial duration on the upper end. On each half-second subwindow the coefficient of determination (R^2) was calculated for each channel on the mean α -band. The five most discriminant channels for each window were used to train an linear discriminant analysis (LDA)-classifier on the activity in each window. The posterior probabilities of all subwindow classifiers were finally concatenated in time to obtain a full vector of posterior probabilities over the whole 5.5-second epoch for every trial. Then the posterior probabilities were exponentially smoothed with equal priors and a smoothing parameter $\rho = 0.96$, yielding one accumulated posterior probability per trial which then was classified according to a 0.5 threshold. All reported results are the outcome of a 10-fold cross validation procedure, which was selected due to the limited

number of samples per class (max. 40 each).

In the second experiment, we based the selection of the classification time window on the results of the first experiment, which revealed the highest discriminant activity from 1.5-3.5 seconds after the trial onset (Figure 3.9). Furthermore, we replaced the classification subwindows of the previous approach with one longer time window spanning the whole 1.5-3.5 seconds, since comparisons showed not significant difference. Ultimately, the LDA classifier was replaced by a random forest (RF) classifier, which held promise of improved classification in BCI systems (Steyrl et al., 2013). The 10-fold cross-validation procedure was kept due to the same arguments.

fNIRS As a first step, all channels which spanned a difference of more than 40 mm and channels with insufficient light detection (too large amplification gain) were excluded. Then we converted the detected light intensity into attenuation values via the modified Beer-Lambert law (Kocsis et al., 2006):

$$A = \ln \frac{I_0}{I} = \mu_a \cdot DPF + G \quad (3.1)$$

where A is the attenuation, I_0 is the emitted light intensity, I is the detected light intensity, μ_a is the absorption coefficient of the tissue, DPF is the differential pathlength factor (mean photon diffuse scattering pathlength from source to detector) and G is the geometry-based scattering loss factor. Even though equation 3.1 is not fully accurate, the differential form approximates small attenuation changes well enough:

$$\Delta A = \ln \frac{I_1}{I_2} = \Delta \mu_a \cdot DPF \quad (3.2)$$

In this case, G is regarded constant and we look at the attenuation changes between the light intensities I_1 and I_2 measured at two close time points t_1 and t_2 . Given that attenuation is caused mainly by the presence of hemoglobin, we can split the observed attenuation change $\Delta \mu_a$ into a weighted sum of the changes in the chromophores of the oxygenized (c_{HbO}) and deoxygenized (c_{HbR}) — also called reduced — form of hemoglobin:

$$\Delta \mu_a = \kappa_{\text{HbO}} \Delta c_{\text{HbO}} + \kappa_{\text{HbR}} \Delta c_{\text{HbR}} \quad (3.3)$$

The two kappas denote the specific molar absorption coefficients. Measuring the attenuation change at two different wavelengths λ_1 and λ_2 allows for the computational extraction of the relative concentration changes of the two chromophores, as long as we also measure (or

estimate) the differential pathlength factor (DPF) for each wavelength:

$$\Delta c_{\text{HbO}} = \frac{\kappa_{\text{HbR}}^{\lambda_1} \frac{\Delta A^{\lambda_2}}{\text{DPF}^{\lambda_2}} - \kappa_{\text{HbR}}^{\lambda_2} \frac{\Delta A^{\lambda_1}}{\text{DPF}^{\lambda_1}}}{\kappa_{\text{HbR}}^{\lambda_1} \kappa_{\text{HbO}}^{\lambda_2} - \kappa_{\text{HbR}}^{\lambda_2} \kappa_{\text{HbO}}^{\lambda_1}} \quad (3.4)$$

$$\Delta c_{\text{HbR}} = \frac{\kappa_{\text{HbO}}^{\lambda_1} \frac{\Delta A^{\lambda_2}}{\text{DPF}^{\lambda_2}} - \kappa_{\text{HbO}}^{\lambda_2} \frac{\Delta A^{\lambda_1}}{\text{DPF}^{\lambda_1}}}{\kappa_{\text{HbO}}^{\lambda_1} \kappa_{\text{HbR}}^{\lambda_2} - \kappa_{\text{HbO}}^{\lambda_2} \kappa_{\text{HbR}}^{\lambda_1}} \quad (3.5)$$

This conversion from light attenuation to concentration changes was done using functions from the HOMER2 toolbox (Huppert et al., 2009). Further, the resulting signal, which now reflects the changes in oxygenated and reduced hemoglobin in the transilluminated tissue, was bandpass filtered between 0.01 and 0.5 Hz which emphasizes the range of the task-induced hemodynamic response by eliminating physiological influences to the signal, most importantly the pulse wave at a frequency around 0.8-1.2 Hz (Naseer and Hong, 2015).

In the first experiment, the HbO and HbR activity was extracted from 2 seconds before until 18 seconds after the cue and then the mean baseline activity (time before cue) removed from the rest of the trial. Analogous to the EEG-classification, also here a windowed approach was implemented, but due to the different time characteristics of the signal, the epoch and window sizes are different. Every 18-second epoch was split into 9 consecutive two-second windows. On each window the coefficient of determination (R^2) was calculated for each channel on the HbO and HbR value means of the two-second window. The five most discriminant features for each window were used to train an LDA-classifier on each window. The results for each test set of a 10-fold cross validation procedure (on each window) were concatenated in time to obtain a full vector of posterior probabilities over the whole 18-second epoch for every trial. Then the posterior probabilities were exponentially smoothed with equal priors and smoothing parameter $\rho = 0.96$, yielding one accumulated posterior probability per trial which then was classified using the 0.5 threshold.

In the second experiment we limited the window for the fNIRS features from 5-12 seconds after the cue, as this was the time with the highest activation found in experiment one. This also corresponds well to the known delay of the hemodynamic response compared to the EEG (Moosmann et al., 2003). Since the hemodynamic activity peaks in this window if the imaged cortical tissue is activated, we averaged the HbO and HbR activity across this window for each trial and channel and used it as input for the classifier. As in the case for the EEG, we employed the same RF classifier with 10-fold cross validation.

In the third experiment, we extracted HbO and HbR as explained above. After a manual removal of trials with signal artifacts, we plotted the resulting trials directly or after baselining to the average pre-cue value.

Classifier fusion Due to the simultaneous recording of EEG and fNIRS in experiment two, a fusion of the information was explored on the classifier level (see Dähne et al. (2015)). Fusion on the feature level was dismissed due to the problems arising with different sampling

frequencies and signal characteristics. For each trial, the two accumulated posterior probabilities were averaged and the resulting value classified with a threshold of 0.5:

$$P_t^{\text{fus}} = \frac{P_t^{\text{eeg}} + P_t^{\text{fnirs}}}{2} \quad (3.6)$$

P_t^{eeg} , P_t^{fnirs} and P_t^{fus} are the posterior probabilities of the EEG, fNIRS and joint classifier, respectively, and t denotes the time. In the first experiment, due to the non-simultaneous recordings of the EEG and fNIRS signals, we performed a pseudo-fusion, by pairing trials of the same condition from two different sessions.

3.2.3 Results

The addition of fNIRS for the CVSA BCI required to extend the trial durations to capture the slow hemodynamic response elicited by the attention shift. This raised the question if subjects could keep full attention to the task throughout the ten second long trials and how blinks, which would be hard to avoid, influence the EEG signal.

Experiment 1

Influence of trial length We observed that the reaction time to the target stimulus appearance is independent of the trial duration (Figure 3.7). This suggests that the CVSA can be sustained over the whole trial, which allows the use of fNIRS as complementary sensory modality.

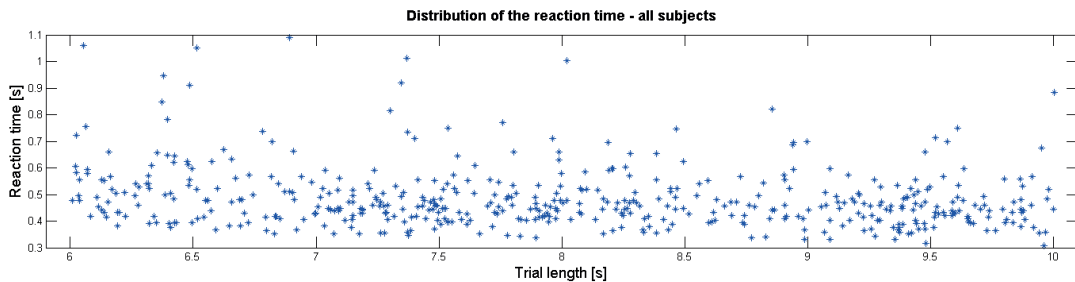


Figure 3.7 – Distribution of reaction time in dependence of the trial duration; pooled data from all subjects in experiment one.

Influence of blinks on occipital electrodes Eye movements produce large artifacts in the EEG recording due to their large dipole nature and additional electrical propagation across the head surface (Schlögl et al., 2007). The consideration of the dynamics of the fNIRS signal required a trial duration which is unusually long for EEG BCIs. Consequently an instruction to not blink during the whole duration of the attention phase (18 seconds) poses a large problem. The correlation between vertical/horizontal EOG and all EEG channels shows a large impact on frontal channels but is negligible in parietooccipital regions (Figure 3.8). Since EEG

correlates of CVSA have been predominantly found in these areas (Posner et al., 1987; Rihs et al., 2007), we conclude that blinking during the attention period has marginal influence on the EEG signal when constrained to the parietooccipital channels.

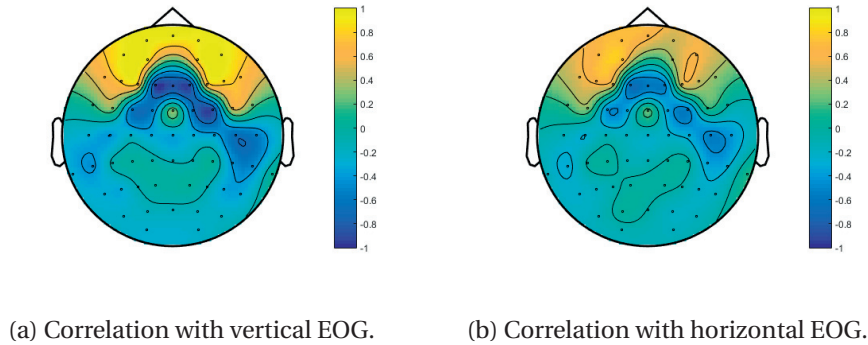


Figure 3.8 – Grand average of the correlation coefficient between the vertical and horizontal EOG with the EEG channels.

EEG: Grand Averages The grand average of the coefficient of determination for the left minus right trials difference in mean α -power is shown in Figure 3.9 in steps of half seconds. Note that the first half-second after the cue is omitted due to only partially filled windows for the PSD calculation. A decrease of α -band oscillations is visible in the contralateral (to the attention focus) parietooccipital cortex, which is especially pronounced from second 1.0 to 3.5 after the cue presentation. This reverses to a strong positive R^2 value in the left parietooccipital regions due to the subtraction of right-side trials. An interesting observation is the reappearance of a distinct lateralization at seconds 5.5-6.

EEG: Correlates of reaction time We split the trials of each subject at the individual median reaction time into a fast and slow group. We then averaged the R^2 -value of left-right difference in α -power over the whole trials and built the across-subject grand averages (Figure 3.10). We see a strong lateralization pattern in the case of the fast reaction times, which is far less pronounced in the case of the slow reaction times. This indicates that the behavioral measure correlates with the hemispheric lateralization in the α -band.

Sensitivity of fNIRS setup The sensitivity simulation using the AtlasViewer tool projected the sensitivity of the modeled light path to the local changes in blood oxygenation onto the cortical surface (Figure 3.11). The detection sensitivity is mapped on a log scale from 0 to -2, where red areas denote high and blue areas low sensitivity. We see that the whole occipital lobes are covered by the fNIRS illumination, where high sensitivity could be achieved on the top of the gyri. This shows that the chosen setup is, at least theoretically, suitable to image CVSA-related changes in blood oxygenation.

fNIRS: hemodynamic response patterns Figure 3.12 shows the grand average changes in HbO levels compared to baseline for the left and right side CVSA trials. We observed the highest

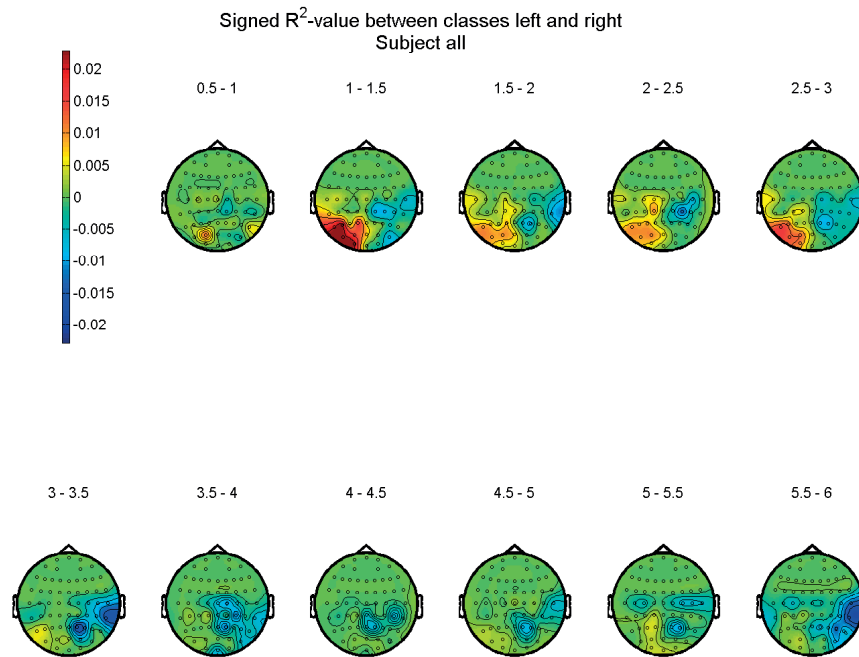


Figure 3.9 – Grand average of the R^2 -value of difference in α -band power for left-right classes across half-second time windows. Time point zero is the cue presentation. A strong lateralization pattern can be observed, especially in the seconds 1-3.5 of the trial.

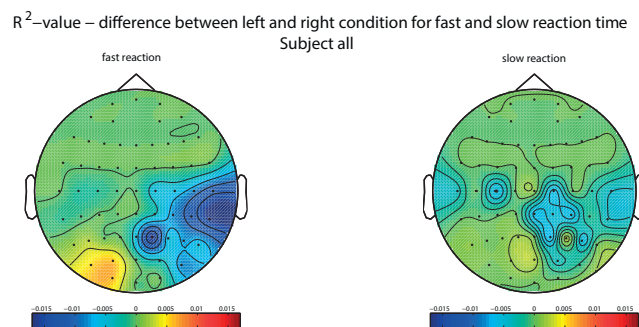


Figure 3.10 – Lateralization topoplots with respect to slow and fast reaction times. The across-subject grand average of the R^2 -value of difference in α -band power for left-right classes is shown for fast reaction time on the left, and the slow reaction time on the right. The color scales are kept equal for both plots for better comparison.

HbO elevations in the lateral parietal cortices, independent of the attended side. Further, the dorsal occipital cortex showed deactivation throughout the trials which is in line with the findings of Sylvester et al. (2007) and Morioka et al. (2014). Sylvester et al. (2007) assumed that the whole occipital cortex gets less activated in favor of the area corresponding to the locus of attention in the retinotopic cortical projection. Interestingly, we observed a side difference in

Sensitivity of the used fNIRS setup to changes in cortical blood flow

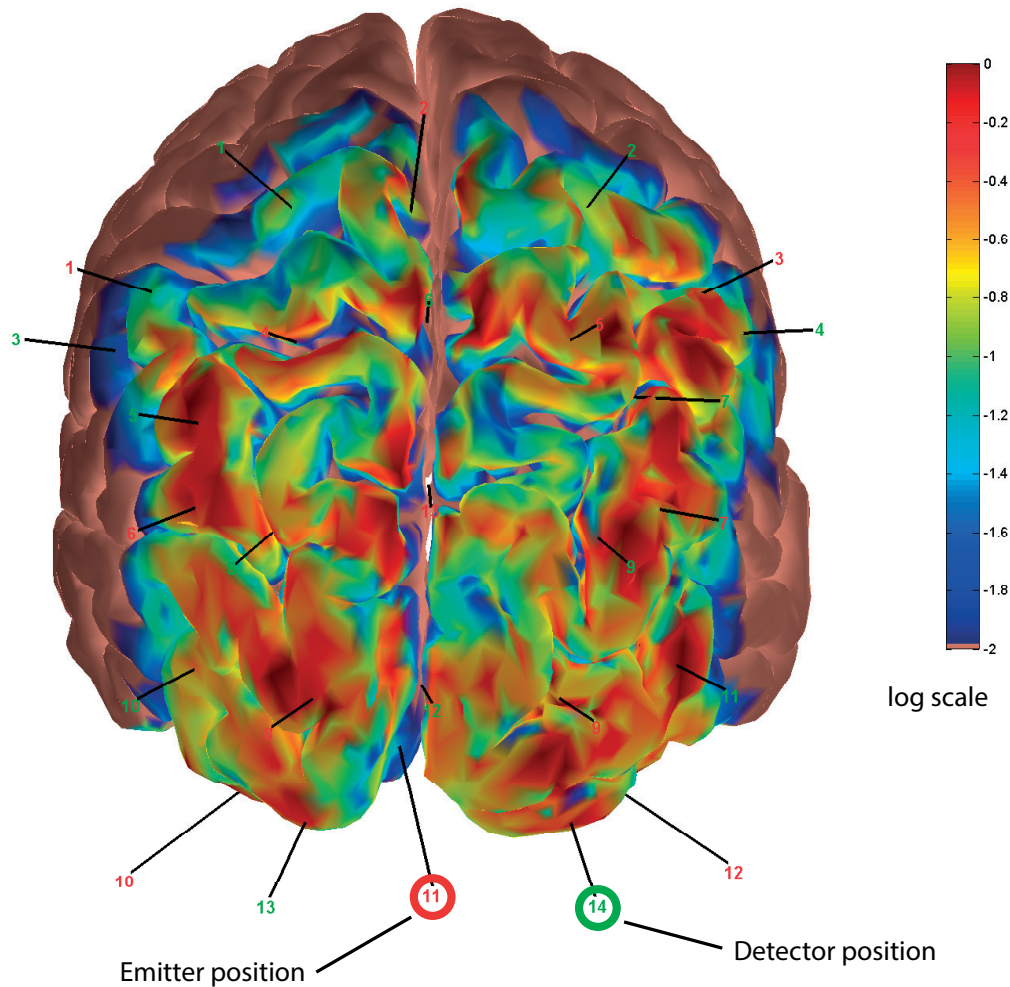


Figure 3.11 – Sensitivity map of the used fNIRS setup; occipital view. High values on the log-scale (red) indicate high sensitivity (no power loss) of the recording setup to cerebral blood flow changes, blue values denote low sensitivity (high power loss). Areas that cannot be imaged with the chosen fNIRS montage are painted in skin color. Thin black lines with small red (source) and green (detector) numbers indicate the projected optode positions.

the dorsooccipital HbO decrease between the left and the right attention condition (located between positions O9 and PO9, as well as O10 and PO10). This supports the asymmetrical inhibition theory of Battelli et al. (2009) which was hypothesized to play also a role in the activation of the visual cortex during covert attention (Harasawa and Shioiri, 2011).

When computing the R^2 -value of left-right difference in the HbO and the HbR signal we did not see clear lateralization patterns when compared with the EEG analysis (Figure 3.13). The

highest differences were observed for the HbR with a peak of discriminability in the right parietooccipital areas between 10 and 14 seconds after cue presentation. This discriminant period, which already falls into the resting period after the trial, could be explained by the observed delay of 8.7 ± 2.5 seconds of the HbR signal with respect to temporal peak in α -oscillations (Moosmann et al., 2003). Nevertheless is hard to explain the lack of a symmetrical difference.

Activation pattern compared to baseline – Subject all

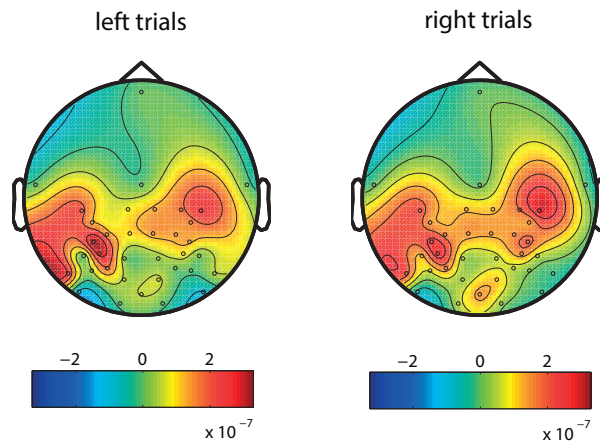


Figure 3.12 – Average changes of HbO throughout the trial compared to baseline. Elevated levels are observed mainly in the lateral parietal cortices whereas decreased levels are found in the dorsal parts of the occipital cortex. The activation patterns look very similar in both conditions, left and right CVSA.

Classification Table 3.1 reports the classification accuracies. For the EEG data alone, we obtained a mean classification accuracy of $63.3 \pm 10.6\%$, which is basically at the chance level of 63.2%, computed as the upper bound of the 95% confidence interval of a random binomial classifier. Individually, the EEG-derived decoder was above chance level for three out of five subjects.

For the fNIRS data, we built two independent classifiers for the HbO and HbR signals respectively. We observed that none of the two classifiers achieved general above-chance level accuracies with $62.8 \pm 9.2\%$ and $60.7 \pm 5.6\%$. Three, respectively two, out of five subjects performed better than chance.

Due to the slightly better classification performance of the classifier built with the HbO signals, we used it to perform the before-mentioned pseudo-fusion. We saw that the combined classifier increased the overall classification performance to $68.9 \pm 4.6\%$ with four out of five subjects above chance level. The mean increase of 5.6 ± 11.6 over the EEG-based classifier is not significant ($p = 0.34$) as is the 6.1 ± 8.26 increase over the HbO-based classifier ($p = 0.17$).

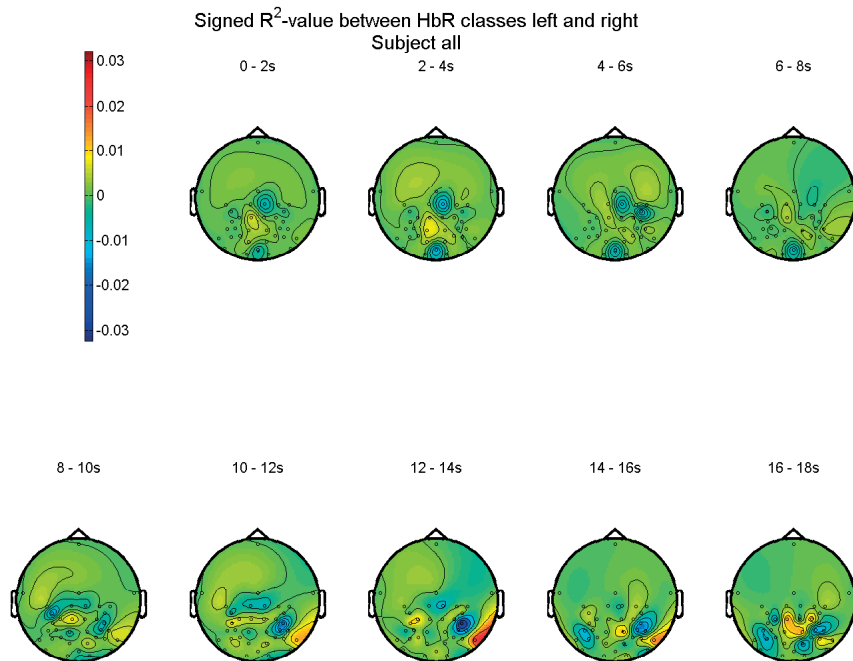


Figure 3.13 – Grand average time series of the R^2 -value of difference in HbR levels for left-right classes across two second time windows (timepoint 0 is the cue presentation). No obvious lateralization pattern is distinguishable. Peak discriminability is focused around two channels in the right side parietooccipital region between 10 and 14 seconds.

Experiment 2

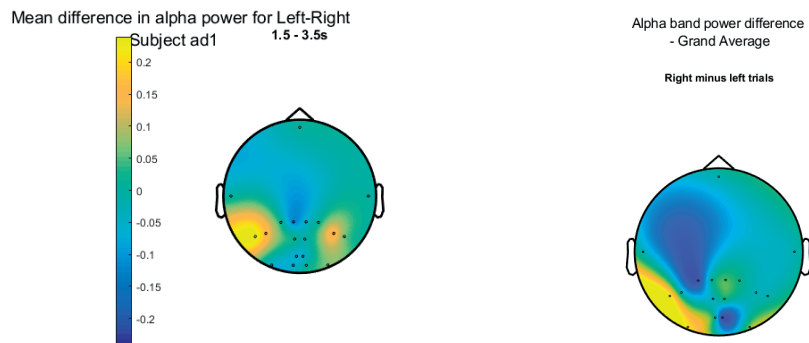
EEG The 16-channel EEG montage fitted in between the fNIRS optodes was covering the parietooccipital cortex only in parts. Although the EEG coverage did not allow to image all the electrodes that usually displaying strong lateralization in a full coverage, we could observe lateralization towards the lateral electrode positions. Figure 3.14a shows the topoplot of CVSA-induced lateralization in the best subject. In this subject, we were able to pick up lateralization towards the correct side, but without the expected α -band depression over the right parietooccipital areas (compare Figures 3.9 and 3.10). The grand average, as can be seen in Figure 3.14b, showed some expected lateralization at electrode location PO7 only.

fNIRS Figure 3.15 shows the topological plot of signed differences in the HbO signal between right and left side covert attention. We observed symmetric patterns of strong differences in the occipital cortex, where the lower and upper areas of the occipital lobes show an inverse in the side differences. Individual patterns are not similar between them (not shown) and the computed grand average is also very different than the one obtained in experiment one (Figure 3.12).

3.2. Functional near-infrared spectroscopy

Modality ↓	Subject →	s1	s2	s3	s4	s5	Average
EEG (α -band)		68.8%	57.5%	47.5%	70.3%	72.5%	63.3 \pm 10.6%
fNIRS (HbO)		65.0%	70.0%	71.3%	58.8%	48.8%	62.8 \pm 9.2%
fNIRS (HbR)		61.3%	65.0%	55.0%	67.3%	55.0%	60.7 \pm 5.6%
EEG (α -band) + fNIRS (HbO)		69.3%	72.6%	66.4%	73.7%	62.6%	68.9 \pm 4.6%

Table 3.1 – Classification accuracies of left vs. right trials for the five subjects using a series of LDA-classifiers on subsequent time windows and integration over the trial period. The last row is the result of the pseudo-fusion of the two classifiers, matching same-side trials from two different recordings.



(a) Left-Right lateralization of the best subject; 16-channel combined montage. (b) Grand average of the left-right lateralization; 16-channel combined montage.

Figure 3.14 – EEG lateralization topoplots for 16-channel montage. (a) Topoplot of the α -band lateralization of the best subject. Colors denote the mean difference in α -power between left and right side attention shifts. Black dots indicate the electrode positions (except the electrode positions at the front and side of the head, which have been added to correctly place the montage). (b) Grand average of right minus left side trials of all four subjects. Electrode position PO7 shows the expected enhanced α -power, but the overall distribution shows no clear lateralization pattern.

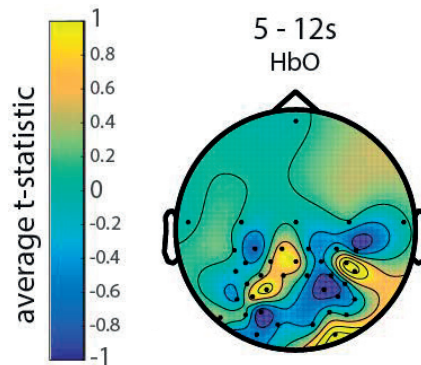


Figure 3.15 – Grand average difference in the HbO signal between right and left side CVSA trials. The colors signal the signed t-statistic (limited to ± 1) between the right and left class. Higher differences from zero indicate higher discriminability between the two classes. The black dots indicate optode positions of the fNIRS montage. The optodes on the coronal midline and frontally were added in the plot and set to zero to reduce interpolation artifacts.

Classification The classification of the EEG signals led to an average accuracy of $56.9 \pm 13.0\%$ which was on par with the HbO classification at $56.0 \pm 7.2\%$. The classification of the HbR signal yielded an average performance of $49.6 \pm 9.5\%$. All mean classification accuracies do not exceed the chance level, which holds also true for the fusion classifier encompassing the EEG and HbO signals. Classification results were significantly above the 95% chance level only for one with the EEG modality and one with the fNIRS. The achieved classification performance after classifier fusion on the trial level was $56.6 \pm 6.6\%$. See Table 3.2 for details of each participant.

Modality ↓	Subject →	s6	s7	s8	s9	Average
EEG (α -band)		76.3%	50.4%	51.8%	49.1%	$56.9 \pm 13.0\%$
fNIRS (HbO)		56.5%	54.6%	47.7%	65.3%	$56.0 \pm 7.2\%$
fNIRS (HbR)		38.9%	53.2%	45.4%	60.8%	$49.6 \pm 9.5\%$
EEG (α -band) + fNIRS (HbO)		64.2%	51.8%	50.4%	59.9%	$56.6 \pm 6.6\%$

Table 3.2 – Classification accuracies of left vs. right trials for the four subjects using an LDA-classifier on the activation means over the whole trial period. The last row is the result of the classifier fusion on the trial level.

3.2. Functional near-infrared spectroscopy

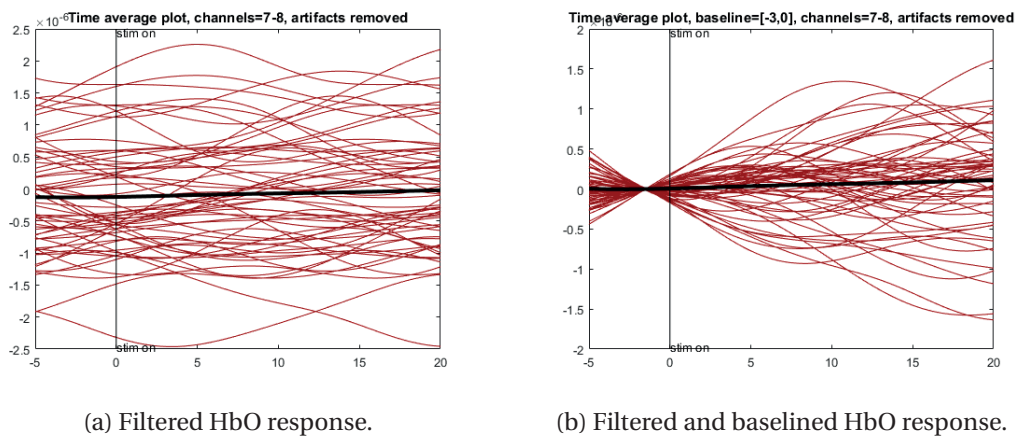


Figure 3.16 – Evoked response in the HbO changes as imaged with the fNIRS device. Data was pooled from all three subjects (= 30 trials) and the tick black line denotes the grand average over all trials. (a) shows the HbO response after filtering (removal of pulse artifacts). (b) depicts HbO response filtered and baselined to a five second pre-cue period.

Experiment 3

We expected a large, time-locked hemodynamic response to the onset of the rotating checkerboard pinwheel, as described for the flickering checkerboard in Ward et al. (2015). The expected activation would have been a rise in the oxygenated hemoglobin (HbO) every time the pinwheel came on. Figure 3.16a shows the pooled single-trial responses and the grand average response to the visual stimulation after filtering out the pulse-wave artifacts. We cannot distinguish the expected *inverted bathtub* shape reported for this kind of experiments (compare Ward et al. (2015)). Further, the grand average response is completely flat. Baselining the signal to the pre-cue interval had no effect on the grand average flat line either (Figure 3.16b). Without a doubt, since no activation can be measured with a very strong external stimulus, small internal variations of blood circulation as expected from shifting the internal locus of covert attention will not be visible when recording with this device.

3.2.4 Discussion

EEG We saw that even though α -power lateralization patterns manifest in the grand averages as shown in experiment one (as well as in the previous chapter about closed-loop feedback), a reduced set of EEG electrodes with sparse cover of the occipital cortex, as used in experiment two, drastically hampers the ability to classify CVSA from the EEG. The mean classification accuracy dropped by 6.2% and, more importantly, came to lie inside the 95% confidence interval for a random classifier. Therefore, we conclude that supplementing the EEG with another brain imaging modality should not come at the expense of reducing the electrode coverage.

fNIRS Our fNIRS results were inconclusive after experiments one and two since the two extracted grand averages did not look alike and also individual averages did not show comparable patterns. Morioka et al. (2014) showed large deactivation (decrease of HbO and increase of HbR) in far occipital fNIRS channels for a visual attention task as compared to rest. Further, Harasawa and Shioiri (2011) reported that increasing the attentional load leads to an asymmetry in the cortical oxygenation, with higher neuronal activity in the left hemisphere. Both reported clearly visible activation to visual attention and stimulation. Specifically, the results of experiment three were worrying, since no activation could be picked up for visual stimulation, while Ward et al. (2015) showcased such activation very well.

The fNIRS device used in our studies clearly picked up the pulsewave, and therefore indeed measured blood oxygenation changes. Nevertheless, the stimulus-evoked response was completely missing over the parieto-occipital cortex. A possible explanation is that the light never reached the cortex and thus only skin blood flow is measured. Scalp thickness is known to be larger in occipital areas while being thinner in frontal and temporal sites (Zhao et al., 2002; Okamoto et al., 2004). While this is a factor that needs to be taken into account, it still does not explain why other studies have indeed been able to image occipital oxygenation changes with a comparable optode montage.

One difference between our device and the devices used in these three studies are the light sources and the wavelengths used. While our device utilized LEDs emitting light at 760 and 850 nm, the other studies all used full laser setups with two or three different wavelengths. The longest wavelength was 830 nm for all devices, while the shorter wavelengths were 690, 780 and 805 nm. As Scholkmann et al. (2014) note, all used wavelength pairs (triplets) are theoretically able to image light absorption due to concentration changes in HbO and HbR. The fact that LEDs are known to produce less exact, and even skewed optical spectra was considered as a possible explanation since this usually leads to a slightly lower signal-to-noise ratio (Myllylä et al., 2015). Myllylä et al. (2015) experimentally found no large differences in the results of both systems when measuring the increase in HbR on the forehead while holding the breath. It must be noted though, that the observed HbR increase is no compelling proof for the equivalency of the systems on cortical imaging. After all, the skin-level blood flow alone would also exhibit the same drop in oxygen.

Classifier fusion The unexpected impasse with the fNIRS-side of the multimodal BCI also made the attempted classifier fusion an effort in vain. Interestingly, the increase in the pseudo-fusion of the data of experiment one could not be replicated in experiment two, where signals were simultaneously recorded. Therefore, it is likely that the fusion of two different sessions added more information than simply recording the two modalities alongside each other. Unfortunately, this is not viable for a closed-loop BCI system. Further, we have gathered evidence that classifier fusion on the trial level might have the potential to allow more people to reach classification performances above chance level, as compared to either modality alone.

3.3 Pupillometry

3.3.1 Introduction

Pupillometry denotes the measurement of pupil size changes due to external and internal influences. One of the oldest uses of the pupil responses to light was outcome prediction in comatose patients in critical medical care (Loewenfeld and Lowenstein, 1993). This evaluation was based on the natural constrictive response of the pupil to bright light. Muscles in the iris control the amount of light entering the eye by constricting (miosis) or dilating the pupil (mydriasis). This is called the pupillary light response (PLR) and is the main human mechanism for light exposure adjustment and to some extent also to protect the retina from too high light intensities (Ellis, 1981).

But the PLR is not the only system that can influence the pupil diameter. Especially in psychological and neuropsychological experiments pupillometry is used to uncover cognitive and emotional processing (Beatty, 1982; Laeng et al., 2012). Studies have linked unconstrictions of pupil size to stress, fear and arousal, while relaxation shows the opposite effect (Laeng et al., 2012). Importantly, changes in pupil size due to cognitive and emotional processing are not to be mixed with the PLR, since they do not share the same neural substrate (Beatty, 1982; Loewenfeld and Lowenstein, 1993; Aston-Jones and Cohen, 2005). Studies have found evidence of a strong top-down influence of the *Locus Coeruleus* — the noradrenergic hub in the brain — on the pupillary constriction and dilation (Aston-Jones and Cohen, 2005; Laeng et al., 2012). The PLR on the other hand, shows strong connections to the *Superior Colliculus* (Wang et al., 2012).

Binocular rivalry studies, where each eye is presented differently with either a bright or dark stimulus, showed that the PLR corresponded to the perceived stimulus, showing that the PLR is not merely related to the physical stimulus but is influenced by perception (Lowe and Ogle, 1966; Naber et al., 2011). Naber and Nakayama (2013) and Binda et al. (2013b) further demonstrated that pupil constriction to images containing the sun was higher as compared to isoluminant images without sun. This was corroborated by Laeng and Sulutvedt (2014) who showed that even imagining bright or dark scenes, whilst actually looking at an isoluminant gray background, influences the pupil size accordingly. Taken together, this clearly points out that the PLR is influenced by cognition.

Binda et al. (2013a) were the first to show that the PLR can be modulated by CVSA. Participants covertly attended to either sides of the screen which contained a bright or dark disk respectively. They observed that covertly attending to bright areas lead to a constriction while attending to dark areas to a dilation of the pupils. This fits well with the premotor theory of attention, where shifts in visuospatial attention are considered to precede overt saccades and covert attention is only a cognitive blocking of the actual saccade (Rizzolatti et al., 1987). In this school of thought it makes sense to adapt the pupil size already to the target region before making the saccade, so that the time delay of adaptation can be minimized.

Chapter 3. Multimodal sensing

Mathôt et al. (2013) extended the idea presented by Binda et al. (2013a) by integrating a split (dark-medium-light) background into a Posner cueing task, probing covert attention (Posner, 1980). They showed that a stronger PLR is linked to a stronger cueing effect, as probed by the orientation detection of a Gabor patch. The similarity between the presented visual protocol and standard protocols in EEG-based CVSA BCIs allows for simultaneous testing of the particular CVSA-related effects. Furthermore, the eye tracker does also not interfere with the EEG setup, making it a very interesting combination for a hybrid BCI.

The goal of our experiment was to explore single trial classification of the PLR in conjunction with simultaneous EEG measurements. We report on the average responses to the CVSA for both modalities, single trial classification results and the performance of a hybrid BCI by using trial-level classifier fusion.

3.3.2 Materials and Methods

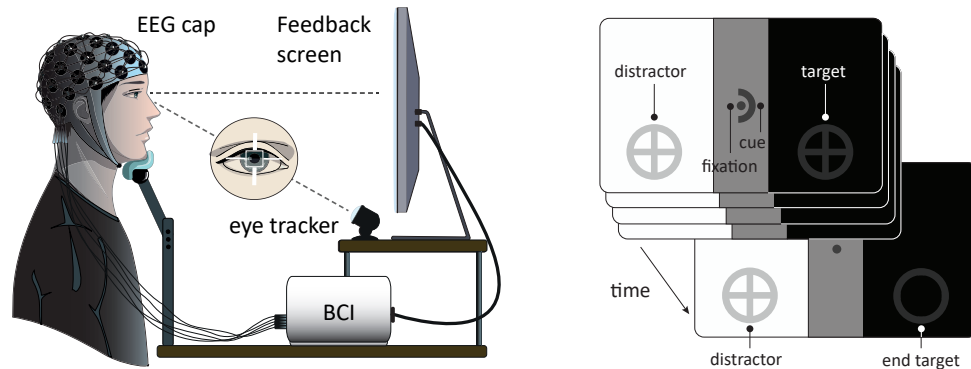
We reanalyzed the data from day one of the study described in Chapter 2, Section 2.2.

Visual display

The main addition to the setup described in Section 2.2 was the background coloring, which was necessary to achieve the luminance contrast between the left and right side target region. Inspired from Mathôt et al. (2013) we split the background into three parts: a central gray vertical band (width 7° visual angle) which contained the central fixation point and the symbolic spatial cues. The remaining side panels which housed the left and right side target placeholders were either black or white, to allow for maximum contrast between the two (Figure 3.17b). The order bright-medium-dark or dark-medium-bright changed pseudorandomly between trials and ensured that the same amount of left and right side CVSA trial targets were displayed on dark or bright background. Apart from the differently colored background, all visual elements are positioned exactly as described in Section 2.2.

Data analysis

The optical eye tracker used (EyeLink 1000 Plus, SR research, Ottawa, Canada) allowed for the automatic tracking of the pupil size in arbitrary units. This allows for the easy extraction of changes in the pupil size when subjects shifted their attention towards areas of higher or lower luminosity. The conversion of the EyeLink 1000 Edf files was done with the Edf2Mat Matlab Toolbox (<https://github.com/uzh/edf-converter>). All further processing was done in MATLAB Release 2017b (The MathWorks, Inc., Natick, Massachusetts, United States). We detrended the pupil size recordings with a moving median filter (60 s window; analog to a highpass filter) and reduced the jitter by applying another moving median filter (0.5 s window; analog to a lowpass filter).



(a) Experimental setup with the EEG cap and amplifier as well as the eye tracker and the feedback screen.

(b) Visual paradigm for the CVSA task throughout the trial on a tricolor background.

Figure 3.17 – Experimental setup and visual paradigm. (a) Experimental setup for the multimodal EEG + pupillometry BCI. The eye tracker was used to monitor gaze fixation in the center of the screen as well as the pupil diameter. (b) Visual display at the time of the cue presentation (foreground) and at the end of the sustained attention phase (background). Subjects were instructed to fixate the center point throughout the trial and shift their attention towards the cued side. At the end of each trial, when the inscribed cross disappeared at the cued (valid trial) or uncued side (invalid trial), subjects responded as fast as possible with a button press. The background was flipped randomly between trials. Note that the symbol sizes are not to scale.

For plotting grand average results encompassing multiple subjects, we baselined every trial by dividing by the average pupil size during the last 100 ms before the cue appearance (Mathôt et al., 2013). This allowed to control for different mean pupil sizes between subjects. To decode the attended side, we first identified the time window that best discriminated bright versus dark side. We then used an LDA classifier based on the average pupil size (relative to baseline) during this time window (0.9 - 1.1 seconds after the cue onset). Additionally, this time window was present in all trials, which lasted 1.1 - 5.1 seconds from the cue onset (1 - 5 s after cue offset). As for the EEG decoding, we used 10-fold cross validation to estimate classifier performance and repeated the classification procedure 100 times to get stable estimates. For details in the classification procedure, please refer to Section 2.2, where the analogous procedure is described for the EEG. The only difference is, that for the pupillometry, due to having only a single input feature, the feature selection step was unnecessary.

Classifier fusion

Following our hypothesis, we fused EEG and pupillometry. For this, we implemented a meta-classifier: we used the posterior probability output from both the EEG and pupillometry classifiers as two-dimensional input space which was fed to another LDA classifier. This resulted in an automatic weighting of the two features, thus naturally weighting each modality

as a function of its performance (Leeb et al., 2011; Dähne et al., 2015).

3.3.3 Results

Figure 3.18 shows the results of a one-person pilot study with a tricolor background in white, gray and black. We found significant difference between the left (bright) and right (dark) sided attention trials from 0.9 to 3.8 seconds after the cue. Pure center fixation led to a pupil size indistinguishable from the attention to the bright side.

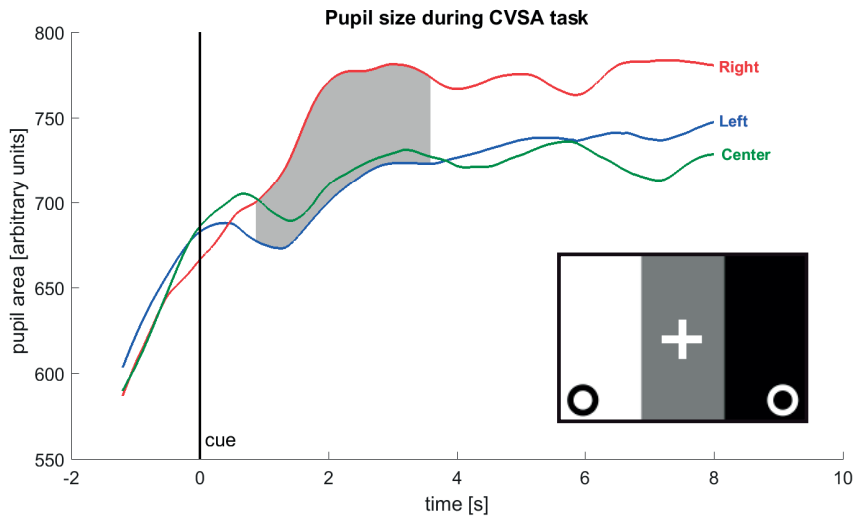


Figure 3.18 – Average pupil size for one pilot subject in response to CVSA to targets on white (left side) or black (right side) background or to center fixation (not baselined). The small inscribed image shows the screen background with one third white, gray and black. The gray area in between the right and left side attention means is statistically significant with $p < .05$, cluster corrected. The fixation cross and target circles are not to scale and in exact positions. The size of the gray screen center area was reduced for the full study in accordance with Mathôt et al. (2013).

For the full study we changed the white fixation cross to a gray fixation point with the same luminosity as the background, so that the fixation trials would not be influenced by the luminosity of the fixation cross. Further, we narrowed the gray vertical center band to 7° visual angle in order to confirm with Mathôt et al. (2013).

Figure 3.19 shows the average pupil size when CVSA was deployed towards the bright (yellow line) or dark (blue line) side. We observed a 2 - 4% difference in pupil size between conditions starting around 750 ms after the cue. This timing also corresponded to a hump present for both conditions and followed by a downwards slope until around 1.2 s. A similar temporal dynamic was observed for center fixation trials, albeit with a weaker downward slope. From this dip on, the pupil size continually grew until the trial ended, which is possibly due to movement preparation for the response task (Richer and Beatty, 1985). Note that the jagged means towards the end of the 5 s period are due to the fewer long trials. Based on these results

and the fact that the shorter trials lasted only one second, we defined the time window for classification as 0.9 – 1.1 s after the cue.

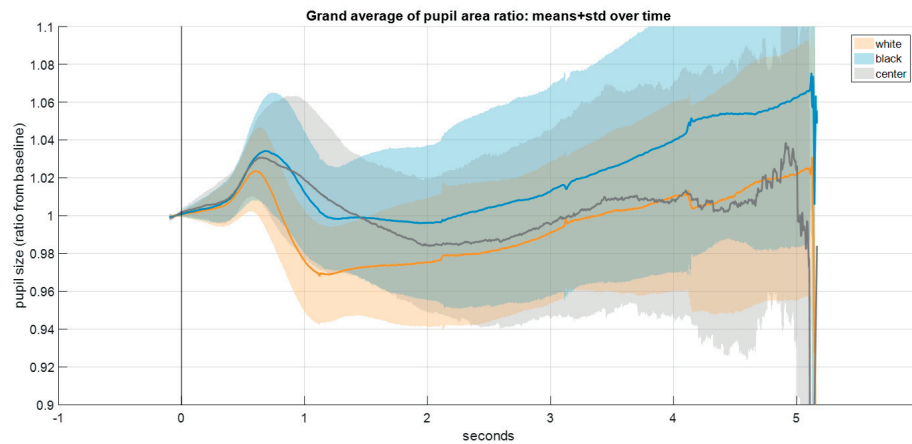
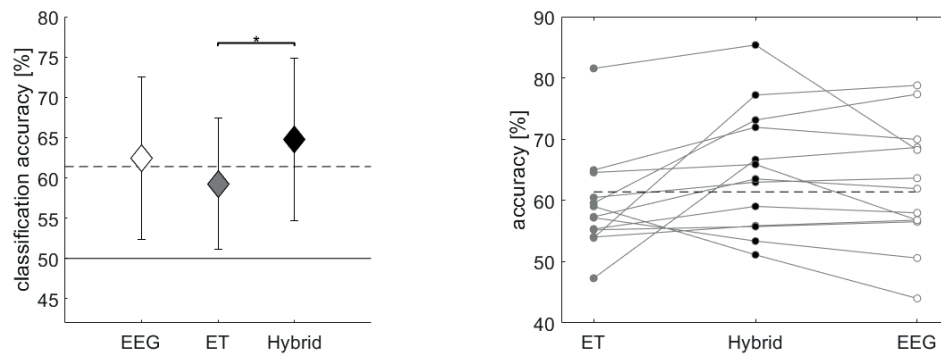


Figure 3.19 – Grand average of the baselined pupil size in response to CVSA to targets on white (yellow line) or black (blue line) background. The gray line depicts the average pupil size in central fixation. Shaded areas are the standard deviations of the subject means. The radical drop in the mean pupil size after five seconds is due to samples already capturing the appearance of the target (temporal jitter in the signal), at which moment the pupil unconstricts rapidly.



(a) Mean classification performance.

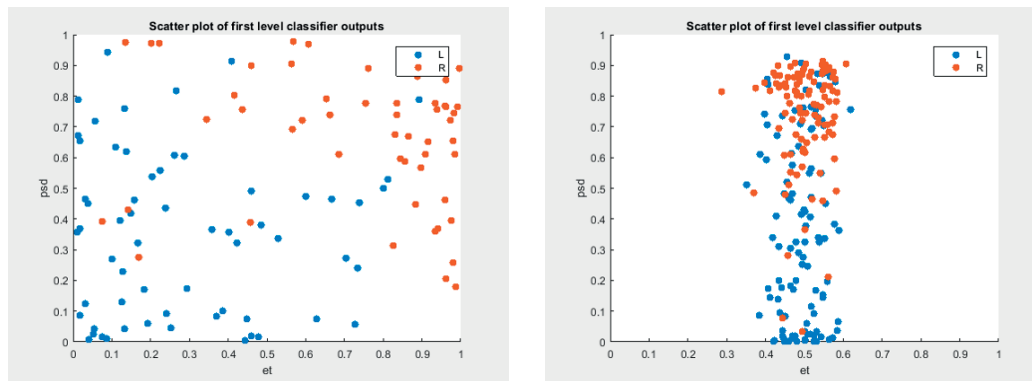
(b) Subject-wise classification performance.

Figure 3.20 – Unimodal and multimodal classification accuracies. (a) Mean classification performance across all subjects for the EEG alone (white), the eye tracker alone (gray) and the hybrid BCI (black). Standard deviations are denoted by the whiskers. The star indicates a p-value lower than .05 in a two-sided t-test. (b) Single-subject classification accuracies for both single modalities and the hybrid BCI (center). The horizontal dashed line denotes the two-class chance level in both figures.

EEG-based classification reached $62.05 \pm 9.75\%$ with a maximum of 78.70% (Figure 3.20). Combining the two modalities with the meta-classifier raised the average classification performance slightly to $63.78 \pm 10.22\%$ and lifted the highest accuracy to 85.24%. Overall, the modality

fusion improved the average pupillometry-based classification by $4.82 \pm 8.70\%$ ($p = .059$) and the EEG-based classification by $1.73 \pm 5.80\%$ ($p = .28$). The hybrid classifier led to an improved classification performance ($>1\%$) in 7 (EEG), respectively 10 (pupillometry) out of 13 subjects and allowed 8 subjects to perform above chance level (above the 95% confidence interval of a random classifier).

When plotting the feature distribution for the two classes (left and right side CVSA) for the metaclassifier we often encountered a case where one of the modalities did not add substantial additional information for the combined classification (Figure 3.21b). In one case — subject af1 — the obtained feature distribution for the meta-classifier was showing a near perfect diagonal dividing line between the two classes, indicating that both modalities contributed equally to the resulting classification (Figure 3.21a). Consequentially, this was also the subject that profited the most from the classifier fusion, increasing its performance by 3.76% compared to the pupillometry only case and by 17.03% compared to the EEG only case.



(a) Two-dimensional feature space for the classes left (L) and right (R) covert attention for the best subject.

(b) Two-dimensional feature space for the classes left (L) and right (R) covert attention for an average subject.

Figure 3.21 – Multimodal feature space of posterior probabilities. (a) The x-axis shows the posterior probabilities from the eye-tracker classifier and the y-axis the posterior probabilities of the EEG-derived PSDs. We see a very clear divide running diagonally between the two classes, which shows that each modality brings information to the meta-classifier for this subject. (b) For most subjects, one modality was performing way better than the other (here the pupillometry classifier is basically random). This results in little to no information gain by employing the meta-classifier.

3.3.4 Discussion

In this second section, we hypothesized that decoding pupillometric correlates of CVSA at the single trial level could improve EEG decoding. Firstly, our experiment corroborated the results of Mathôt et al. (2013) insofar as the pupil size is modulated by CVSA. Moreover, we attempted single trial classification of these pupillometric correlates of CVSA and could achieve significant decoding in 4 out of 14 subjects.

We used a similar paradigm to our previous EEG-only paradigms, implying that classification decisions had to be issued rapidly. This contrasts with a previous proof of concept study in which the authors let the stimuli luminance vary periodically, so that initially dark disks became bright, then dark again, etc. and vice versa for initially bright disks. This allowed them to keep the trial going until the decoder was sufficiently sure about the selected stimulus (initially white or black disk). This shows that implementing dynamical luminance changes can aid the pupil pattern matching for classification. Therefore it can be assumed that periodical smooth changes between white and black (offset for the two sides, see Mathôt et al. (2016)) could increase the classification performance. Further, a multimodal closed-loop system could be envisioned, that keeps trials running to accumulate evidence in both modalities until the meta-classifier is sure of the attended side.

Compared with the EEG, where the patterns introduced by CVSA are retionotopically dependent on the locus of attention, the pupillometry data needs to be complemented with the information of the luminance of the available targets. Not only does this make the hybrid BCI dependent on the screen presentation, but it also needs to be performed in settings with controlled lighting. This would prohibit the use of such a system outside or at places with changing light, but it would offer a viable option for an in-clinic rehabilitation device.

Finally, we have demonstrated that the combined classification of pupillometry and EEG data allowed one more person to achieve above-chance classification, which is a success in constructing such BCI systems to work with a large part of the population. We observed that the problematic cases for a successful classifier fusion were subjects with a modality that had random classification performance, mostly in the pupillometry case. Therefore we expect that if the inclusion of dynamic luminance changes into the visual protocol will lead to better pupillometry classification results, the metaclassification will result in an even higher gain over the unimodal classifiers.

In conclusion, if the controlled environment is not detrimental to the intended application of the BCI (e.g. rehabilitation) we recommend the fusion of pupillometry with the EEG to improve CVSA BCIs and we are positive that the discussed changes in the visual protocol will further enhance such systems.

3.4 Conclusion

In this chapter we implemented classifier fusion on the classifier level in two different ways: (i) by simply taking the mean of the posterior probabilities of the individual LDA classifiers and classifying it with a 0.5 threshold and (ii) by building an LDA meta-classifier on the posterior probabilities of the individual classifiers. While the first method gives the same weight to both modalities, the second method should, at least theoretically, weight both modalities according to their specific classification performance (Leeb et al., 2011).

The main observed outcome after combined classification for both hybrid BCIs (EEG + fNIRS

and EEG + pupillometry) was that mean classification accuracies did not significantly increase for simultaneous recordings. This stands in contrast to the paper of Fazli et al. (2012), who reported a significant 5% increase in classification accuracy for using an equivalent meta-classifier on EEG, HbO and HbR signals. Similarly, Putze et al. (2014) reported a significant performance increase through the application of a meta-classifier. Both studies used the combination EEG and fNIRS, which did not work in our experiments due to the inability of the fNIRS to pick up meaningful signals from the visual cortex. But also in combination with the pupillometry we could not observe a significant increase in classification accuracy. Even though for one third of the subjects the combination of EEG and pupillometry allowed for higher classification results than any of the unimodal classifiers, the mean increase of 1.8% is neither statistically nor in real life an important gain. This opens the question if the PLR and the occipital α -band oscillations represent two orthogonal information spaces, or if they are rather highly correlated. In the latter case, combining the information might not be as helpful compared to more orthogonal signals like the hemodynamic response.

Other data combination techniques, especially such of early fusion, i.e. fusion on the feature level, are described by Dähne et al. (2015) but to our knowledge have never been investigated in the classification framework of a multimodal BCI. This might be due to the very different temporal dynamics of the two signals, which do not allow for a straightforward integration into a joint feature space. Further, we are not aware of any studies exploring the potential benefits of long-term use of multimodal BCI systems. It is thinkable that the inclusion of another sensing modality can remedy somewhat the inter-session variability observed with EEG-based BCIs (Corsi-Cabrera et al., 2007). Future studies should be devoted to answering these open questions.

Finally, it also needs to be discussed if or when such hybrid BCIs are actually an improvement of the current situation. Taking the combination EEG + fNIRS as an example, we have two brain imaging modalities which operate on very different temporal scales. EEG is capable of depicting fast brain responses like evoked potentials, which happen on the timescale of a few hundred milliseconds, to comparatively slower endogenous brain commands via changes in the power in the μ or α band, which usually happens over seconds. When used for spelling on a screen, such types of BCIs can achieve information transfer rates (ITRs) of up to 105 bits/min for evoked signals (Chen et al., 2014) and up to 35 bits/min for oscillatory activity (Blankertz et al., 2007). Even if the overall decoding accuracy could be improved by 5-10% with the introduction of a second sensing modality like fNIRS, the ITR would suffer strongly from the sluggish temporal dynamics of the HbO and HbR signals. Since the ITR would be limited to the slower of the two modalities, the ITR would be comparable to the one from fNIRS-only BCIs, which lies between 1 and 4 bits/min (Zimmermann et al., 2013; Koo et al., 2015). Fortunately, when looking at the application of BCI technology in rehabilitation settings, the ITR is less important than the overall decoding accuracy. Studies showed that delayed feedback from fMRI or fNIRS does not hinder the learning process in neurofeedback and closed-loop BCI setups (Andersson et al., 2013b; Robineau et al., 2014; Kober et al., 2014).

In conclusion, we found that the fusion of two orthogonal sensing modalities has the theoretical possibility to improve decoding performance of a BCI, but it does not work for everybody and in every setting. Hybrid BCIs come with their own set of disadvantages like longer setup time, an ITR limited by the slower modality and the possibility that the joint classifier performs worse than the better of the two simple classifiers — especially for subjects with a large difference between these two. It is possible to put the work in to resolve many of these problems, but it comes at the cost of a very complex classification procedure which might lead to a *blackbox* system with hard-to-interpret results.

4 Brain stimulation

In Chapter 2 of the present thesis, we investigated how lateralization in parieto-occipital α -band power can be used as a control signal for a brain-computer interface (BCI) and attempted to improve the decoding using real-time feedback. However, these lateralization shifts are observed only in part of the population. Since many of the people with no lateralization also have a naturally low power to their α -oscillations, it is conceivable that the lateralization is happening during covert visuospatial attention (CVSA), but is not observable due to the low signal-to-noise ratio. On the other hand, previous works have shown that α -band power can be enhanced by applying transcranial alternating current stimulation (tACS). We thus hypothesized that tACS can boost the individual α -band power and subsequently enhance the lateralization elicited by CVSA, which, in turn, would also increase the BCI decoding accuracy. We enrolled six subjects in a crossover pilot study and asked them to perform a CVSA task before and after 20 minutes of occipital high definition tACS (HD-tACS) at their individual peak α -frequency. As a control condition, we repeated the procedure on a different day but stimulating at a β -frequency. We predicted that the α -stimulation condition would lead to enhanced baseline levels of α -power and would result in a clearer lateralization pattern as compared to the β -frequency stimulation. Contrary to our expectations, we did not observe any consistent differences between the stimulation conditions, neither in the baseline α -power nor the lateralization pattern. Also classification and behavioral results did not diverge significantly. An additional test contrasting α -stimulation with rest (i.e. no stimulation) likewise did not reveal any consistent differences between the groups. Although our pilot data revealed a mild overall increase in alpha power, it did not translate in behavioral changes nor in differences in task-related electrophysiological activity. Moreover, additional tests revealed inconsistent stimulation effects on alpha power.

4.1 Introduction

As shown in previous chapters, CVSA BCI hinges greatly on the achieved decoding accuracy, which indicates if users feel in control, and if so, how efficient the communication runs. Decoders that are not better than random not only defy the purpose of the BCI as a tool to interact or rehabilitate, but also discourage people from any further use (Huggins et al., 2011). Electroencephalography (EEG)-based decoding of left and right sided CVSA is based on the lateralization of occipital α -oscillations; α -power decreases contralateral to the attended side and increases in the ipsilateral hemisphere. Rihs et al. (2007) made the interesting observation that subjects which achieved substantial α -lateralization during a CVSA task also showed high α -power levels during baseline, and that the baseline levels are very subject-dependent. Conversely, participants with low baseline α -activity showed little to no lateralization during CVSA. This raises the question of whether enhancing the occipital α -power would by itself also enhance the lateralization observed during CVSA, which, in turn, would allow for higher classification performances.

We decided to test this hypothesis by utilizing tACS — a noninvasive brain stimulation technique, shown to be able to enhance occipital α -rhythms (Zaehle et al., 2010; Helfrich et al., 2014b; Vossen et al., 2015; Kasten et al., 2016). A large part of the literature focuses on the stimulation at the individual alpha frequency (IAF), which is defined as the frequency with the highest peak in the α -band from 8-14 Hz. It is believed that the IAF is the intrinsic frequency of the individual α -rhythm network, and so, stimulation in this frequency should have the largest effect, since the neural networks are already tuned to it (Thut et al., 2011). A power increase after tACS in the individual α -band is has been shown with a set of patch electrodes over locations Cz and Oz in the international 10-10 system (Neuling et al., 2013; Helfrich et al., 2014b; Kasten et al., 2016; Ruhnau et al., 2016), as well as in a bilateral arrangement over locations PO9 and PO10 (Zaehle et al., 2010; Thut, 2014; Vossen et al., 2015; Saturnino et al., 2017). Further, Helfrich et al. (2014a) also showed similar results with a high definition (HD)-tACS setup with smaller electrodes in a 4-1 configuration over each occipital hemisphere. The elevations in α -power achieved through tACS in these studies ranged from an averaged 14% (Zaehle et al., 2010) to 80% increase (Kasten et al., 2016) of the power of the IAF compared with the pre-stimulus levels.

Therefore, we tested our hypothesis on pilot data in a double-blind crossover study, where participants would engage in an CVSA task before and after tACS, either in the IAF or a control frequency in the β -band range. We report on the influence of α and β -tACS on the power in the individual alpha band (IAB), the induced changes in electrophysiology during CVSA and any difference in behavioral proxies to CVSA.

4.2 Materials and Methods

4.2.1 Participants

For this crossover pilot study we enrolled six participants with a mean age of 29.2 ± 4.9 years. All subjects reported normal or corrected-to-normal vision. All participants were right handed and 4 and 2 participants displayed right and left ocular dominance respectively. The study confirmed with the requirements of the Declaration of Helsinki (World Medical Association, 2013) and was covered under the ethical protocol N° PB_2017-00295 of the ethical commissions of the cantons of Vaud and Geneva, Switzerland. All participants gave their written informed consent.

4.2.2 Experimental setup

During the CVSA task subjects sat in a dark, shielded room, with their head in a headrest that was fixed 50 cm in front of a 24" LCD monitor. The EEG was recorded with an active 64 channel HIamp EEG amplifier (g.tec, Schiedlberg, Austria) at 512 Hz and referenced to the linked ear potential. The electrodes were positioned according to the international 10-20 system with the ground electrode on FCz. Eye movements and blinks were monitored with an eyeLink 1000 optical eye tracker (ET) (SR research, Ottawa, Canada) at 500 Hz, calibrated on the dominant eye (Holmqvist et al., 2011). tACS was administered via five HD electrodes of a neuroConn DC-stimulator plus (neuroCare Group GmbH, Munich, Germany, see Section 4.2.3 for details). While tACS was administered, subjects sat in dim light (as compared to darkness) to relieve the eyes and prevent excessive sleepiness. The recording setup is displayed visually in Figure 4.1. All software for recording, real-time eye-tracker processing and the on-screen display was written inhouse.

4.2.3 Session structure

Each participant was recorded on two different days, with both recordings being one week apart. Half of the participants started with tACS at the IAF and received β -frequency stimulation on the second recording day. The other half of the subjects started with β -frequency stimulation, followed by tACS at the IAF on the second day (see Section 4.2.3 for more details). Each recording session included the following steps:

- A) Resting state with eyes open / eyes closed (1 minutes each)
- B) Covert attention task left / right with response times (15 minutes)
- A) Resting state with eyes open / eyes closed (1 minutes each)
- C) tACS while doing an attention keeping task (20 minutes)
- A) Resting state with eyes open / eyes closed (1 minutes each)
- B) Covert attention task left / right with response times (15 minutes)

Chapter 4. Brain stimulation

A) Resting state with eyes open / eyes closed (1 minutes each)

Figure 4.1b gives a graphical overview of the session structure. Together with the EEG and tACS setup and intermittent breaks the total experiment duration per day was around 120 - 140 minutes, depending on the amount of aborted and restarted trials due to eye movements and blinks (see Section 4.2.3).

Resting state

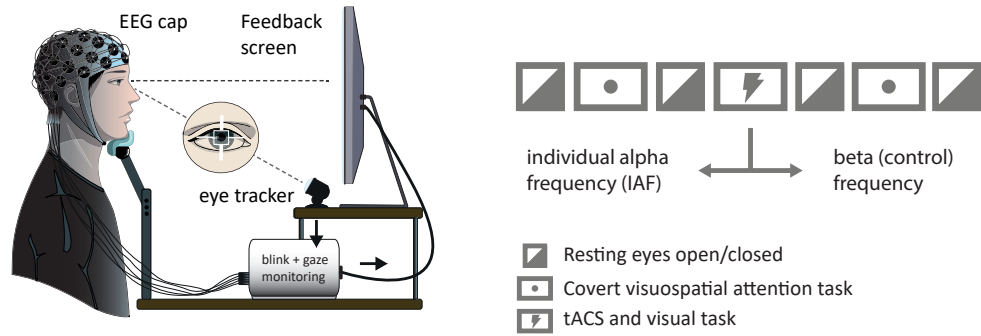
We recorded one minute of eyes open and eyes closed resting state EEG activity at four different points in one session: before and after the pre-stimulation CVSA task as well as before and after the post-stimulation CVSA task (Figure 4.1b). This was done on the one hand to determine the IAF which was needed to set the correct tACS frequency, and on the other hand to monitor the changes in the power of the IAB ($= IAF \pm 2$ Hz) throughout the recording session (see Section 4.2.5).

CVSA task

In the pre- and post-stimulation CVSA tasks, subjects were instructed to always maintain eye gaze on a central fixation dot while shifting the covert attention to one of two (left and right) target placeholders as instructed by a central cue. The background color was chosen a medium gray to relieve strain on the eyes in the dark experimental room. To encourage the attention shifts via increased target detection difficulty, all onscreen symbols were of low contrast to the background.

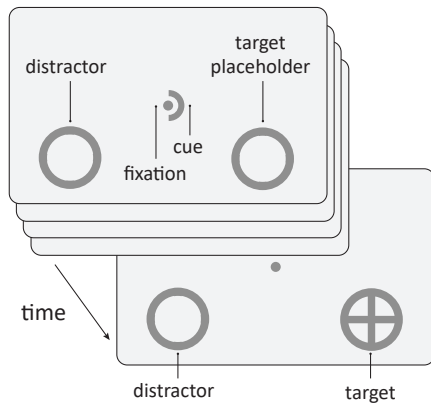
Each trial started with the appearance of the central fixation point (0.5° visual angle) for 1-1.5 s, followed by a 100 ms presentation of a central cue in the form of a half-circle (line width 0.1° , radius 2°) pointing towards the side to attend. Subjects then shifted their covert attention towards the indicated target placeholder (circles with a diameter of radius 2° and a line width of 0.2° , centered at 12° extremity from the center point and at a downward angle of 30° from the horizontal center line, see Figure 4.1c. After 2-4 s in this so-called attention period, a visual target stimulus appeared in the form of an X-shape (line width 0.1°) inscribed in the target placeholder circle. As the subjects detected the target stimulus, they were requested to respond as fast as possible with a button press using their right index finger. Then subjects could blink and relax during an intertrial time of 2-3 s while the current trial number and last reaction time were shown on the screen to inform participants of the experimental progress and their performance. The recorded reaction times were used as a behavioral measure for CVSA (Posner, 1980).

To ensure that subjects did not overtly attend the target regions, and that the recorded EEG-signal is free from blink artifacts, we implemented a real-time monitoring of the gaze position and blinks. Whenever subjects blinked or deviated their gaze from the central fixation for more

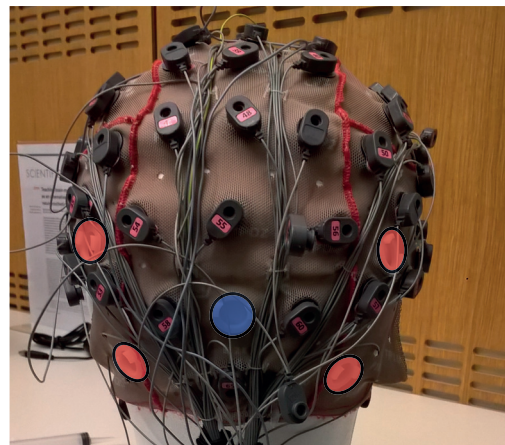


(a) Participant and device setup for the CVSA task.

(b) Run sequence for the two recording days.



(c) Visual protocol presentation during CVSA task.



(d) EEG cap with stimulation positions.

Figure 4.1 – Experimental design, visual protocol, stimulation setup. (a) Experimental setup for the CVSA task. Blinks and gaze deviation from the screen fixation point were detected in real time and resulted in the abortion and restart of the affected trial. (b) Graphic representation of the run order in one session. Each recording session had four eyes open/closed resting state recordings (1 minute each) at the beginning and the end of the experiment, as well as directly before and after stimulation. 120 trials of left and right CVSA were done pre and post stimulation to assess the influence of the stimulation on the CVSA-induced brain patterns. Subjects were randomly assigned to start either with tACS in the α - or β -frequency. (c) Visual display at the time of the cue presentation (foreground) and at the end of the sustained attention phase (background). Subjects were instructed to fixate the center point throughout the trial and shift their attention towards the cued side. At the end of each trial, when the inscribed cross disappeared at the cued (valid trial) or uncued side (invalid trial), subjects responded as fast as possible with a button press. Note that the symbol sizes are not to scale. (d) Sketch of the EEG-cap with the EEG electrodes in gray and the added stimulation electrodes in blue and red. The color coding of the stimulation electrodes does not reflect polarity since alternating current stimulation was applied, but the center electrode (in blue) received the full stimulation current while current was split in four to feed the surrounding electrodes (in red).

Chapter 4. Brain stimulation

than 2° the trial was automatically aborted and restarted after the intertrial waiting period (Roijsdijk et al., 2013; Horschig et al., 2015).

Each CVSA run comprised 120 trials, 60 left and 60 right. In 80% of the time, the target appeared at the indicated side (valid cues) whereas in 20% of the time the target appeared on the opposite side (invalid cues). The inclusion of catch trials allowed to compute the validity effect (VE) as a behavioral measure of CVSA (Schneider et al., 2018).

Transcranial alternating current stimulation

We administered 20 minutes of tACS at either their IAF or a control frequency in a double-blinded crossover design. To preserve as many EEG recording positions possible for the CVSA decoding, we decided against the widely used 5 × 7 cm patch electrodes and for an HD tACS montage which could be fitted between the EEG electrodes. Unfortunately, preliminary tests showed that subjects could easily distinguish between stimulation and sham (i.e. no stimulation) throughout the whole session. This forced us to choose a control frequency instead, which we set at a beta frequency (2.3 × IAF, to avoid harmonics of the IAF), since θ , α and γ -frequencies have been shown modulate attention-related processes (Laczó et al., 2012; Brignani et al., 2013; Clayton et al., 2015).

For the HD tACS we used five circular HD stimulation electrodes with an electrode surface of approximately 113 mm² (disk electrodes with 6 mm radius) in a 4-1 montage. The center electrode was positioned on Oz in the international 10-10 system, while the four surrounding electrodes were placed on the positions PPO7h, PPO8h, PO9 and PO10 (Figure 4.1d). Based on published literature we decided to stimulate at 1000 μ A peak-to-peak (Zaehle et al., 2010; Helfrich et al., 2014b; Helfrich et al., 2014a; Fekete et al., 2018). A neuroConn Equalizer Box (neuroCare Group GmbH, Munich, Germany) supplied the center electrode with the full current 1000 μ A while splitting the induced current for the surrounding electrodes by four (250 μ A each). The electrode impedance was tried to be kept below 10 k Ω , but for two subjects we could not achieve values below 20 k Ω . At the beginning and the end of the stimulation we ramped the current up and down for 3 seconds to dampen the skin sensations induced by the stimulation on- and offset. As in Helfrich et al. (2014a) and in Fekete et al. (2018), no subject reported phosphenes with the chosen stimulation intensity. To compare our HD montage with other setups reported in literature, we modeled the resulting electric fields using the *roast* toolbox (Figure 4.9; Huang et al., 2018).

During the stimulation we employed a visual attention task modeled after (Kasten et al., 2016), which was developed to keep subjects awake and their eyes open. Subjects were required to keep their head in the chinrest and focus to the center of the screen, which presented a gray ring of 2° diameter with four white markings at 3, 6, 9 and 12 o' clock positions. They had to respond with a button press whenever this circle rotated (rotation duration 250 ms). This happened randomly 40 times during the 20 minutes stimulation run, leading to one rotation per 30 s on average.

4.2.4 Questionnaire

To document stimulation-related subjective effects, we included a questionnaire based on the one proposed in (Brunoni et al., 2011). Further, we also included fatigue ratings at the beginning and end of the session, since fatigue is known to increase α -power levels and could therefore be a contributing factor to α -increases from pre to post stimulation (Boksem et al., 2005).

4.2.5 Data processing

Data processing and analysis was done in MATLAB Release 2017b (The MathWorks, Inc., Natick, Massachusetts, United States). The topographical plots were produced with the EEGlab toolbox (Delorme and Makeig, 2004). The conversion of the EyeLink 1000 Edf files was done with the Edf2Mat Matlab Toolbox (<https://github.com/uzh/edf-converter>).

EEG preprocessing

We inspected the EEG signals visually and replaced channels with abnormal signature ($N = 2.48 \pm 1.26$) by an interpolation of the channels in a 50 mm radius. Trials with visible artifacts as well as trials with button presses outside of a one second window after the target onset were excluded from further processing. This resulted in an average exclusion rate of $2.6 \pm 5.0\%$. We employed a fast Fourier transformation with one second long Hanning windows and 62.5 s shift (16 Hz resolution) to obtain the power spectral density (PSD) values in single-Hertz bands.

Individual alpha frequency

The spectral decomposition of an EEG recording of a person at rest reveals a peak (frequency dominance) in the α -band from 8 - 14 Hz, which is the definition of the individual alpha frequency (IAF) (Klimesch, 1999; Helfrich et al., 2014b). This α -peak is most prominent over occipital areas, where α -band oscillations are believed to be the main contributing rhythm to coordinate visual attention (Sauseng et al., 2005; Rihs et al., 2007; Foxe and Snyder, 2011). Therefore, the IAF is a logical target for tACS for endogenous oscillation patterns (Rosanova et al., 2009; Vossen et al., 2015).

We computed the IAF within a 60 second eyes open resting period at the beginning of the experiment. To this end we averaged the PSDs of the EEG electrodes PO3, PO4, O1, O2 and identified the highest peak in the frequency range from 8 - 14 Hz (Ruhnau et al., 2016; Fekete et al., 2018). This was the IAF used to compute the individual stimulation frequency (see Section 4.2.3). We repeated the extraction of the IAF and the mean power in the surrounding α -band ($\text{IAF} \pm 2$ Hz) for all four resting state blocks in each recording to monitor the stability of the IAF and the change in power due to the CVSA task and tACS.

Alpha lateralization index

We defined the α -power lateralization index (α -LI) as the difference of the mean activity of the electrode clusters (P6, P8, PO8) and (P5, P7, PO7) in the IAB (Thut et al., 2006):

$$\alpha\text{-LI} = \alpha \left(\frac{P6 + P8 + PO8}{3} \right) - \alpha \left(\frac{P5 + P7 + PO7}{3} \right) \quad (4.1)$$

The resulting α -LI is negative when the left visual hemifield is attended and positive when the right visual hemifield is attended. We then defined the α -LI span as the average difference between the mean α -LI for right and left trials throughout a run. As such, the α -LI span increases when the area between the two mean α -LI curves (one for left and one for right side CVSA) gets larger.

Discriminative analysis

Apart from the immediate effects of the tACS on the levels of α -band power in the resting state, we also wanted to explore the impact of the different stimulation frequencies on EEG classification performance during the CVSA task. For the topographical plots, we averaged the power in the IAB over all trials and over the trial duration and then subtracted right from left-side trials, to emphasize the occipital α -power lateralization.

To decode the attended side on a trial-by-trial basis, we trained and tested linear discriminant analysis (LDA) classifiers and assessed their performance with 10-fold cross validation. The initial feature space was chosen as the *channels* \times *frequency bands* array containing the PSDs of the electrodes located across the parieto-occipital cortex (P7, P5, P3, P1, Pz, P2, P4, P6, P8, PO7, PO3, POz, PO4, PO8, O1, Oz, O2) in five one-Hertz wide bands spanning the IAB. Then we used canonical variate analysis (CVA) (Galán et al., 2007) to limit the number of features to a maximum of 10 to prevent overfitting, and then trained a regularized ($\gamma = 0.5$) LDA. We classified each sample (16 samples per second) and then took the mean posterior probabilities across each trial to classify them into left and right side CVSA. To avoid results introduced by the random split in the cross validation procedure, we repeated the whole process of performance estimation 100 times and reported the average over these repetitions.

The chance level was computed as the upper bound of the 95% confidence interval of a binomial distribution with an expectation value 0.5 for 120 trials.

4.3 Results

4.3.1 Effect of tACS on alpha power

Our main hypothesis was that tACS at the IAF would lead to increases in the power of the IAB over the stimulated areas. Figure 4.2 shows the pre- and post-stimulation levels in the IAB. The power in the IAB grew by $24.1 \pm 63.6\%$ ($p > .05$) in the α -stimulation condition and by

$6.1 \pm 14.3\%$ ($p > .05$) in the β -stimulation condition. In the α -stimulation condition, as well as with β -stimulation four out of six subjects showed increases after the stimulation. Figure 4.3 displays the mean power spectra over the electrodes PO3, PO4, O1 and O2 for each subject before and after each stimulation condition. Subjects S4 and S5 showed a higher α -peak after the α -stimulation and subject S2 displayed a shifted α -peak (not at the stimulation frequency). In the β -stimulation condition, S1, S2, S3 and S6 showed elevated spectra over the β -band region, while S5 showed an increased α -peak. According to the questionnaire, subjects felt moderate itching (in 80% of the sessions), moderate tingling (in 50% of the sessions) and mild burning (in 33% of the sessions).

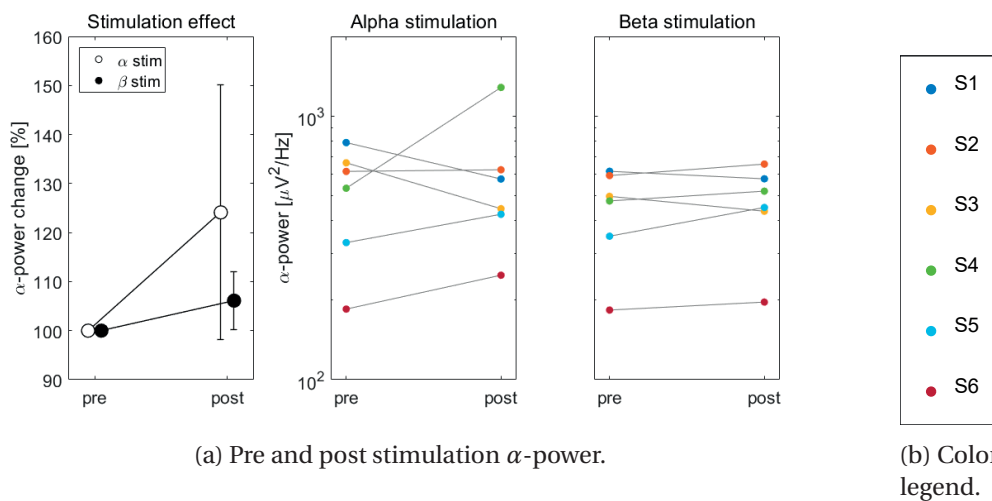


Figure 4.2 – Alpha power changes as a result of tACS in the α - or β -band. (a) Average relative change in the IAB power for both conditions (leftmost panel). The error bars indicate the standard error of the mean. Changes in the power (log scale) of the IAB for each subject from pre to post tACS, at either the IAF (left) or the β control frequency. (b) Every subject (S1 - S6) has a unique color code as shown here, which can be used to track the results of an individual subject throughout the different analyses.

4.3.2 Effect of tACS on alpha-power lateralization during CVSA

Our second hypothesis stated that an increased baseline α -power due to tACS should lead to more lateralization during the CVSA task. Figure 4.4 shows the averages and individual changes in the α -LI span in the α - and β -stimulation condition. The means did not change significantly ($p > .05$). Three out of six subjects increased their α -LI span after tACS in the α -stimulation condition, while only one out of six did after β -stimulation. Figure 4.5 displays the individual results for the pre- and post-stimulation α -LI — mean values for left (red) and right (blue) sided CVSA throughout the trial duration — as well as the topographical lateralization patterns (means over the IAB and trial duration, right minus left side attention). We observed lateralization patterns in S2, S3 and S5, although for the latter, the chosen electrodes for the α -LI computation were not the most discriminant ones. Subjects S1, S4 and S6 showed no

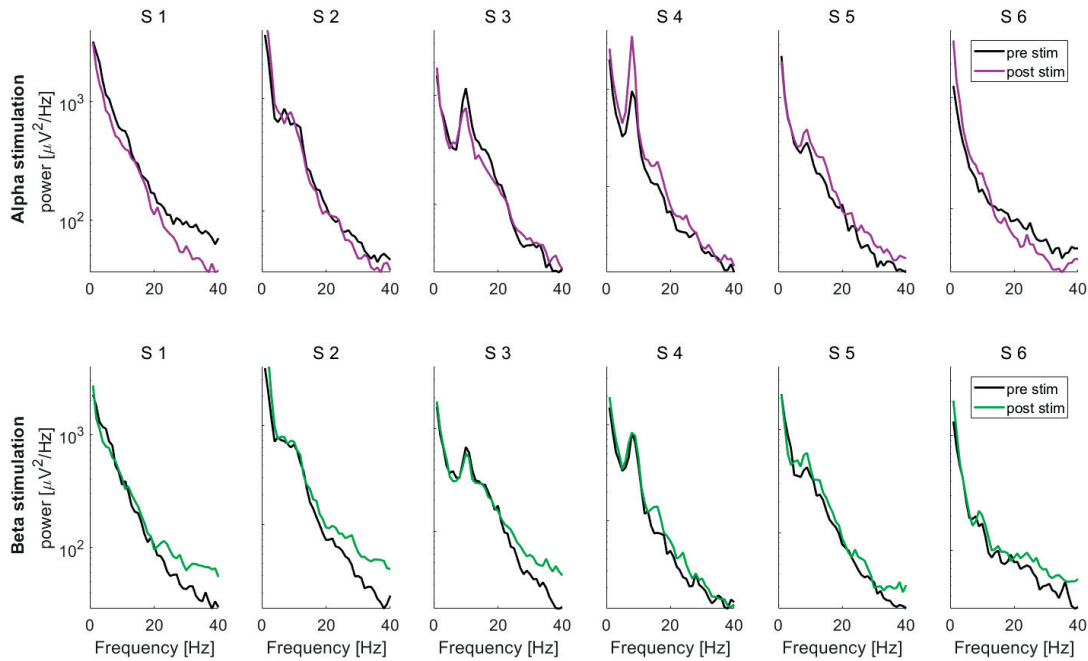


Figure 4.3 – PSDs pre and post stimulation for single subjects. The upper row presents the pre- (black) and post-stimulation (magenta) PSDs for tACS in the IAF. The lower row depicts the pre- (black) and post-stimulation (green) PSDs for tACS in the control frequency. All graphs have a logarithmic y-axis.

clear signs of a task-induced lateralization.

4.3.3 Changes in classification accuracy

The classifier accuracy in the binary left and right side CVSA paradigm is tightly coupled with the induced lateralization patterns. The mean classification accuracies increased from $64.6 \pm 11.8\%$ to $66.2 \pm 11.3\%$ in the case of the α -stimulation and from $60.4 \pm 9.9\%$ to $64.9 \pm 6.8\%$ for the β -stimulation (Figure 4.6). On an individual basis, subjects S2, S5 and S6 showed increased classification performance after the α -stimulation, and subjects S2, S4 and S6 after the β -stimulation.

4.3.4 Behavioral effect

Our behavioral proxy to CVSA was the validity effect (VE), which is defined as the reaction time difference between catch trials and validly cued trials. Figure 4.7 presents the average and individual changes in the VE pre and post stimulation in both conditions. Three and two subjects out of the six showed increases in the VE after stimulation at the α - and β -frequency, respectively.

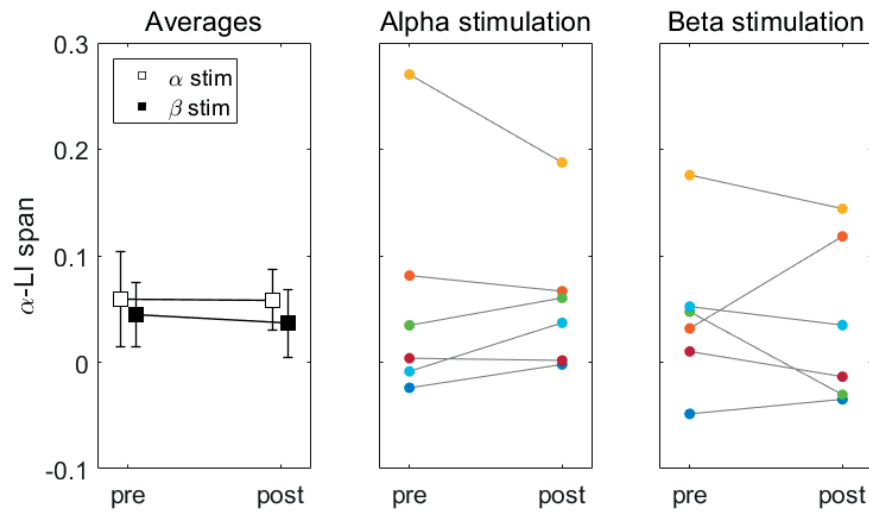


Figure 4.4 – Mean α -lateralization index span pre and post tACS. The left panel shows the grand averages of the α -LI span for all subjects and conditions. The error bars indicate the standard error of the mean. The middle panel shows the individual changes in the α -stimulation condition and the right panel for the β -stimulation condition. The color codes for individual subjects can be found in Figure 4.2b.

4.3.5 Comparison with no-stimulation condition

Since the results of our tACS intervention on alpha power were inconsistent across subjects, four out of six subjects agreed to come back to test stimulation at the IAF versus rest (i.e. no stimulation) with the same electrode setup. Figure 4.8 displays the pre- and post-stimulation power in the IAB for the same four subjects across the four recording days (α - vs. β -stimulation and α - vs. no stimulation). Therefore, we can observe twice as many data points in the middle panel, which allows us to estimate the replicability of the observed effects. Subjects S1 and S3 showed very similar behavior (one increasing and one decreasing) in both recording days, whereas S5 and S6 showed an opposite effect. In the no-stimulation condition, three subjects show no changes, while one subject still presents an elevation in α -power in the post measurement. No clear patterns are visible that set apart one of the conditions.

4.4 Discussion

In this pilot experiment we used tACS at the IAF to boost the levels of endogenous parieto-occipital α -power in order to study its effects on the electrophysiological and behavioral correlates of CVSA. Our preliminary results do not show consistent power increases in the IAB, neither after α - nor β -stimulation. Further tests also found no difference to absent stimulation in the same protocol. A CVSA task before and after the stimulation showed no significant differences ($p > .05$) in lateralization, classification or the validity effect (VE).

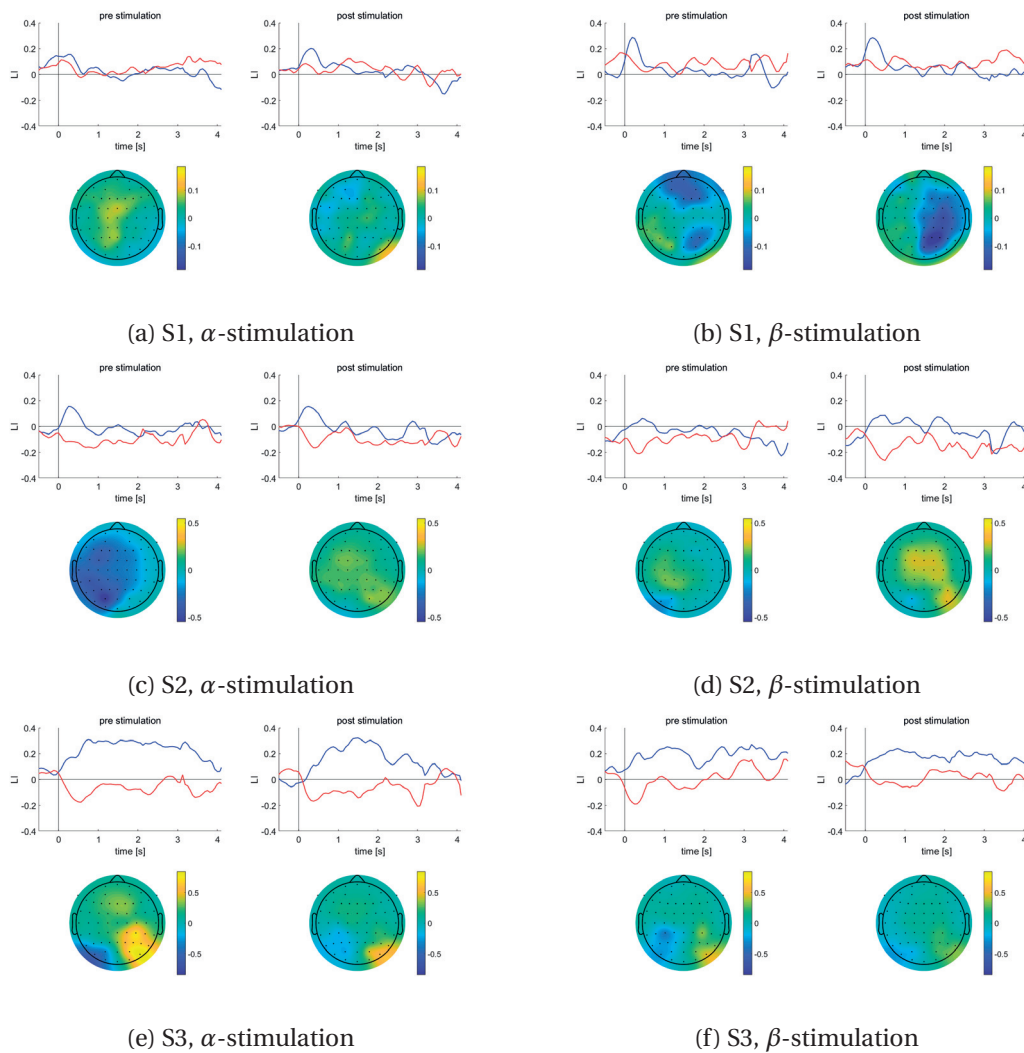


Figure 4.5 – Individual α -LI over time and topographical lateralization patterns (a-f). Pre- and post-stimulation plots of the average α -LI time course on the top and the mean topographical lateralization pattern in the IAB (right minus left side attention trials) on the bottom. The lateralization index is colored red for left-side trials and blue for right-side trials; the y-axis is kept the same for all subjects. The color axis for the topographical plots is kept constant for each individual subject, but changes between subjects due to large individual differences in the α -power base level. (continued on next page)

4.4.1 tACS parameter choices

The role of occipital α -power in visual and attentional processes has made it an interesting target to manipulate with noninvasive brain stimulation (Klimesch, 1999; Foxe and Snyder, 2011; Thut, 2014). tACS is still a rather novel tool for influencing ongoing oscillatory activity, and its mechanism of action is still the focus of ongoing research (Antal and Paulus, 2013; Fröhlich, 2015). Multiple studies have attempted to modulate ongoing α -band activity via

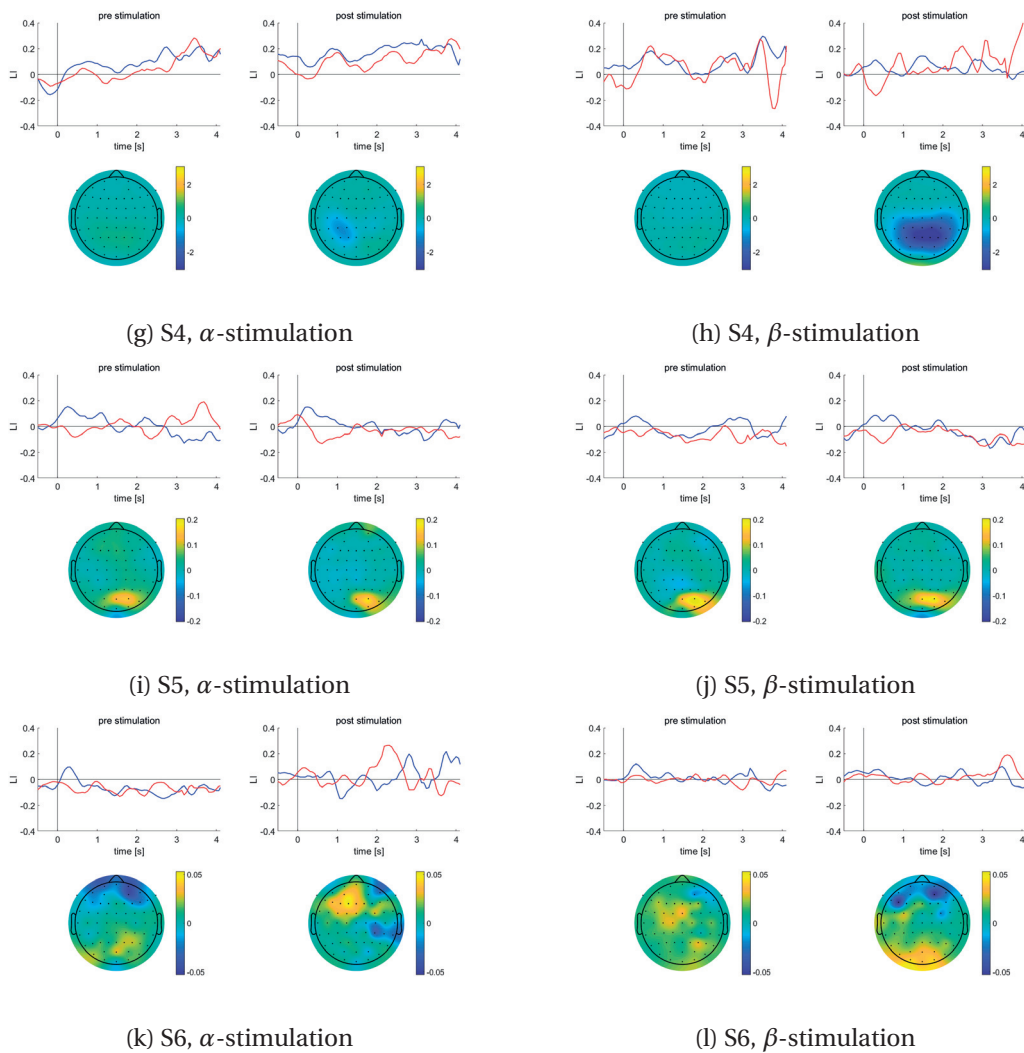


Figure 4.5 – Individual α -LI over time and topographical lateralization patterns (g-l). Pre- and post-stimulation plots of the average α -LI time course on the top and the mean topographical lateralization pattern in the IAB (right minus left side attention trials) on the bottom. The lateralization index is colored red for left-side trials and blue for right-side trials; the y-axis is kept the same for all subjects. The color axis for the topographical plots is kept constant for each individual subject, but changes between subjects due to large individual differences in the α -power base level.

tACS but the large search space of possible setup and parameters makes it hard to summarize the findings. Table 4.1 gives an overview of the most important parameters used in recent studies for tACS-driven amplification of parietooccipital α -power.

Five out of the six studies found significant differences between tACS stimulation in the IAB compared to sham stimulation. The only other study that reported no difference in groups was also the only study (apart from ours) using HD stimulation electrodes instead of patches

Source	Subject number	Subject design	EEG positions	Stimulation electrodes & positions	Stimulation frequency	Stimulation intensity	Stimulation duration	Result
Zaehle et al. (2010)	20	inter	CPz, Pz, POz	5 × 7 cm patch P09, PO10	1120 ± 489 μ A	IAF vs. sham	10 min	+ 14% (tACS) - 2% (sham)
Neuling et al. (2013)	22	inter	Pz	5 × 7 cm patch Cz, Oz	877 ± 48 μ A	IAF vs. sham	20 min	+ 50% (tACS) + 10% (sham)
Helfrich et al. (2014b)	14	intra	POz	5 × 7 cm patch Cz, Oz	1000 μ A	10 Hz vs. sham	20 min	+ 40% (tACS) + 10% (sham)
Vossen et al. (2015)	12	intra	FPz, Fz, Cz, CPz, Pz, POz	5 × 7 cm patch PO7 - P09 PO8 - PO10	1350 μ A - 2000 μ A	IAF vs. sham	25 min	+ 45% (tACS) + 15% (sham)
Kasten et al. (2016)	17	inter	F7, F3, Fz, F4, F8, P7, P3, Pz, P4, P8	5 × 7 cm patch Cz, Oz	1200 ± 440 μ A	IAF vs. sham	20 min	+ 50% (tACS) + 10% (sham)
Fekete et al. (2018)	78	inter	F3, F4, C4, C4 P3, P4, O1, O2	disc \varnothing 1 cm F3, F4, C4, C4 P3, P4, O1, O2	1089 ± 72 μ A	IAF vs. sham	20 min	+ 30% (tACS) + 30% (sham)
This study	6 (+ 4)	intra	PO3, PO4, O1, O2	disc \varnothing 1.2 cm PPO7h, PPO8h PO9, PO10	1000 μ A	IAF vs. no or β -band	20 min	+ 33% (IAF) + 20% (β)

Table 4.1 – Literature comparison of stimulation parameters and setup. For easier comparison of our study with the presented literature, we combined all recordings from both sessions (= 10 sessions α -stimulation) and the recordings from both the β - (6 sessions) as well as the no-stimulation (4 sessions) group. All reported differences in changes between stimulation and sham groups were significant, except for Fekete et al. (2018) and this study.

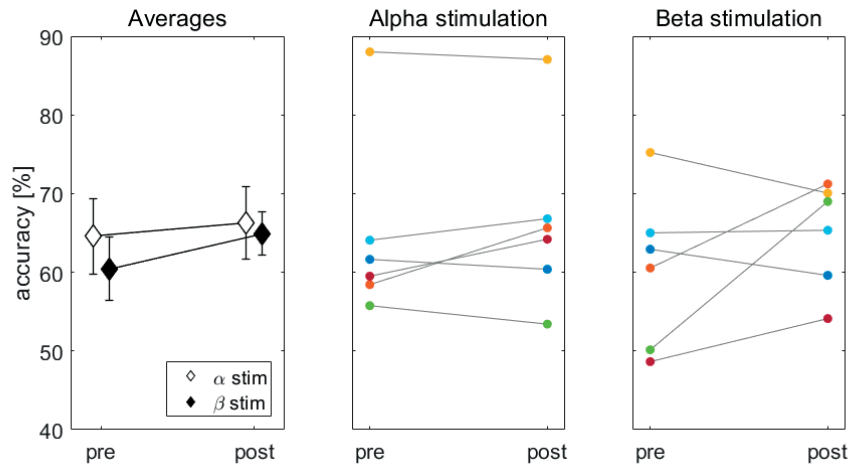


Figure 4.6 – Classification accuracy pre and post tACS. The left panel shows the grand average classification accuracies pre and post stimulation in both conditions. The error bars indicate the standard error of the mean. The two other panels present the pre- and post-stimulation decoding of the attended side in the CVSA task. The left side shows the changes in the α -stimulation condition, the right side for β -stimulation. The color codes for individual subjects can be found in Figure 4.2b.

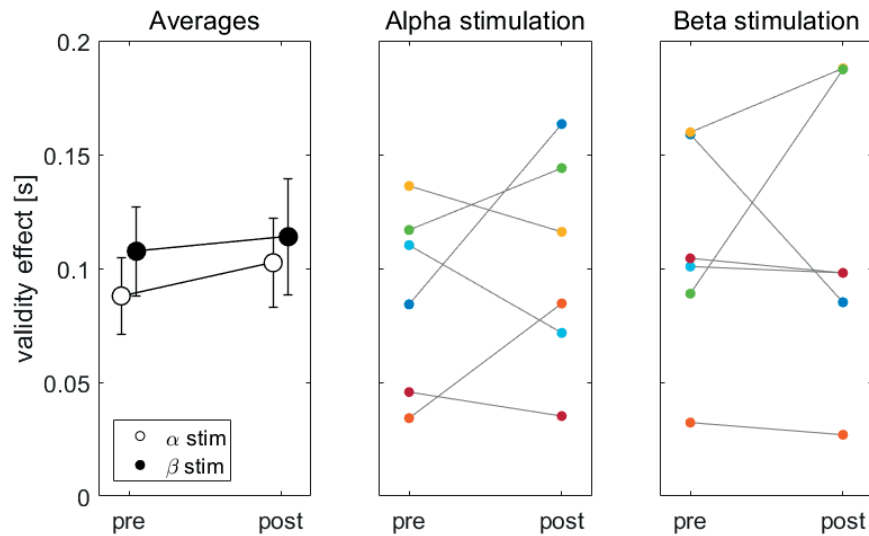


Figure 4.7 – Behavioral changes due to tACS. The left panel shows the grand averages in the validity effect in both conditions pre and post stimulation. The error bars indicate the standard error of the mean. The middle and right panel show the pre- and post-stimulation levels of the VE for stimulation in the α (left) and β (right) band. The color codes for individual subjects can be found in Figure 4.2b.

(Fekete et al., 2018). This suggests that HD-tACS is not powerful enough to influence the natural α -power levels. Although Helfrich et al. (2014a) used HD electrodes in occipital γ -

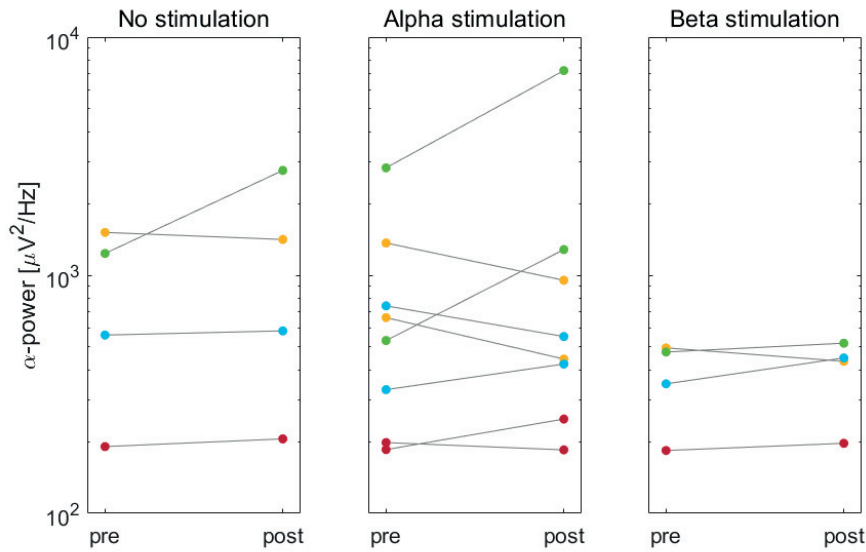


Figure 4.8 – Comparison of tACS-induced effects for α , β and no stimulation. The left panel shows the measured changes in the IAB when no stimulation was applied. The middle panel contains both IAF-tACS recordings for the four subjects and can serve as a measure for reproducibility of the stimulation effect in individual subjects. The right panel depicts the IAB-changes measured after tACS in the control frequency (β -band). The color codes for individual subjects can be found in Figure 4.2b. Note that the y-axes are logarithmic.

band stimulation and showed a significant decrease in α -band power, no study to our best knowledge has managed to see an increase in alpha power by stimulating at the IAF with an HD montage.

4.4.2 Simulation of the electric field

To shed further light on this topic, we simulated the induced electric field during tACS for our setup and for the setup described in the papers from Table 4.1. The results can be seen in Figure 4.9. The maximally induced field strengths range from 0.05 V/m. to 0.11 V/m (0.07 V/m). Our setup was thus towards the lower end of the range in field strength but covered the occipital cortex much more evenly than all other setups. Further, the setup of Zaehle et al. (2010) achieved less field strength and still resulted in significant increases in α -power after the stimulation. Therefore, judging by the simulated values of the stimulation coverage and the induced electric field, no evident conclusions can be drawn as to why our setup did not produce comparable results.

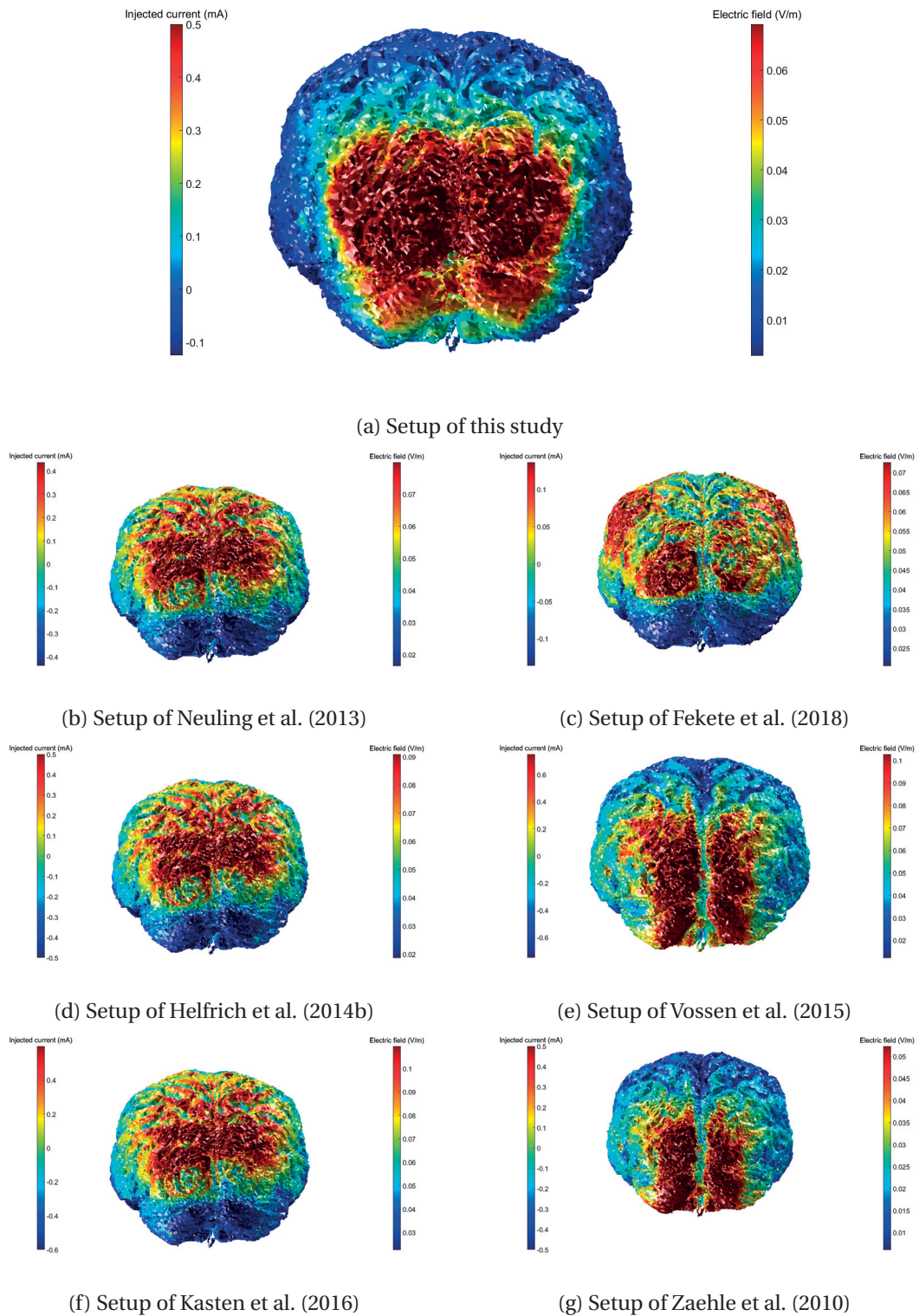


Figure 4.9 – Simulation of the induced electric field (view from behind). All simulations were done using the *roast* toolbox (Huang et al., 2018). The right-side color bar indicates the electric field strength and corresponds to the colors shown on the brain surface. The left-side color bar shows the input values for the positive and negative currents at the electrode level. Note that for multi-electrode setups peak-to-peak current needs to be divided by the number of electrodes attached.

4.4.3 Choice of control condition

One obvious difference between all studies reported in Table 4.1 and our experiment was the choice of the control condition. The usual choice was to evaluate an active stimulation condition versus a sham condition. To this end, current levels were tested and the highest possible current below the sensitivity threshold was chosen for stimulation (Vossen et al., 2015; Kasten et al., 2016). In pre-tests subjects reported to feel the stimulation at levels as low as 250 μ V over an extended period of time. This ruled out a traditional sham setup since we wanted the subjects to be blinded to the stimulation condition. Therefore we opted to stimulate in the β -frequency instead (avoiding harmonics of the IAF). Indeed, Kanai et al. (2008) demonstrated increased sensitivity to phosphenes after β -stimulation, but no study reports changes in α -power as a consequence of β -band tACS. The similar changes in parieto-occipital α -power after α - or β -band stimulation could be due to similar influences on the cortical networks, but is unlikely since the no-stimulation condition was not different either.

4.4.4 Role of enhanced alpha power in CVSA

Overall, we observed a large intersubject variance in the measured levels of α -band power. Lower baseline α -power has rather been connected to better memory retention (Klimesch et al., 2007), better visual perception of covert stimuli (Thut et al., 2006) and a lower transcranial magnetic stimulation (TMS) threshold for evoked phosphenes (Romei et al., 2008). But all these results were obtained from intra-subject comparisons, i.e. the gating mechanism of the α -oscillations most probably depends on relative changes in cortical oscillatory activity and not on the absolute levels. Thus, compared to the experiment in Chapter 2, where real-time feedback was able to improve behavioral correlates of CVSA, a general increase in parietooccipital α -power as induced by the tACS would not necessarily enhance CVSA by itself. Nevertheless, even if an elevated α -power level would show no functional effect, it could still lead to enhanced BCI classification performance due to a better signal-to-noise ratio of the α -lateralization patterns.

4.5 Conclusion

The modulation of ongoing natural oscillatory activity with tACS is an interesting approach to increase the discriminability of brain activity patterns for the use in BCIs. Unfortunately, our pilot study did not show conclusive evidence for a link between baseline alpha power and behavioral and electrophysiological correlates of CVSA. Although no statistical analysis could be conducted at the group level and more participants should thus be recorded, arguably, not enough is known yet about the neuroscientific mechanism of action of tACS and the choice of setup and useful parameters is far from being standardized. This study adds a small piece of evidence to the body of literature and calls especially for a more thorough investigation of the differences in stimulation effects achieved with setups with patch or HD electrodes.

5 Discussion and conclusion

Covert visuospatial attention (CVSA) has been proposed as an endogenous and natural control signal for brain-computer interfaces (BCIs) (Van Gerven and Jensen, 2009). However, implementation studies highlighted the problem that CVSA could not be reliably decoded in approximately one third to one half of the population (Tonin et al., 2013; Horschig et al., 2015). The aim of this thesis was to explore and open up new ways to improve CVSA-based BCI performance. To this end, I studied three complementary facets of CVSA BCIs: (i) the impact of continuous real-time feedback on CVSA-related behavior and electrophysiology, (ii) the integration of additional sensing modalities with the electroencephalography (EEG) into a hybrid BCI and (iii) the effects of transcranial alternating current stimulation (tACS) on the cortical patterns induced by CVSA.

5.0.1 Contributions

To explore the first approach, I designed the first online EEG-based CVSA-BCI with continuous feedback and used it to conduct a sham-controlled crossover study to investigate the effect of real-time feedback as compared to sham feedback. I could show a significant increase in the validity effect (VE) — a behavioral proxy to CVSA (Posner, 1980) — in the experimental group. This is interesting evidence that EEG could be used as a cheaper and mobile alternative to the functional magnetic resonance imaging (fMRI) for the use in patient neurofeedback training (Scharnowski et al., 2012; Sulzer et al., 2013; Robineau et al., 2017). Interestingly, the behavioral improvements after real-time feedback could not be connected to changes in the ongoing brain activity during CVSA. This could be due to the higher measurement noise in the EEG-signal as compared to the behavioral task, masking any slight changes, or be an indicator that internal shifts of covert attention and the observable lateralization patterns are not linked directly.

In the first part of the hybrid BCI approach, I investigated the feasibility of using functional near-infrared spectroscopy (fNIRS) in conjunction with the EEG in a multimodal BCI. The obtained results suggest that the fNIRS was not capable of detecting oxygenation-related

Chapter 5. Discussion and conclusion

changes in the occipital cortex. Since occipital signals have been measured before with Laser-based fNIRS devices (Harasawa and Shioiri, 2011; Morioka et al., 2014; Ward et al., 2015), it opens the question if the used light emitting diode (LED)-based fNIRS system was underpowered for measurements in occipital areas where the scalp-cortex distance is larger than, for example, on the forehead.

In the second part of the hybrid BCI approach, I combined CVSA-related information from the EEG with pupillometry measurements. I could demonstrate that the visual protocol developed by Mathôt et al. (2013) can be used to decode CVSA-related pupil size on a single-trial basis. Further, I showed that a fusion of both single-modality classifiers led to a higher average BCI performance, higher maximal accuracy and a higher number of subjects above the chance level than any of the single modalities alone.

To explore the neuromodulation approach, I utilized tACS at the individual alpha frequency (IAF) to raise the baseline level of occipital α -power and compared the effects to stimulation at an unrelated β -band frequency. Based on the findings in Rihs et al. (2009), I hypothesized that higher baseline α -power would translate into a larger lateralization pattern during CVSA. Results showed no significant difference between the two stimulation groups nor a consistent increase from the starting α -level. Not surprisingly, measures extracted from the pre- and post-stimulation CVSA tasks did not show any dependable changes either. Comparison of the employed stimulation setup with respect to the literature and of the simulations of the induced electric field did not yield a conclusive explanation for the missing effect. Fekete et al. (2018) and my study are the only ones so far that attempted to amplify α -power by stimulating at the IAF with an high definition (HD) electrode setup — and both yielded negative results. If the simulations of the induced electric fields are to be trusted, the comparison of recent tACS studies for occipital α -power enhancement implies that the intensity and location of the electric field during the stimulation and the duration of the latter are not the only important factors necessary for increasing cortical excitability through tACS. Future work is needed to shed light on the still little understood principles of tACS.

5.0.2 Proposed future work

The work presented in this thesis raised interesting questions and gave indications of where we should focus next to expand the current body of knowledge. Some of the following proposed research aims at answering open questions while other parts aim at practical implementations to achieve better working CVSA BCIs.

[Real-time feedback] Longitudinal training In this thesis, I did not observe significant changes in the CVSA-related brain patterns in EEG as a consequence of the real-time feedback intervention. One of the reasons might have been the short exposure to the feedback (around 20 minutes). Recently, Perdakis et al. (2018) have shown that longitudinal training of motor-related patterns with an online BCI significantly increased the discriminant features in the EEG. Therefore it would be interesting to explore the effects of long term and frequent real-

time feedback on the CVSA-induced patterns. The same recording setup and protocols that I described in Chapter 2 could be used to test the incorporation of multiple (e.g. 2×5) training sessions.

[fNIRS] Hardware changes and updates FMRI measurements have shown that blood flow changes during CVSA in the uppermost cortical layer can be used to decode the locus of covert attention (Andersson et al., 2013b). Thus, it is not unreasonable to assume that the same information can be obtained with modern laser-based fNIRS systems that employ short separation channels to filter out the superficial signal (Saager et al., 2011; Gagnon et al., 2012; Gagnon et al., 2014) and make use of a denser multi-channel optode grid to increase the spatial resolution (Shin et al., 2017). A BCI based on such an advanced fNIRS recording setup could be used as standalone or combined with EEG to benefit from multimodal integration.

[Pupillometry] Dynamic luminosity changes The visual protocol described in Chapter 3.3 uses different luminosities at the two screen target areas to get a different modulation of pupil size depending on the side of the covert attention. Even though I showed that a single-trial decoder can work with this paradigm, the classification accuracy was largely below what Mathôt et al. (2016) reported for their speller application. Two major changes to our protocol are most likely the reason for it. Firstly, they made the luminosity change dynamically over time, allowing to employ a pattern-matching process on the pupil size dynamics. Secondly, they continued each trial until a previously set threshold value was reached. The more conservative the threshold is set, the higher will be the accuracy, but also the longer the trials will last. (Mathôt et al., 2016) reported around 90% classification accuracy for an average trial duration of above 20 seconds. Both principles could be easily integrated into our design and the combination where the combination with the EEG has the potential to drastically reduce the mean time to selection.

[tACS] Change of stimulation electrodes Due to the lack of a stimulation-related effect in the occipital α -band, I could not verify the hypothesis that changing α -levels would also influence the prominence of CVSA-induced lateralization patterns. Since three studies have reported consistent α -power amplification with the application of 5×7 cm patch electrodes over electrode positions Cz and Oz, I propose to attempt to replicate their findings independently (of note, all three studies come from the same research group). Once the same effect is established, this electrode setup can replace the one used in Chapter 4 (the cap setup will be more complicated) and be used to probe the original hypothesis.

[tACS] Electrode comparison As discussed in Chapter 4, crucial insights on the workings of tACS are still missing. The field of neurostimulation needs a more in-depth investigation of the effects of different stimulation setups and parameters. For example, why did our stimulation setup achieve no effects, although stimulating the same brain regions with the same intensity had an effect with differently shaped and sized electrodes? The gold standard for uncovering the effects of noninvasive brain stimulation is simultaneous recording from

Chapter 5. Discussion and conclusion

implanted electrodes (Vöröslakos et al., 2018). Even though theoretically possible in humans, a systematic exploration most certainly has to be done in animal experiments initially due to the size of the free parameter space. Once sound models and simulation tools have been developed, a move towards testing these models in humans would be the next step.

5.0.3 Conclusion

The inability to observe CVSA patterns in the EEG from a substantial part of the population hinders the employment of an otherwise very promising control signal for BCI applications. Even though I could not effectively address this issue with the work that I have put into this thesis, I gathered valuable information about the rules that govern the investigated approaches. The real-time feedback CVSA BCI might become a promising tool for neurorehabilitation. The hybrid BCI was the most encouraging approach to overcome low BCI accuracies and could enable more people to use BCIs. Finally, while the noninvasive brain stimulation approach bears large potential, it also holds the most unanswered questions. Future research should and will improve our current knowledge and technology until, one day, we will be able to offer a BCI to every person that needs it.

“Does the cosmos contain keys for opening my diving bell? A subway line with no terminus? A currency strong enough to buy my freedom back? We must keep looking.”

— Jean-Dominique Bauby, *The Diving Bell and the Butterfly*

Bibliography

- Adam, Jos J., Jimmy H. Nieuwenstein, Raoul Huys, Fred G.W.C. Paas, Herman Kingma, Paul Willems, and Marieke Werry (2000). "Control of rapid aimed hand movements: The one-target advantage". In: *Journal of Experimental Psychology: Human Perception and Performance* 26.1, pp. 295–312.
- Ahn, Minkyu and Sung Chan Jun (2015). "Performance variation in motor imagery brain-computer interface: A brief review". In: *Journal of Neuroscience Methods* 243, pp. 103–110.
- Ajiboye, A. Bolu, Francis R. Willett, Daniel R. Young, William D. Memberg, Brian A. Murphy, Jonathan P. Miller, Benjamin L. Walter, Jennifer A. Sweet, Harry A. Hoyen, Michael W. Keith, P. Hunter Peckham, John D. Simeral, John P. Donoghue, Leigh R. Hochberg, and Robert F. Kirsch (2017). "Restoration of reaching and grasping movements through brain-controlled muscle stimulation in a person with tetraplegia: a proof-of-concept demonstration". In: *The Lancet* 389.10081, pp. 1821–1830.
- Aloise, Fabio, Pietro Aricò, Francesca Schettini, Angela Riccio, Serenella Salinari, Donatella Mattia, Fabio Babiloni, and Febo Cincotti (2012). "A covert attention P300 - based brain - computer interface: Geospell". In: *Ergonomics* 55.5, pp. 538–551.
- Andersson, Patrik, Josien P W Pluim, Max a. Viergever, and Nick F Ramsey (2013a). "Navigation of a telepresence robot via Covert Visuospatial Attention and real-time fMRI". In: *Brain Topography* 26.1, pp. 177–185.
- Andersson, Patrik, Nick F. Ramsey, Mathijs Raemaekers, Max A. Viergever, and Josien P W Pluim (2012). "Real-time decoding of the direction of covert visuospatial attention". In: *Journal of Neural Engineering* 9.4, p. 045004.
- Andersson, Patrik, Nick F. Ramsey, Max a. Viergever, and Josien P W Pluim (2013b). "7T fMRI reveals feasibility of covert visual attention-based brain-computer interfacing with signals obtained solely from cortical grey matter accessible by subdural surface electrodes". In: *Clinical Neurophysiology* 124.11, pp. 2191–2197.
- Ang, Kai Keng, Karen Sui Geok Chua, Kok Soon Phua, Chuanchu Wang, Zheng Yang Chin, Christopher Wee Keong Kuah, Wilson Low, and Cuntai Guan (2015). "A Randomized Controlled Trial of EEG-Based Motor Imagery Brain-Computer Interface Robotic Rehabilitation for Stroke". In: *Clinical EEG and Neuroscience* 46.4, pp. 310–320.
- Ang, Kai Keng, Cuntai Guan, Karen Sui Geok Chua, Beng Ti Ang, Christopher Wee Keong Kuah, Chuanchu Wang, Kok Soon Phua, Zheng Yang Chin, and Haihong Zhang (2011). "A

Bibliography

- Large Clinical Study on the Ability of Stroke Patients to Use an EEG-Based Motor Imagery Brain-Computer Interface". In: *Clinical EEG and Neuroscience* 42.4, pp. 253–258.
- Antal, Andrea and Walter Paulus (2013). "Transcranial alternating current stimulation (tACS)". In: *Frontiers in Human Neuroscience* 7.June, p. 317.
- Anwar, Abdul Rauf, Makii Muthalib, Stephane Perrey, Andreas Galka, Oliver Granert, Stephan Wolff, Ulrich Heute, Günther Deuschl, Jan H. Raethjen, and Muthuraman Muthuraman (2016). "Effective Connectivity of Cortical Sensorimotor Networks During Finger Movement Tasks: A Simultaneous fNIRS, fMRI, EEG Study." In: *Brain topography* 29, pp. 645–660.
- Appelros, Peter, Gunnel M. Karlsson, Åke Seiger, and Ingegerd Nydevik (2002). "Neglect and anosognosia after first-ever stroke: Incidence and relationship to disability". In: *Journal of Rehabilitation Medicine* 34.5, pp. 215–220.
- Arenth, Patricia M., Joseph H. Ricker, and Maria T. Schultheis (2007). "Applications of Functional Near-Infrared Spectroscopy (fNIRS) to Neurorehabilitation of Cognitive Disabilities". In: *The Clinical Neuropsychologist* 21.1, pp. 38–57.
- Arvaneh, Mahnaz, Cuntai Guan, Kai Keng Ang, and Chai Quek (2013). "EEG Data Space Adaptation to Reduce Intersession Nonstationarity in Brain-Computer Interface". In: *Neural Computation* 25.8, pp. 2146–2171.
- Aston-Jones, Gary and Jonathan D. Cohen (2005). "An Integrative Theory of Locus Coeruleus-Norepinephrine Function: Adaptive Gain and Optimal Performance". In: *Annual Review of Neuroscience* 28.1, pp. 403–450.
- Astrand, Elaine, Claire Wardak, and Suliann Ben Hamed (2014). "Selective visual attention to drive cognitive brain-machine interfaces: from concepts to neurofeedback and rehabilitation applications". In: *Frontiers in Systems Neuroscience* 8.August, pp. 1–16.
- Bahramisharif, Ali, Marcel Van Gerven, Tom Heskes, and Ole Jensen (2010). "Covert attention allows for continuous control of brain-computer interfaces". In: *European Journal of Neuroscience* 31.8, pp. 1501–1508.
- Baldauf, Daniel and Heiner Deubel (2010). "Attentional landscapes in reaching and grasping". In: *Vision Research* 50.11, pp. 999–1013.
- Banerjee, Snigdha, Adam C. Snyder, Sophie Molholm, and John J. Foxe (2011). "Oscillatory Alpha-Band Mechanisms and the Deployment of Spatial Attention to Anticipated Auditory and Visual Target Locations: Supramodal or Sensory-Specific Control Mechanisms?" In: *Journal of Neuroscience* 31.27, pp. 9923–9932.
- Battelli, Lorella, George A. Alvarez, Thomas Carlson, and Alvaro Pascual-Leone (2009). "The Role of the Parietal Lobe in Visual Extinction Studied with Transcranial Magnetic Stimulation". In: *Journal of Cognitive Neuroscience* 21.10, pp. 1946–1955.
- Bauernfeind, Günther, Reinhold Scherer, Gert Pfurtscheller, and Christa Neuper (2011). "Single-trial classification of antagonistic oxyhemoglobin responses during mental arithmetic". In: *Medical and Biological Engineering and Computing* 49.9, pp. 979–984.
- Beatty, Jackson (1982). "Task-evoked pupillary responses, processing load, and the structure of processing resources." In: *Psychological bulletin* 91.2, pp. 276–92.

- Beauchamp, Michael S., Laurent Petit, Timothy M. Ellmore, John Ingeholm, and James V. Haxby (2001). "A parametric fMRI study of overt and covert shifts of visuospatial attention". In: *NeuroImage* 14.2, pp. 310–321.
- Belyusar, Daniel, Adam C. Snyder, Hans Peter Frey, Mark R. Harwood, Josh Wallman, and John J. Foxe (2013). "Oscillatory alpha-band suppression mechanisms during the rapid attentional shifts required to perform an anti-saccade task". In: *NeuroImage* 65, pp. 395–407.
- Bestmann, Sven, Christian C. Ruff, Colin Blakemore, Jon Driver, and Kai V. Thilo (2007). "Spatial Attention Changes Excitability of Human Visual Cortex to Direct Stimulation". In: *Current Biology* 17.2, pp. 134–139.
- Biasiucci, Andrea, Robert Leeb, Iñaki Iturrate, Serafeim Perdakis, Abdul Al-Khodairy, Tiffany Corbet, A. Schnider, T. Schmidlin, Huaijian Zhang, Manuela Bassolino, D. Viceic, P. Vuadens, A. G. Guggisberg, and José del R. Millán (2018). "Brain-actuated functional electrical stimulation elicits lasting arm motor recovery after stroke". In: *Nature Communications* 9.1, pp. 1–13.
- Bießmann, Felix, Sergey Plis, Frank C. Meinecke, Tom Eichele, and Klaus-Robert Müller (2011). "Analysis of Multimodal Neuroimaging Data". In: *IEEE Reviews in Biomedical Engineering* 4, pp. 26–58.
- Binda, P., M. Pereverzeva, and S. O. Murray (2013a). "Attention to Bright Surfaces Enhances the Pupillary Light Reflex". In: *Journal of Neuroscience* 33.5, pp. 2199–2204.
- Binda, P., M. Pereverzeva, and S. O. Murray (2013b). "Pupil constrictions to photographs of the sun". In: *Journal of Vision* 13(6).8, pp. 1–9.
- Blankertz, Benjamin, Guido Dornhege, Matthias Krauledat, Klaus Robert Müller, and Gabriel Curio (2007). "The non-invasive Berlin Brain-Computer Interface: Fast acquisition of effective performance in untrained subjects". In: *NeuroImage* 37.2, pp. 539–550.
- Blokland, Yvonne, Loukianos Spyrou, Dick Thijssen, Thijs Eijsvogels, Willy Colier, Marianne Floor-Westerdijk, Rutger Vlek, Jorgen Bruhn, and Jason Farquhar (2014). "Combined EEG-fNIRS decoding of motor attempt and imagery for brain switch control: An offline study in patients with tetraplegia". In: *IEEE Transactions on Neural Systems and Rehabilitation Engineering* 22.2, pp. 222–229.
- Boksem, Maarten A.S., Theo F. Meijman, and Monicque M. Lorist (2005). "Effects of mental fatigue on attention: An ERP study". In: *Cognitive Brain Research* 25.1, pp. 107–116.
- Boto, Elena, Niall Holmes, James Leggett, Gillian Roberts, Vishal Shah, Sofie S. Meyer, Leonardo Duque Muñoz, Karen J. Mullinger, Tim M. Tierney, Sven Bestmann, Gareth R. Barnes, Richard Bowtell, and Matthew J. Brookes (2018). "Moving magnetoencephalography towards real-world applications with a wearable system". In: *Nature* 555.7698, pp. 657–661.
- Brigham, Katharine and B. V. K. Vijaya Kumar (2010). "Imagined Speech Classification with EEG Signals for Silent Communication: A Preliminary Investigation into Synthetic Telepathy". In: *2010 4th International Conference on Bioinformatics and Biomedical Engineering*. IEEE, pp. 1–4.

Bibliography

- Brignani, Debora, Manuela Ruzzoli, Piercarlo Mauri, and Carlo Miniussi (2013). “Is Transcranial Alternating Current Stimulation Effective in Modulating Brain Oscillations?” In: *PLoS ONE* 8.2. Ed. by Lawrence M. Ward, e56589.
- Brunner, P, S Joshi, S Briskin, J R Wolpaw, H Bischof, and G Schalk (2010). “Does the ‘P300’ speller depend on eye gaze?” In: *Journal of Neural Engineering* 7.5, p. 056013.
- Brunoni, Andre Russowsky, Joao Amadera, Bruna Berbel, Magdalena Sarah Volz, Brenno Gomes Rizzerio, and Felipe Fregni (2011). “A systematic review on reporting and assessment of adverse effects associated with transcranial direct current stimulation”. In: *International Journal of Neuropsychopharmacology* 14.8, pp. 1133–1145.
- Buccino, Alessio Paolo, Hasan Onur Keles, and Ahmet Omurtag (2016). “Hybrid EEG-fNIRS asynchronous brain-computer interface for multiple motor tasks”. In: *PLoS ONE* 11.1, pp. 1–16.
- Bunce, Scott C., Meltem Izzetoglu, Kurtulus Izzetoglu, Banu Onaral, and Kambiz Pourrezaei (2006). “Functional near-infrared spectroscopy”. In: *IEEE Engineering in Medicine and Biology Magazine* 25.4, pp. 54–62.
- Carlson, Tom and José del R. Millán (2013). “Brain-controlled wheelchairs: A robotic architecture”. In: *IEEE Robotics and Automation Magazine* 20.1, pp. 65–73.
- Cazzoli, Dario, René M. Müri, Rahel Schumacher, Sebastian Von Arx, Silvia Chaves, Klemens Gutbrod, Stephan Bohlhalter, Daniel Bauer, Tim Vanbellinghen, Manuel Bertschi, Stefan Kipfer, Clive R. Rosenthal, Christopher Kennard, Claudio L. Bassetti, and Thomas Nyffeler (2012). “Theta burst stimulation reduces disability during the activities of daily living in spatial neglect”. In: *Brain* 135.11, pp. 3426–3439.
- Chang, Pyung-Hun, Seung-Hee Lee, Gwang Min Gu, Seung-Hyun Lee, Sang-Hyun Jin, Sang Seok Yeo, Jeong Pyo Seo, and Sung Ho Jang (2014). “The cortical activation pattern by a rehabilitation robotic hand: a functional NIRS study.” In: *Frontiers in human neuroscience* 8. February, p. 49.
- Chavarriaga, Ricardo, Aleksander Sobolewski, and José del R. Millán (2014). “Errare machinale est: The use of error-related potentials in brain-machine interfaces”. In: *Frontiers in Neuroscience* 8. July, pp. 1–13.
- Chen, Xiaogang, Zhikai Chen, Shangkai Gao, and Xiaorong Gao (2014). “A high-ITR SSVEP-based BCI speller”. In: *Brain-Computer Interfaces* 1.3-4, pp. 181–191.
- Chen, Xiaogang, Yijun Wang, Masaki Nakanishi, Xiaorong Gao, Tzyy-Ping Jung, and Shangkai Gao (2015). “High-speed spelling with a noninvasive brain-computer interface”. In: *Proceedings of the National Academy of Sciences* 112.44, E6058–E6067.
- Ciavarro, Marco, Ettore Ambrosini, Annalisa Tosoni, Giorgia Committeri, Patrizia Fattori, and Claudio Galletti (2013). “rTMS of Medial Parieto-occipital Cortex Interferes with Attentional Reorienting during Attention and Reaching Tasks”. In: *Journal of Cognitive Neuroscience* 26.10, pp. 1–10.
- Clayton, Michael S., Nick Yeung, and Roi Cohen Kadosh (2015). “The roles of cortical oscillations in sustained attention”. In: *Trends in Cognitive Sciences* 19.4, pp. 188–195.
- Collura, Thomas F. (1993). “History and Evolution of Electroencephalographic Instruments and Techniques”. In: *Journal of Clinical Neurophysiology* 10.4, pp. 476–504.

- Corbetta, Maurizio, Erbil Akbudak, Thomas E. Conturo, Abraham Z. Snyder, John M. Ollinger, Heather A. Drury, Martin R. Linenweber, Steven E. Petersen, Marcus E. Raichle, David C. Van Essen, and Gordon L. Shulman (1998). "A common network of functional areas for attention and eye movements". In: *Neuron* 21.4, pp. 761–773.
- Corbetta, Maurizio, J. Michelle Kincade, John M. Ollinger, Marc P. McAvoy, and Gordon L. Shulman (2000). "Voluntary orienting is dissociated from target detection in human posterior parietal cortex". In: *Nature Neuroscience* 3.3, pp. 292–297.
- Corbetta, Maurizio, Michelle J. Kincade, Chris Lewis, Abraham Z. Snyder, and Ayelet Sapir (2005). "Neural basis and recovery of spatial attention deficits in spatial neglect." In: *Nature Neuroscience* 8.11, pp. 1603–1610.
- Corbetta, Maurizio, Francis M. Miezin, Gordon L. Shulman, and Steven E. Petersen (1993). "A PET study of visuospatial attention." In: *The Journal of Neuroscience* 13.3, pp. 1202–26.
- Corbetta, Maurizio and Gordon L. Shulman (2011). "Spatial Neglect and Attention Networks". In: *Annual Review of Neuroscience* 34.1, pp. 569–599.
- Corbetta, Maurizio and Gordon L. Shulman (2002). "Control of goal-directed and stimulus-driven attention in the brain." In: *Nature Reviews Neuroscience* 3.3, pp. 201–215.
- Corsi-Cabrera, María, Luz María Galindo-Vilchis, Yolanda Del-Río-Portilla, Consuelo Arce, and Julieta I. Ramos-Loyo (2007). "Within-subject reliability and inter-session stability of EEG power and coherent activity in women evaluated monthly over nine months". In: *Clinical Neurophysiology* 118.1, pp. 9–21.
- Coyle, Shirley M., Tomás E. Ward, and Charles M. Markham (2007). "Brain-computer interface using a simplified functional near-infrared spectroscopy system." In: *Journal of neural engineering* 4.3, pp. 219–226.
- Coyle, Shirley, Tomás Ward, Charles Markham, and Gary McDarby (2004). "On the suitability of near-infrared (NIR) systems for next-generation brain-computer interfaces". In: *Physiological Measurement* 25.4, pp. 815–822.
- Crawford, Trevor J. and Herrmann J. Muller (1992). "Spatial and temporal effects of spatial attention on human saccadic eye movements". In: *Vision Research* 32.2, pp. 293–304.
- Cui, Xu, Signe Bray, and Allan L. Reiss (2010). "Speeded Near Infrared Spectroscopy (NIRS) Response Detection". In: *PLoS ONE* 5.11. Ed. by Fabien Tell, e15474.
- Cuntai, Guan, Manoj Thulasidas, and Wu Jiankang (2004). "High performance p300 speller for brain-computer interface". In: *IEEE International Workshop on Biomedical Circuits and Systems, 2004*. IEEE, pp. 293–296.
- Curran, Eleanor A. and Maria J. Stokes (2003). "Learning to control brain activity: A review of the production and control of EEG components for driving brain-computer interface (BCI) systems". In: *Brain and Cognition* 51.3, pp. 326–336.
- Curtis, Howard J. (1940). "Intercortical Connections of Corpus Callosum as Indicated by Evoked Potentials". In: *Journal of Neurophysiology* 3.5, pp. 407–413.
- Dähne, Sven, Felix Bießmann, Wojciech Samek, Stefan Haufe, Dominique Goltz, Christopher Gundlach, Arno Villringer, Siamac Fazli, and Klaus-Robert Müller (2015). "Multivariate Machine Learning Methods for Fusing Multimodal Functional Neuroimaging Data". In: *Proceedings of the IEEE* 103.9, pp. 1507–1530.

Bibliography

- Dale, Anders M., Arthur K. Liu, Bruce R. Fischl, Randy L. Buckner, John W. Beldave, Jeffrey D. Lewine, and Eric Halgren (2000). "Dynamic Statistical Parametric Mapping". In: *Neuron* 26.1, pp. 55–67.
- DaSalla, Charles S., Hiroyuki Kambara, Makoto Sato, and Yasuharu Koike (2009). "Single-trial classification of vowel speech imagery using common spatial patterns". In: *Neural Networks* 22.9, pp. 1334–1339.
- De Bettencourt, Megan T., Jonathan D. Cohen, Ray F. Lee, Kenneth A. Norman, and Nicholas B. Turk-Browne (2015). "Closed-loop training of attention with real-time brain imaging". In: *Nature Neuroscience* 18.3, pp. 470–478.
- De Schotten, Michel Thiebaut, Flavio Dell'Acqua, Stephanie J. Forkel, Andrew Simmons, Francesco Vergani, Declan G. M. Murphy, and Marco Catani (2011). "A lateralized brain network for visuospatial attention". In: *Nature Neuroscience* 14.10, pp. 1245–1246.
- Decety, Jean and David H. Ingvar (1990). "Brain Structures Participating in Mental Simulation of Motor Behavior: A Neuropsychological Interpretation". In: *Acta Psychologica* 73, pp. 13–34.
- Delorme, Arnaud and Scott Makeig (2004). "EEGLAB: An open source toolbox for analysis of single-trial EEG dynamics including independent component analysis". In: *Journal of Neuroscience Methods* 134.1, pp. 9–21.
- Desimone, Robert and John Duncan (1995). "Neural Mechanisms of Selective Visual Attention". In: *Annual Review of Neuroscience* 18.1, pp. 193–222.
- Dickhaus, Thorsten, Claudia Sannelli, Klaus-Robert Müller, Gabriel Curio, and Benjamin Blankertz (2009). "Predicting BCI performance to study BCI illiteracy". In: *BMC Neuroscience* 10.Suppl 1, P84.
- Donchin, Emanuel and David B. D. Smith (1970). "The contingent negative variation and the late positive wave of the average evoked potential". In: *Electroencephalography and Clinical Neurophysiology* 29.2, pp. 201–203.
- Downing, Paul, Jia Liu, and Nancy Kanwisher (2001). "Testing cognitive models of visual attention with fMRI and MEG". In: *Neuropsychologia* 39.12, pp. 1329–1342.
- Eimer, Martin, José Van Velzen, Elena Gherri, and Clare Press (2006). "Manual response preparation and saccade programming are linked to attention shifts: ERP evidence for covert attentional orienting and spatially specific modulations of visual processing". In: *Brain Research* 1105.1, pp. 7–19.
- Ellis, C. J. K. (1981). "The pupillary light reflex in normal subjects." In: *British Journal of Ophthalmology* 65.11, pp. 754–759.
- Engel, Stephen A., Gary H. Glover, and Brian A. Wandell (1997). "Retinotopic organization in human visual cortex and the spatial precision of functional MRI". In: *Cerebral Cortex* 7.2, pp. 181–192.
- Escolano, Carlos, Ander Ramos Murguialday, Tamara Matuz, Niels Birbaumer, and Javier Minguez (2010). "A telepresence robotic system operated with a P300-based brain-computer interface: Initial tests with ALS patients". In: *2010 Annual International Conference of the IEEE Engineering in Medicine and Biology*. IEEE, pp. 4476–4480.

- Fabiani, Monica, Gabriele Gratton, and Demetrios Karis (1987). "Reliability of Measurement of the P300 Component of the Event-Related Brain Potential". In: *Advances in Psychophysiology* 2, pp. 1–78.
- Falkenstein, Michael, Jörg Hoormann, Stefan Christ, and Joachim Hohnsbein (2000). "ERP components on reaction errors and their functional significance: A tutorial". In: *Biological Psychology* 51.2-3, pp. 87–107.
- Fard, Pouyan R. and Moritz Grosse-Wentrup (2014). "The Influence of Decoding Accuracy on Perceived Control: A Simulated BCI Study". In: *ArXiv* 1410.6752v1.
- Farwell, Lawrence A. and Emanuel Donchin (1988). "Talking off the top of your head: toward a mental prosthesis utilizing event-related brain potentials". In: *Electroencephalography and Clinical Neurophysiology* 70.6, pp. 510–523.
- Fazli, Siamac, Jan Mehnert, Jens Steinbrink, Gabriel Curio, Arno Villringer, Klaus Robert Müller, and Benjamin Blankertz (2012). "Enhanced performance by a hybrid NIRS-EEG brain computer interface". In: *NeuroImage* 59.1, pp. 519–529.
- Fekete, Tomer, Andrey R. Nikolaev, Floris De Knijf, Aleksandra Zharikova, and Cees van Leeuwen (2018). "Multi-Electrode Alpha tACS During Varying Background Tasks Fails to Modulate Subsequent Alpha Power". In: *Frontiers in Neuroscience* 12.June.
- Ferrari, M., I. Giannini, G. Sideri, and E. Zanette (1985). *Oxygen Transport to Tissue VII*. Ed. by F. Kreuzer, S. M. Cain, Z. Turek, and T. K. Goldstick. Vol. 191. *Advances in Experimental Medicine and Biology*. Boston, MA: Springer US, pp. 873–82.
- Ferrari, Marco and Valentina Quaresima (2012). "A brief review on the history of human functional near-infrared spectroscopy (fNIRS) development and fields of application". In: *NeuroImage* 63.2, pp. 921–935.
- Ferrez, Pierre W. and José del R. Millán (2008). "Error-Related EEG Potentials Generated During Simulated Brain–Computer Interaction". In: *IEEE Transactions on Biomedical Engineering* 55.3, pp. 923–929.
- Findlay, John M. (1997). "Saccade target selection during visual search". In: *Vision Research* 37.5, pp. 617–631.
- Foxe, John J. and Adam C. Snyder (2011). "The role of alpha-band brain oscillations as a sensory suppression mechanism during selective attention". In: *Frontiers in Psychology* 2.July, pp. 1–13.
- Fröhlich, Flavio (2015). "Experiments and models of cortical oscillations as a target for noninvasive brain stimulation". In: *Progress in Brain Research*. Vol. 222, pp. 41–73.
- Funane, Tsukasa, Hirokazu Atsumori, Takusige Katura, Akiko N. Obata, Hiroki Sato, Yukari Tanikawa, Eiji Okada, and Masashi Kiguchi (2014). "Quantitative evaluation of deep and shallow tissue layers' contribution to fNIRS signal using multi-distance optodes and independent component analysis". In: *NeuroImage* 85, pp. 150–165.
- Gagnon, Louis, Robert J. Cooper, Meryem A. Yücel, Katherine L. Perdue, Douglas N. Greve, and David A. Boas (2012). "Short separation channel location impacts the performance of short channel regression in NIRS". In: *NeuroImage* 59.3, pp. 2518–2528.

Bibliography

- Gagnon, Louis, Meryem A. Yücel, David A. Boas, and Robert J. Cooper (2014). “Further improvement in reducing superficial contamination in NIRS using double short separation measurements”. In: *NeuroImage* 85, pp. 127–135.
- Galán, Ferran, Pierre W. Ferrez, Francesc Oliva, Joan Guàrdia, and José del R Millán (2007). “Feature extraction for multi-class BCI using canonical variates analysis”. In: *2007 IEEE International Symposium on Intelligent Signal Processing*.
- Garipelli, Gangadhar, Ricardo Chavarriaga, and José del R Millán (2013). “Single trial analysis of slow cortical potentials: a study on anticipation related potentials”. In: *Journal of Neural Engineering* 10.3, p. 036014.
- Gitelman, Darren R., Anna C. Nobre, Todd B. Parrish, Kevin S. LaBar, Yun-Hee Kim, Joel R. Meyer, and M. Marsel Mesulam (1999). “A large-scale distributed network for covert spatial attention”. In: *Brain* 122.6, pp. 1093–1106.
- Goldenholz, Daniel M., Seppo P. Ahlfors, Matti S. Hämäläinen, Dahlia Sharon, Mamiko Ishitobi, Lucia M. Vaina, and Steven M. Stufflebeam (2009). “Mapping the signal-to-noise-ratios of cortical sources in magnetoencephalography and electroencephalography”. In: *Human Brain Mapping* 30.4, pp. 1077–1086.
- Gu, Ying, Kim Dremstrup, and Dario Farina (2009). “Single-trial discrimination of type and speed of wrist movements from EEG recordings”. In: *Clinical Neurophysiology* 120.8, pp. 1596–1600.
- Guger, Christoph, Shahab Daban, Eric Sellers, Clemens Holzner, Gunther Krausz, Roberta Carabalona, Furio Gramatica, and Guenter Edlinger (2009). “How many people are able to control a P300-based brain-computer interface (BCI)?” In: *Neuroscience Letters* 462.1, pp. 94–98.
- Gunduz, Aysegul, Peter Brunner, Amy Daitch, Eric C. Leuthardt, Anthony L. Ritaccio, Bijan Pesaran, and Gerwin Schalk (2012). “Decoding covert spatial attention using electrocorticographic (ECoG) signals in humans”. In: *NeuroImage* 60.4, pp. 2285–2293.
- Hanslmayr, Simon, Alp Aslan, Tobias Staudigl, Wolfgang Klimesch, Christoph S. Herrmann, and Karl Heinz Bäuml (2007). “Prestimulus oscillations predict visual perception performance between and within subjects”. In: *NeuroImage* 37, pp. 1465–1473.
- Harasawa, Masamitsu and Satoshi Shioiri (2011). “Asymmetrical brain activity induced by voluntary spatial attention depends on the visual hemifield: A functional near-infrared spectroscopy study”. In: *Brain and Cognition* 75.3, pp. 292–298.
- Helfrich, Randolph F., Hannah Knepper, Guido Nolte, Daniel Strüber, Stefan Rach, Christoph S. Herrmann, Till R. Schneider, and Andreas K. Engel (2014a). “Selective Modulation of Interhemispheric Functional Connectivity by HD-tACS Shapes Perception”. In: *PLoS Biology* 12.12, e1002031.
- Helfrich, Randolph F., Till R. Schneider, Stefan Rach, Sina A. Trautmann-Lengsfeld, Andreas K. Engel, and Christoph S. Herrmann (2014b). “Entrainment of brain oscillations by transcranial alternating current stimulation”. In: *Current Biology* 24.3, pp. 333–339.
- Herff, Christian, Dominic Heger, Ole Fortmann, Johannes Hennrich, Felix Putze, and Tanja Schultz (2014). “Mental workload during n-back task—quantified in the prefrontal cortex using fNIRS”. In: *Frontiers in Human Neuroscience* 7.January, pp. 1–9.

- Hesse, Constanze and Heiner Deubel (2011). "Efficient grasping requires attentional resources". In: *Vision Research* 51.11, pp. 1223–1231.
- Hochberg, Leigh R., Daniel Bacher, Beata Jarosiewicz, Nicolas Y. Masse, John D. Simeral, Joern Vogel, Sami Haddadin, Jie Liu, Sydney S. Cash, Patrick Van Der Smagt, and John P. Donoghue (2012). "Reach and grasp by people with tetraplegia using a neurally controlled robotic arm". In: *Nature* 485.7398, pp. 372–375.
- Holmqvist, Kenneth, Marcus Nyström, Richard Andersson, Richard Dewhurst, Halszka Jarodzka, and Joost Van de Weijer (2011). *Eye Tracking: A Comprehensive Guide To Methods And Measures*. Oxford University Press.
- Horschig, Jörn M., Wouter Oosterheert, Robert Oostenveld, and Ole Jensen (2015). "Modulation of Posterior Alpha Activity by Spatial Attention Allows for Controlling A Continuous Brain – Computer Interface". In: *Brain Topography* 28.6, pp. 852–864.
- Huang, Yu, Abhishek Datta, Marom Bikson, and Lucas C. Parra (2018). "ROAST: An Open-Source, Fully-Automated, Realistic Volumetric-Approach-Based Simulator For TES". In: *2018 40th Annual International Conference of the IEEE Engineering in Medicine and Biology Society (EMBC)*. IEEE, pp. 3072–3075.
- Huggins, Jane E., Patricia A. Wren, and Kirsten L. Gruis (2011). "What would brain-computer interface users want? Opinions and priorities of potential users with amyotrophic lateral sclerosis". In: *Amyotrophic Lateral Sclerosis* 12.5, pp. 318–324.
- Huppert, Theodore J., Solomon G. Diamond, Maria A. Franceschini, and David A. Boas (2009). "HomER: a review of time-series analysis methods for near-infrared spectroscopy of the brain." In: *Applied optics* 48.10, pp. D280–D298.
- Huster, Rene J., Stefan Debener, Tom Eichele, and Christoph S. Herrmann (2012). "Methods for Simultaneous EEG-fMRI: An Introductory Review". In: *Journal of Neuroscience* 32.18, pp. 6053–6060.
- Hwang, Han-Jeong, Soyoun Kim, Soobeom Choi, and Chang-Hwan Im (2013). "EEG-Based Brain-Computer Interfaces: A Thorough Literature Survey". In: *International Journal of Human-Computer Interaction* 29.12, pp. 814–826.
- Iturrate, Iñaki, Jonathan Grizou, Jason Omedes, Pierre Yves Oudeyer, Manuel Lopes, and Luis Montesano (2015). "Exploiting task constraints for self-calibrated brain-machine interface control using error-related potentials". In: *PLoS ONE* 10.7, pp. 1–15.
- Jarosiewicz, Beata, Anish A. Sarma, Daniel Bacher, Nicolas Y. Masse, John D. Simeral, Brittany Sorice, Erin M. Oakley, Christine Blabe, Chethan Pandarinath, Vikash Gilja, Sydney S. Cash, Emad N. Eskandar, Gerhard Friehs, Jaimie M. Henderson, Krishna V. Shenoy, John P. Donoghue, and Leigh R. Hochberg (2015). "Virtual typing by people with tetraplegia using a self-calibrating intracortical brain-computer interface". In: *Science Translational Medicine* 7.313, 313ra179–313ra179.
- Jensen, Ole and Ali Mazaheri (2010). "Shaping Functional Architecture by Oscillatory Alpha Activity: Gating by Inhibition". In: *Frontiers in Human Neuroscience* 4.November, pp. 1–8.
- Jespersen, Sune N. and Leif Østergaard (2012). "The roles of cerebral blood flow, capillary transit time heterogeneity, and oxygen tension in brain oxygenation and metabolism". In: *Journal of Cerebral Blood Flow and Metabolism* 32.2, pp. 264–277.

Bibliography

- Jiang, Ning, Leonardo Gizzi, Natalie Mrachacz-Kersting, Kim Dremstrup, and Dario Farina (2015). "A brain-computer interface for single-trial detection of gait initiation from movement related cortical potentials". In: *Clinical Neurophysiology* 126.1, pp. 154–159.
- Jöbsis, Frans F. (1977). "Noninvasive, infrared monitoring of cerebral and myocardial oxygen sufficiency and circulatory parameters". In: *Science* 198.4323, pp. 1264–1267.
- Kajihara, Takafumi, Muhammad Nabeel Anwar, Masahiro Kawasaki, Yuji Mizuno, Kimitaka Nakazawa, and Keiichi Kitajo (2015). "Neural dynamics in motor preparation: From phase-mediated global computation to amplitude-mediated local computation". In: *NeuroImage* 118, pp. 445–455.
- Kanai, Ryota, Leila Chaieb, Andrea Antal, Vincent Walsh, and Walter Paulus (2008). "Frequency-Dependent Electrical Stimulation of the Visual Cortex". In: *Current Biology* 18.23, pp. 1839–1843.
- Karnath, Hans Otto and Christopher Rorden (2012). "The anatomy of spatial neglect". In: *Neuropsychologia* 50.6, pp. 1010–1017.
- Karnath, Hans-Otto (2015). "Spatial attention systems in spatial neglect". In: *Neuropsychologia* 75, pp. 61–73.
- Kasten, Florian H., James Dowsett, and Christoph S. Herrmann (2016). "Sustained Aftereffect of α -tACS Lasts Up to 70 min after Stimulation". In: *Frontiers in Human Neuroscience* 10.May, pp. 1–9.
- Kastner, Sabine, Mark A. Pinsk, Peter De Weerd, Robert Desimone, and Leslie G. Ungerleider (1999). "Increased activity in human visual cortex during directed attention in the absence of visual stimulation." In: *Neuron* 22.4, pp. 751–761.
- Kelly, Simon P., Edmund C. Lalor, Ciaran Finucane, and Richard B. Reilly (2004). "A comparison of covert and overt attention as a control option in a steady-state visual evoked potential-based brain computer interface." In: *Annual International Conference of the IEEE Engineering in Medicine and Biology Society (EMBC)*. Vol. 7, pp. 4725–4728.
- Kelly, Simon P., Edmund C. Lalor, Richard B. Reilly, and John J. Foxe (2005). "Visual spatial attention tracking using high-density SSVEP data for independent brain-computer communication". In: *IEEE Transactions on Neural Systems and Rehabilitation Engineering* 13.2, pp. 172–178.
- Kelly, Simon P., Edmund C. Lalor, Richard B. Reilly, and John J. Foxe (2006). "Increases in alpha oscillatory power reflect an active retinotopic mechanism for distracter suppression during sustained visuospatial attention." In: *Journal of neurophysiology* 95.6, pp. 3844–3851.
- Kerkhoff, Georg, Leandra Bucher, Michael Brasse, Eva Leonhart, Manfred Holzgraefe, Volker Völzke, Ingo Keller, and Stefan Reinhart (2014). "Smooth Pursuit "Bedside" Training Reduces Disability and Unawareness During the Activities of Daily Living in Neglect: A Randomized Controlled Trial." In: *Neurorehabilitation and neural repair* 28.6, pp. 554–563.
- Kerkhoff, Georg, Stefan Reinhart, Wolfram Ziegler, Frank Artinger, Christian Marquardt, and Ingo Keller (2013). "Smooth Pursuit Eye Movement Training Promotes Recovery From Auditory and Visual Neglect". In: *Neurorehabilitation and Neural Repair* 27.9, pp. 789–798.
- Kerlin, J. R., A. J. Shahin, and L. M. Miller (2010). "Attentional Gain Control of Ongoing Cortical Speech Representations in a "Cocktail Party"". In: *Journal of Neuroscience* 30.2, pp. 620–628.

- Khan, M. Jawad and Keum-Shik Hong (2015). "Passive BCI based on drowsiness detection: an fNIRS study". In: *Biomedical Optics Express* 6.10, p. 4063.
- Kinsbourne, Marcel (1987). "Mechanisms of Unilateral Neglect". In: *Advances in Psychology*. Vol. 45. C, pp. 69–86.
- Kirschstein, Timo and Rüdiger Köhling (2009). "What is the Source of the EEG?" In: *Clinical EEG and Neuroscience* 40.3, pp. 146–149.
- Klimesch, Wolfgang (1999). "EEG alpha and theta oscillations reflect cognitive and memory performance: A review and analysis". In: *Brain Research Reviews* 29.2-3, pp. 169–195.
- Klimesch, Wolfgang, Paul Sauseng, and Simon Hanslmayr (2007). "EEG alpha oscillations: The inhibition-timing hypothesis". In: *Brain Research Reviews* 53.1, pp. 63–88.
- Klinke, Marianne E., Thóra B. Hafsteinsdóttir, Haukur Hjaltason, and Helga Jónsdóttir (2015). "Ward-based interventions for patients with hemispatial neglect in stroke rehabilitation: A systematic literature review". In: *International Journal of Nursing Studies* 52.8, pp. 1375–1403.
- Kober, Silvia E., Guilherme Wood, Jürgen Kurzmann, Elisabeth V.C. Friedrich, Matthias Stangl, Theresa Wippel, Aleksander Väljamäe, and Christa Neuper (2014). "Near-infrared spectroscopy based neurofeedback training increases specific motor imagery related cortical activation compared to sham feedback". In: *Biological Psychology* 95.1, pp. 21–30.
- Kocsis, László, Peter Herman, and Andras Eke (2006). "The modified Beer–Lambert law revisited". In: *Physics in Medicine and Biology* 51.5, N91–N98.
- Koo, Bonkon, Hwan-Gon Lee, Yunjun Nam, Hyohyeong Kang, Chin Su Koh, Hyung-Cheul Shin, and Seungjin Choi (2015). "A hybrid NIRS-EEG system for self-paced brain computer interface with online motor imagery". In: *Journal of Neuroscience Methods* 244, pp. 26–32.
- Kornhuber, Hans H. and Lüder Deecke (1965). "Hirnpotentialänderungen bei Willkürbewegungen und passiven Bewegungen des Menschen: Bereitschaftspotential und reafferente Potentiale". In: *Pflügers Archiv für die Gesamte Physiologie des Menschen und der Tiere* 284.1, pp. 1–17.
- Krusienski, Dean J., Eric W. Sellers, Dennis J. McFarland, Theresa M. Vaughan, and Jonathan R. Wolpaw (2008). "Toward enhanced P300 speller performance". In: *Journal of Neuroscience Methods* 167.1, pp. 15–21.
- Kübler, Andrea, Nicola Neumann, Barbara Wilhelm, Thilo Hinterberger, and Niels Birbaumer (2004). "Predictability of Brain-Computer Communication". In: *Journal of Psychophysiology* 18.(2-3), pp. 121–129.
- Laczó, Bence, Andrea Antal, Robert Niebergall, Stefan Treue, and Walter Paulus (2012). "Transcranial alternating stimulation in a high gamma frequency range applied over V1 improves contrast perception but does not modulate spatial attention". In: *Brain Stimulation* 5.4, pp. 484–491.
- Laeng, Bruno, Sylvain Sirois, and Gustaf Gredebäck (2012). "Pupillometry: A Window to the Preconscious?" In: *Perspectives on psychological science* 7.1, pp. 18–27.
- Laeng, Bruno and Unni Sulutvedt (2014). "The Eye Pupil Adjusts to Imaginary Light". In: *Psychological Science* 25.1, pp. 188–197.

Bibliography

- LaFleur, Karl, Kaitlin Cassady, Alexander Doud, Kaleb Shades, Eitan Rogin, and Bin He (2013). “Quadcopter control in three-dimensional space using a noninvasive motor imagery-based brain–computer interface”. In: *Journal of Neural Engineering* 10.4, p. 046003.
- Lal, Thomas Navin, Niels Birbaumer, Bernhard Schölkopf, Michael Schröder, N. Jeremy Hill, Hubert Preissl, Thilo Hinterberger, Jürgen Mellinger, Martin Bogdan, Wolfgang Rosenstiel, and Thomas Hofmann (2005). “A brain computer interface with online feedback based on magnetoencephalography”. In: *Proceedings of the 22nd international conference on Machine learning - ICML '05*, pp. 465–472.
- Leeb, Robert, Hesam Sagha, Ricardo Chavarriaga, and José del R. Millán (2011). “A hybrid brain–computer interface based on the fusion of electroencephalographic and electromyographic activities”. In: *Journal of Neural Engineering* 8.2, p. 025011.
- Leff, Daniel Richard, Felipe Orihuela-Espina, Clare E. Elwell, Thanos Athanasiou, David T. Delpy, Ara W. Darzi, and Guang Zhong Yang (2011). “Assessment of the cerebral cortex during motor task behaviours in adults: A systematic review of functional near infrared spectroscopy (fNIRS) studies”. In: *NeuroImage* 54.4, pp. 2922–2936.
- Lemm, Steven, Benjamin Blankertz, Thorsten Dickhaus, and Klaus-Robert Müller (2011). “Introduction to machine learning for brain imaging”. In: *NeuroImage* 56.2, pp. 387–399.
- Leuthardt, Eric C., Charles Gaona, Mohit Sharma, Nicholas Szrama, Jarod Roland, Zac Freudenberger, Jamie Solis, Jonathan Breshears, and Gerwin Schalk (2011). “Using the electrocorticographic speech network to control a brain–computer interface in humans”. In: *Journal of Neural Engineering* 8.3, p. 036004.
- Leuthardt, Eric C., Kai J. Miller, Gerwin Schalk, Rajesh P.N. Rao, and Jeffrey G. Ojemann (2006). “Electrocorticography-based brain computer interface - The seattle experience”. In: *IEEE Transactions on Neural Systems and Rehabilitation Engineering* 14.2, pp. 194–198.
- Leuthardt, Eric C., Gerwin Schalk, Jonathan R. Wolpaw, Jeffrey G. Ojemann, and Daniel W. Moran (2004). “A brain-computer interface using electrocorticographic signals in humans”. In: *Journal of Neural Engineering* 1.2, pp. 63–71.
- Lindquist, Martin A., Ji Meng Loh, Lauren Y. Atlas, and Tor D. Wager (2009). “Modeling the hemodynamic response function in fMRI: Efficiency, bias and mis-modeling”. In: *NeuroImage* 45.1, S187–S198.
- Liparas, Dimitris, Stavros I. Dimitriadis, Nikolaos A. Laskaris, Areti Tzelepi, Konstantinos Charalambous, and Lefteris Angelis (2014). “Exploiting the temporal patterning of transient VEP signals: A statistical single-trial methodology with implications to brain–computer interfaces (BCIs)”. In: *Journal of Neuroscience Methods* 232, pp. 189–198.
- Liu, Yang, Zongtan Zhou, and Dwen Hu (2011). “Gaze independent brain-computer speller with covert visual search tasks”. In: *Clinical Neurophysiology* 122.6, pp. 1127–1136.
- Liu, Yuelu, Jesse Bengson, Haiqing Huang, George R. Mangun, and Mingzhou Ding (2016). “Top-down Modulation of Neural Activity in Anticipatory Visual Attention: Control Mechanisms Revealed by Simultaneous EEG-fMRI”. In: *Cerebral Cortex* 26.2, pp. 517–529.
- Loewenfeld, Irene E. and Otto Lowenstein (1993). *The pupil: Anatomy, physiology, and clinical applications*. Vol. 2. Wiley-Blackwell.

- Lotte, Fabien, Marco Congedo, Anatole Lécuyer, Fabrice Lamarche, and Bruno Arnaldi (2007). “A review of classification algorithms for EEG-based brain–computer interfaces”. In: *Journal of Neural Engineering* 4.2, R1–R13.
- Lowe, Stanley W. and Kenneth N. Ogle (1966). “Dynamics of the Pupil During Binocular Rivalry”. In: *Archives of Ophthalmology* 75.3, pp. 395–403.
- Luu, Sheena and Tom Chau (2009). “Decoding subjective preference from single-trial near-infrared spectroscopy signals”. In: *Journal of Neural Engineering* 6.1, p. 016003.
- Mangun, George R. and Lindy A. Buck (1998). “Sustained visual spatial attention produces costs and benefits in response time and evoked neural activity”. In: *Neuropsychologia* 36.3, pp. 189–200.
- Marshall, John C. and Peter W. Halligan (1988). “Blindsight and insight in visuo-spatial neglect”. In: *Nature* 336.6201, pp. 766–767.
- Martin, Stephanie, Peter Brunner, Iñaki Iturrate, José del R. Millán, Gerwin Schalk, Robert T. Knight, and Brian N. Pasley (2016). “Word pair classification during imagined speech using direct brain recordings”. In: *Scientific Reports* 6.1, p. 25803.
- Mathôt, Sebastiaan, Lotje van der Linden, Jonathan Grainger, and Françoise Vitu (2013). “The pupillary light response reveals the focus of covert visual attention.” In: *PLoS ONE* 8.10, e78168.
- Mathôt, Sebastiaan, Jean Baptiste Melmi, Lotje Van Der Linden, and Stefan Van Der Stigchel (2016). “The mind-writing pupil: A human-computer interface based on decoding of covert attention through pupillometry”. In: *PLoS ONE* 11.2, pp. 1–15.
- Matthews, Fiachra, Barak A. Pearlmutter, Tomas E. Ward, Christopher Soraghan, and Charles Markham (2008). “Hemodynamics for brain-computer interfaces”. In: *IEEE Signal Processing Magazine* 25.1, pp. 87–94.
- Maynard, Edwin M., Craig T. Nordhausen, and Richard A. Normann (1997). “The Utah Intracortical Electrode Array: A recording structure for potential brain-computer interfaces”. In: *Electroencephalography and Clinical Neurophysiology* 102.3, pp. 228–239.
- McConnell, George C., Howard D. Rees, Allan I. Levey, Claire-Anne Gutekunst, Robert E. Gross, and Ravi V. Bellamkonda (2009). “Implanted neural electrodes cause chronic, local inflammation that is correlated with local neurodegeneration”. In: *Journal of Neural Engineering* 6.5, p. 056003.
- Mellinger, Jürgen, Gerwin Schalk, Christoph Braun, Hubert Preissl, Wolfgang Rosenstiel, Niels Birbaumer, and Andrea Kübler (2007). “An MEG-based brain-computer interface (BCI)”. In: *NeuroImage* 36.3, pp. 581–593.
- Mestais, Corinne S., Guillaume Charvet, Fabien Sauter-Starace, Michael Foerster, David Ratel, and Alim Louis Benabid (2015). “WIMAGINE: Wireless 64-channel ECoG recording implant for long term clinical applications”. In: *IEEE Transactions on Neural Systems and Rehabilitation Engineering* 23.1, pp. 10–21.
- Mesulam, M. Marsel (1999). “Spatial attention and neglect: Parietal, frontal and cingulate contributions to the mental representation and attentional targeting of salient extrapersonal events”. In: *Philosophical Transactions of the Royal Society B: Biological Sciences* 354.1387, pp. 1325–1346.

Bibliography

- Mihara, Masahito, Noriaki Hattori, Megumi Hatakenaka, Hajime Yagura, Teiji Kawano, Taro Hino, and Ichiro Miyai (2013). “Near-infrared spectroscopy-mediated neurofeedback enhances efficacy of motor imagery-based training in poststroke victims: A pilot study”. In: *Stroke* 44.4, pp. 1091–1098.
- Mihara, Masahito, Ichiro Miyai, Noriaki Hattori, Megumi Hatakenaka, Hajime Yagura, Teiji Kawano, Masaki Okibayashi, Nobuyoshi Danjo, Akihiro Ishikawa, Yoshihiro Inoue, and Kisou Kubota (2012). “Neurofeedback Using Real-Time Near-Infrared Spectroscopy Enhances Motor Imagery Related Cortical Activation”. In: *PLoS ONE* 7.3, e32234.
- Millán, José del R., Josep Mouriño, Marco Franzé, Febo Cincotti, Markus Varsta, Jukka Heikkonen, and Fabio Babiloni (2002). “A local neural classifier for the recognition of EEG patterns associated to mental tasks”. In: *IEEE Transactions on Neural Networks* 13.3, pp. 678–686.
- Min, Byoung Kyong, Matthew J. Marzelli, and Seung Schik Yoo (2010). “Neuroimaging-based approaches in the brain-computer interface”. In: *Trends in Biotechnology* 28.11, pp. 552–560.
- Moosmann, Matthias, Petra Ritter, Ina Krastel, Andrea Brink, Sebastian Thees, Felix Blankenburg, Birol Taskin, Hellmuth Obrig, and Arno Villringer (2003). “Correlates of alpha rhythm in functional magnetic resonance imaging and near infrared spectroscopy”. In: *NeuroImage* 20.1, pp. 145–158.
- Morioka, Hiroshi, Atsunori Kanemura, Satoshi Morimoto, Taku Yoshioka, Shigeyuki Oba, Motoaki Kawanabe, and Shin Ishii (2014). “Decoding spatial attention by using cortical currents estimated from electroencephalography with near-infrared spectroscopy prior information”. In: *NeuroImage* 90, pp. 128–139.
- Müller-Putz, Gernot R. and Gert Pfurtscheller (2008). “Control of an electrical prosthesis with an SSVEP-based BCI”. In: *IEEE Transactions on Biomedical Engineering* 55.1, pp. 361–364.
- Müller-Putz, Gernot R., Reinhold Scherer, Christian Brauneis, and Gert Pfurtscheller (2005). “Steady-state visual evoked potential (SSVEP)-based communication: impact of harmonic frequency components.” In: *Journal of neural engineering* 2.4, pp. 123–130.
- Müller, Hermann J. and John M. Findlay (1988). “The effect of visual attention of peripheral discrimination thresholds in single and multiple element displays”. In: *Acta Psychologica* 69.2, pp. 129–155.
- Müller, Hermann J. and Patrick M.A. Rabbitt (1989). “Reflexive and Voluntary Orienting of Visual Attention: Time Course of Activation and Resistance to Interruption”. In: *Journal of Experimental Psychology: Human Perception and Performance* 15.2, pp. 315–330.
- Muthukumaraswamy, Suresh D. (2013). “High-frequency brain activity and muscle artifacts in MEG/EEG: a review and recommendations”. In: *Frontiers in Human Neuroscience* 7.April, pp. 1–11.
- Myllylä, Teemu, Vesa Korhonen, Vesa Kiviniemi, and Valery Tuchin (2015). “Experimental studies with selected light sources for NIRS of brain tissue: quantifying tissue chromophore concentration”. In: *Optical Techniques in Neurosurgery, Neurophotonics, and Optogenetics II*. Vol. 9305. March 2015, 93051S.
- Naber, Marnix, Stefan Frässle, and Wolfgang Einhäuser (2011). “Perceptual Rivalry: Reflexes Reveal the Gradual Nature of Visual Awareness”. In: *PLoS ONE* 6.6, e20910.

- Naber, Marnix and Ken Nakayama (2013). "Pupil responses to high-level image content". In: *Journal of Vision* 13.6, pp. 1–8.
- Naito, Masayoshi, Yohko Michioka, Kuniaki Ozawa, Yoshitoshi Ito, Masashi Kiguchi, and Tsuneo Kanazawa (2007). "A Communication Means for Totally Locked-in ALS Patients Based on Changes in Cerebral Blood Volume Measured with Near-Infrared Light". In: *IEICE Transactions on Information and Systems* E90-D.7, pp. 1028–1037.
- Naseer, Noman and Keum-Shik Hong (2015). "fNIRS-based brain-computer interfaces: a review". In: *Frontiers in Human Neuroscience* 9.January, pp. 1–15.
- Naseer, Noman, Melissa Jiyoun Hong, and Keum Shik Hong (2014). "Online binary decision decoding using functional near-infrared spectroscopy for the development of brain-computer interface". In: *Experimental Brain Research* 232.2, pp. 555–564.
- Neuling, Toralf, Stefan Rach, and Christoph S. Herrmann (2013). "Orchestrating neuronal networks: sustained after-effects of transcranial alternating current stimulation depend upon brain states". In: *Frontiers in Human Neuroscience* 7.April, pp. 1–12.
- Newman, Daniel P., Redmond G. O'Connell, and Mark A. Bellgrove (2013). "Linking time-on-task, spatial bias and hemispheric activation asymmetry: A neural correlate of rightward attention drift". In: *Neuropsychologia* 51.7, pp. 1215–1223.
- Nicolas-Alonso, Luis Fernando and Jaime Gomez-Gil (2012). "Brain computer interfaces, a review". In: *Sensors* 12.2, pp. 1211–1279.
- Nijholt, Anton and Desney Tan (2008). "Brain-Computer Interfacing for Intelligent Systems". In: *IEEE Intelligent Systems* 23.3, pp. 72–79.
- Nobre, Anna C., Gillian N. Sebestyen, Darren R. Gitelman, M. Marsel Mesulam, Richard S.J. Frackowiak, and Chris D. Frith (1997). "Functional localization of the system for visuospatial attention using positron emission tomography". In: *Brain* 120.3, pp. 515–533.
- Okamoto, Masako, Haruka Dan, Kuniko Sakamoto, Kazuhiro Takeo, Koji Shimizu, Satoru Kohno, Ichiro Oda, Seiichiro Isobe, Tateo Suzuki, Kaoru Kohyama, and Ippeita Dan (2004). "Three-dimensional probabilistic anatomical cranio-cerebral correlation via the international 10-20 system oriented for transcranial functional brain mapping". In: *NeuroImage* 21.1, pp. 99–111.
- Okazaki, Yuka O., Jörn M. Horschig, Lisa Luther, Robert Oostenveld, Ikuya Murakami, and Ole Jensen (2015). "Real-time MEG neurofeedback training of posterior alpha activity modulates subsequent visual detection performance". In: *NeuroImage* 107, pp. 323–332.
- Oostenveld, Robert, Pascal Fries, Eric Maris, and Jan-Mathijs Schoffelen (2011). "FieldTrip: Open Source Software for Advanced Analysis of MEG, EEG, and Invasive Electrophysiological Data". In: *Computational Intelligence and Neuroscience* 2011, pp. 1–9.
- Oostenveld, Robert and Peter Praamstra (2001). "The five percent electrode system for high-resolution EEG and ERP measurements". In: *Clinical Neurophysiology* 112.4, pp. 713–719.
- Ordikhani-Seyedlar, Mehdi, Helge B. D. Sorensen, Troels W. Kjaer, Hartwig R. Siebner, and Sadasivan Puthusserypady (2014). "SSVEP-modulation by covert and overt attention: Novel features for BCI in attention neuro-rehabilitation". In: *36th Annual International Conference of the IEEE Engineering in Medicine and Biology Society (EMBC)*. IEEE, pp. 5462–5465.

Bibliography

- Palankar, Mayur, K.J. De Laurentis, Redwan Alqasemi, Eduardo Veras, Rajiv Dubey, Yael Arbel, and Emanuel Donchin (2009). "Control of a 9-DoF Wheelchair-mounted robotic arm system using a P300 Brain Computer Interface: Initial experiments". In: *2008 IEEE International Conference on Robotics and Biomimetics*, pp. 348–353.
- Parton, Andrew, Paresh Malhotra, and Masud Husain (2004). "Hemispatial neglect". In: *Journal of neurology, neurosurgery, and psychiatry* 75.1, pp. 13–21.
- Perdikis, Serafeim, Robert Leeb, John Williamson, Amy Ramsay, Michele Tavella, Lorenzo Desideri, Evert-Jan E-J Hoogerwerf, Abdul Al-Khodairy, Roderick Murray-Smith, and José del R. Millán (2014). "Clinical evaluation of BrainTree, a motor imagery hybrid BCI speller." In: *Journal of Neural Engineering* 11.3, p. 036003.
- Perdikis, Serafeim, Luca Tonin, Sareh Saeedi, Christoph Schneider, and José del R. Millán (2018). "The Cybathlon BCI race: Successful longitudinal mutual learning with two tetraplegic users". In: *PLoS Biology* 16.5, pp. 1–28.
- Pfurtscheller, Gert, Clemens Brunner, Alois Schlögl, and Fernando. H. Lopes da Silva (2006). "Mu rhythm (de) synchronization and EEG single-trial classification of different motor imagery tasks". In: *NeuroImage* 31.1, pp. 153–159.
- Pfurtscheller, Gert and Fernando H. Lopes Da Silva (1999). "Event-related EEG/MEG synchronization and desynchronization: Basic principles". In: *Clinical Neurophysiology* 110.11, pp. 1842–1857.
- Pichiorri, Floriana, Giovanni Morone, Manuela Petti, Jlenia Toppi, Iolanda Pisotta, Marco Molinari, Stefano Paolucci, Maurizio Inghilleri, Laura Astolfi, Febo Cincotti, and Donatella Mattia (2015). "Brain-computer interface boosts motor imagery practice during stroke recovery". In: *Annals of Neurology* 77.5, pp. 851–865.
- Piper, Sophie K., Arne Krueger, Stefan P. Koch, Jan Mehnert, Christina Habermehl, Jens Steinbrink, Hellmuth Obrig, and Christoph H. Schmitz (2014). "A wearable multi-channel fNIRS system for brain imaging in freely moving subjects". In: *NeuroImage* 85, pp. 64–71.
- Plichta, Michael M., Sebastian Heinzel, Ann-Christine Ehlis, Paul Pauli, and Andreas J. Fallgatter (2007). "Model-based analysis of rapid event-related functional near-infrared spectroscopy (NIRS) data: A parametric validation study". In: *NeuroImage* 35.2, pp. 625–634.
- Polich, John and Albert Kok (1995). "Cognitive and biological determinants of P300: an integrative review". In: *Biological Psychology* 41.2, pp. 103–146.
- Polikov, Vadim S., Patrick A. Tresco, and William M. Reichert (2005). "Response of brain tissue to chronically implanted neural electrodes". In: *Journal of Neuroscience Methods* 148.1, pp. 1–18.
- Posner, Michael I. (1980). "Orienting of attention." In: *The Quarterly journal of experimental psychology* 32.1, pp. 3–25.
- Posner, Michael I., John A. Walker, Frances A. Friedrich, and Robert D. Rafal (1987). "How do the parietal lobes direct covert attention?" In: *Neuropsychologia* 25.1A, pp. 135–145.
- Power, Sarah D., Tiago H. Falk, and Tom Chau (2010). "Classification of prefrontal activity due to mental arithmetic and music imagery using hidden Markov models and frequency domain near-infrared spectroscopy". In: *Journal of Neural Engineering* 7.2, p. 026002.

- Putze, Felix, Sebastian Hesslinger, Chun-Yu Tse, YunYing Huang, Christian Herff, Cuntai Guan, and Tanja Schultz (2014). "Hybrid fNIRS-EEG based classification of auditory and visual perception processes". In: *Frontiers in Neuroscience* 8.November, pp. 1–13.
- Rahmandad, Hazhir, Nelson Repenning, and John Serman (2009). "Effects of feedback delay on learning". In: *System Dynamics Review* 25.4, pp. 309–338.
- Randazzo, Luca, Iñaki Iturrate, Serafeim Perdikis, and José del R. Millán (2018). "mano: A Wearable Hand Exoskeleton for Activities of Daily Living and Neurorehabilitation". In: *IEEE Robotics and Automation Letters* 3.1, pp. 500–507.
- Rea, Massimiliano, Mohit Rana, Nicola Lugato, Pavel Terekhin, Leonardo Gizzi, Doris Brötz, Andreas J. Fallgatter, Niels Birbaumer, Ranganatha Sitaram, and Andrea Caria (2014). "Lower Limb Movement Preparation in Chronic Stroke: A Pilot Study Toward an fNIRS-BCI for Gait Rehabilitation." In: *Neurorehabilitation and Neural Repair* 28.6, pp. 564–575.
- Reif, Philipp S., Adam Strzelczyk, and Felix Rosenow (2016). "The history of invasive EEG evaluation in epilepsy patients". In: *Seizure* 41, pp. 191–195.
- Richer, Francois and Jackson Beatty (1985). "Pupillary Dilations in Movement Preparation and Execution". In: *Psychophysiology* 22.2, pp. 204–207.
- Rihs, Tonia A., Christoph M. Michel, and Gregor Thut (2007). "Mechanisms of selective inhibition in visual spatial attention are indexed by alpha-band EEG synchronization". In: *European Journal of Neuroscience* 25.2, pp. 603–610.
- Rihs, Tonia A., Christoph M. Michel, and Gregor Thut (2009). "A bias for posterior α -band power suppression versus enhancement during shifting versus maintenance of spatial attention". In: *NeuroImage* 44.1, pp. 190–199.
- Ritter, Petra and Arno Villringer (2006). "Simultaneous EEG–fMRI". In: *Neuroscience & Biobehavioral Reviews* 30.6, pp. 823–838.
- Rizzolatti, Giacomo, Lucia Riggio, Isabella Dascola, and Carlo Umiltá (1987). "Reorienting attention across the horizontal and vertical meridians: Evidence in favor of a premotor theory of attention". In: *Neuropsychologia* 25.1, pp. 31–40.
- Robineau, Fabien, Sebastian W. Rieger, Christophe Mermoud, Swann Pichon, Yuri Koush, Dimitri Van De Ville, Patrik Vuilleumier, and Frank Scharnowski (2014). "Self-regulation of inter-hemispheric visual cortex balance through real-time fMRI neurofeedback training". In: *NeuroImage* 100, pp. 1–14.
- Robineau, Fabien, Arnaud Saj, Rémi Neveu, Dimitri Van De Ville, Frank Scharnowski, and Patrik Vuilleumier (2017). "Using real-time fMRI neurofeedback to restore right occipital cortex activity in patients with left visuo-spatial neglect: proof-of-principle and preliminary results". In: *Neuropsychological Rehabilitation*, pp. 1–22.
- Roijendijk, Linsey, Jason Farquhar, Marcel van Gerven, Ole Jensen, and Stan Gielen (2013). "Exploring the Impact of Target Eccentricity and Task Difficulty on Covert Visual Spatial Attention and Its Implications for Brain Computer Interfacing". In: *PLoS ONE* 8.12. Ed. by Susana Martinez-Conde, e80489.
- Romanelli, Pantaleo, Marco Piangerelli, David Ratel, Christophe Gaude, Thomas Costecalde, Cosimo Puttilli, Mauro Picciafuoco, Alim Benabid, and Napoleon Torres (2018). "A novel neural prosthesis providing long-term electrocortigraphy recording and cortical stimu-

Bibliography

- lation for epilepsy and brain-computer interface”. In: *Journal of Neurosurgery* May, pp. 1–14.
- Romei, Vincenzo, Verena Brodbeck, Christoph Michel, Amir Amedi, Alvaro Pascual-Leone, and Gregor Thut (2008). “Spontaneous fluctuations in posterior alpha-band EEG activity reflect variability in excitability of human visual areas”. In: *Cerebral Cortex* 18.9, pp. 2010–2018.
- Romei, Vincenzo, Joachim Gross, and Gregor Thut (2010). “On the role of prestimulus alpha rhythms over occipito-parietal areas in visual input regulation: correlation or causation?” In: *The Journal of neuroscience* 30.25, pp. 8692–8697.
- Rosanova, Mario, Adenauer Casali, Valentina Bellina, Federico Resta, Maurizio Mariotti, and Marcello Massimini (2009). “Natural Frequencies of Human Corticothalamic Circuits”. In: *Journal of Neuroscience* 29.24, pp. 7679–7685.
- Rossetti, Yves, Gilles Rode, Laure Pisella, Alessandro Farné, Ling Li, Dominique Boisson, and Marie-Thérèse Perenin (1998). “Prism adaptation to a rightward optical deviation rehabilitates left hemispatial neglect”. In: *Nature* 395.6698, pp. 166–169.
- Ruhnau, Philipp, Toralf Neuling, Marco Fuscá, Christoph S. Herrmann, Gianpaolo Demarchi, and Nathan Weisz (2016). “Eyes wide shut: Transcranial alternating current stimulation drives alpha rhythm in a state dependent manner”. In: *Scientific Reports* 6.1, p. 27138.
- Saager, Rolf B., Nicole L. Telleri, and Andrew J. Berger (2011). “Two-detector Corrected Near Infrared Spectroscopy (C-NIRS) detects hemodynamic activation responses more robustly than single-detector NIRS”. In: *NeuroImage* 55.4, pp. 1679–1685.
- Saturnino, Guilherme Bicalho, Kristoffer Hougaard Madsen, Hartwig Roman Siebner, and Axel Thielscher (2017). “How to target inter-regional phase synchronization with dual-site Transcranial Alternating Current Stimulation”. In: *NeuroImage* 163, pp. 68–80.
- Sauseng, Paul, Wolfgang Klimesch, Waltraud Stadler, Manuel Schabus, Michael Doppelmayr, Simon Hanslmayr, Walter R. Gruber, and Niels Birbaumer (2005). “A shift of visual spatial attention is selectively associated with human EEG alpha activity”. In: *European Journal of Neuroscience* 22.11, pp. 2917–2926.
- Schaefer, Rebecca S., Jason Farquhar, Yvonne Blokland, Makiko Sadakata, and Peter Desain (2011a). “Name that tune: Decoding music from the listening brain”. In: *NeuroImage* 56.2, pp. 843–849.
- Schaefer, Rebecca S., Rutger J. Vlek, and Peter Desain (2011b). “Music perception and imagery in EEG: Alpha band effects of task and stimulus”. In: *International Journal of Psychophysiology* 82.3, pp. 254–259.
- Schaeff, Sulamith, Matthias Sebastian Treder, Bastian Venthur, and Benjamin Blankertz (2012). “Exploring motion VEPs for gaze-independent communication”. In: *Journal of Neural Engineering* 9.4, p. 045006.
- Schalk, Gerwin, Kai J. Miller, Nicholas R. Anderson, J. Adam Wilson, Matthew D. Smyth, Jeffrey G. Ojemann, Daniel W. Moran, Jonathan R. Wolpaw, and Eric C. Leuthardt (2008). “Two-dimensional movement control using electrocorticographic signals in humans”. In: *Journal of Neural Engineering* 5.1, pp. 75–84.

- Schalk, Gerwin, Jonathan R. Wolpaw, Dennis J. McFarland, and Gert Pfurtscheller (2000). "EEG-based communication: Presence of an error potential". In: *Clinical Neurophysiology* 111.12, pp. 2138–2144.
- Scharnowski, Frank, Chloe Hutton, Oliver Josephs, Nikolaus Weiskopf, and Geraint Rees (2012). "Improving Visual Perception through Neurofeedback". In: *Journal of Neuroscience* 32.49, pp. 17830–17841.
- Schindler, Andreas and Andreas Bartels (2013). "Parietal cortex codes for egocentric space beyond the field of view". In: *Current Biology* 23.2, pp. 177–182.
- Schlögl, Alois, Claudia Keinrath, Doris Zimmermann, Reinhold Scherer, Robert Leeb, and Gert Pfurtscheller (2007). "A fully automated correction method of EOG artifacts in EEG recordings". In: *Clinical Neurophysiology* 118.1, pp. 98–104.
- Schmidt, Nico M., Benjamin Blankertz, and Matthias S. Treder (2012). "Online detection of error-related potentials boosts the performance of mental typewriters". In: *BMC Neuroscience* 13.1, p. 19.
- Schneider, Christoph, Michael Pereira, Luca Tonin, and José del R. Millán (2018). "Real-time EEG feedback on alpha power lateralization leads to behavioral improvements in a covert attention task". In: *NeuroImage* Submitted.
- Scholkmann, Felix, Stefan Kleiser, Andreas Jaakko Metz, Raphael Zimmermann, Juan Mata Pavia, Ursula Wolf, and Martin Wolf (2014). "A review on continuous wave functional near-infrared spectroscopy and imaging instrumentation and methodology". In: *NeuroImage* 85, pp. 6–27.
- Sherlin, Leslie H., Martijn Arns, Joel Lubar, Hartmut Heinrich, Cynthia Kerson, Ute Strehl, and M. Barry Serman (2011). "Neurofeedback and Basic Learning Theory: Implications for Research and Practice". In: *Journal of Neurotherapy* 15.4, pp. 292–304.
- Shibata, Kazuhisa, Takeo Watanabe, Yuka Sasaki, and Mitsuo Kawato (2011). "Perceptual Learning Incepted by Decoded fMRI Neurofeedback Without Stimulus Presentation". In: *Science* 334.6061, pp. 1413–1415.
- Shin, Jaeyoung, Jinuk Kwon, Jongkwan Choi, and Chang-Hwan Im (2017). "Performance enhancement of a brain-computer interface using high-density multi-distance NIRS". In: *Scientific Reports* 7.1, p. 16545.
- Shin, Jaeyoung, Klaus-Robert Müller, and Han-Jeong Hwang (2016). "Near-infrared spectroscopy (NIRS)-based eyes-closed brain-computer interface (BCI) using prefrontal cortex activation due to mental arithmetic". In: *Scientific Reports* 6.1, p. 36203.
- Sitaram, Ranganatha, Tomas Ros, Luke Stoeckel, Sven Haller, Frank Scharnowski, Jarrod Lewis-Peacock, Nikolaus Weiskopf, Maria Laura Blefari, Mohit Rana, Ethan Oblak, Niels Birbaumer, and James Sulzer (2017). "Closed-loop brain training: The science of neurofeedback". In: *Nature Reviews Neuroscience* 18.2, pp. 86–100.
- Spüler, Martin, Michael Bensch, Sonja Kleih, Wolfgang Rosenstiel, Martin Bogdan, and Andrea Kübler (2012). "Online use of error-related potentials in healthy users and people with severe motor impairment increases performance of a P300-BCI". In: *Clinical Neurophysiology* 123.7, pp. 1328–1337.

Bibliography

- Steyrl, David, Reinhold Scherer, and Gernot R. Müller-Putz (2013). “Random Forests for Feature Selection in Non-invasive Brain-Computer Interfacing”. In: *Human-Computer Interaction and Knowledge Discovery in Complex, Unstructured, Big Data. Lecture Notes in Computer Science (HCI-KDD)*. Vol. 7947, pp. 207–216.
- Strangman, Gary, Maria Angela Franceschini, and David A. Boas (2003). “Factors affecting the accuracy of near-infrared spectroscopy concentration calculations for focal changes in oxygenation parameters”. In: *NeuroImage* 18.4, pp. 865–879.
- Sulzer, James, Sven Haller, Frank Scharnowski, Nikolaus Weiskopf, Niels Birbaumer, Maria Laura Blefari, Annette B. Bruehl, Leonardo G. Cohen, R. Christopher DeCharms, Roger Gassert, Rainer Goebel, Uwe Herwig, Steven LaConte, David E. J. Linden, Andreas R. Luft, Erich Seifritz, and Ranganatha Sitaram (2013). “Real-time fMRI neurofeedback: Progress and challenges”. In: *NeuroImage* 76, pp. 386–399.
- Sylvester, Chad M., Gordon L. Shulman, Anthony I. Jack, and Maurizio Corbetta (2007). “Asymmetry of anticipatory activity in visual cortex predicts the locus of attention and perception.” In: *The Journal of Neuroscience* 27.52, pp. 14424–14433.
- Tai, Kelly and Tom Chau (2009). “Single-trial classification of NIRS signals during emotional induction tasks: Towards a corporeal machine interface”. In: *Journal of NeuroEngineering and Rehabilitation* 6.1, pp. 1–14.
- Thut, Gregor (2014). “Modulating Brain Oscillations to Drive Brain Function”. In: *PLoS Biology* 12.12, e1002032.
- Thut, Gregor and Carlo Miniussi (2009). “New insights into rhythmic brain activity from TMS-EEG studies”. In: *Trends in Cognitive Sciences* 13.4, pp. 182–189.
- Thut, Gregor, Annika Nietzel, Stephan Brandt, and Alvaro Pascual-Leone (2006). “Alpha-band electroencephalographic activity over occipital cortex indexes visuospatial attention bias and predicts visual target detection.” In: *The Journal of Neuroscience* 26.37, pp. 9494–9502.
- Thut, Gregor, Domenica Veniero, Vincenzo Romei, Carlo Miniussi, Philippe Schyns, and Joachim Gross (2011). “Rhythmic TMS causes local entrainment of natural oscillatory signatures”. In: *Current Biology* 21.14, pp. 1176–1185.
- Tonin, Luca, Robert Leeb, and José del R. Millán (2012). “Time-dependent approach for single trial classification of covert visuospatial attention.” In: *Journal of neural engineering* 9.4, p. 045011.
- Tonin, Luca, Robert Leeb, Aleksander Sobolewski, and José del R. Millán (2013). “An online EEG BCI based on covert visuospatial attention in absence of exogenous stimulation.” In: *Journal of Neural Engineering* 10.5, p. 56007.
- Tonin, Luca, Marco Pitteri, Robert Leeb, Huaijian Zhang, Emanuele Menegatti, Francesco Piccione, and José del R. Millán (2017). “Behavioral and Cortical Effects during Attention Driven Brain-Computer Interface Operations in Spatial Neglect: A Feasibility Case Study”. In: *Frontiers in Human Neuroscience* 11.June, pp. 1–8.
- Treder, Matthias S., Ali Bahramisharif, Nico M. Schmidt, Marcel A. J. Van Gerven, and Benjamin Blankertz (2011a). “Brain-computer interfacing using modulations of alpha activity induced by covert shifts of attention.” In: *Journal of neuroengineering and rehabilitation* 8.1, p. 24.

- Treder, Matthias S. and Benjamin Blankertz (2010). "(C)overt attention and visual speller design in an ERP-based brain-computer interface". In: *Behavioral and Brain Functions* 6.1, p. 28.
- Treder, Matthias S., Nico M. Schmidt, and Benjamin Blankertz (2011b). "Gaze-independent brain – computer interfaces based on covert attention and feature attention". In: *Journal of Neural Engineering* 8.6, p. 066003.
- Van der Stigchel, Stefan and Jan Theeuwes (2007). "The relationship between covert and overt attention in endogenous cuing." In: *Perception & psychophysics* 69.5, pp. 719–731.
- Van Dijk, Hanneke, Jan-Mathijs Schoffelen, Robert Oostenveld, and Ole Jensen (2008). "Pre-stimulus Oscillatory Activity in the Alpha Band Predicts Visual Discrimination Ability". In: *Journal of Neuroscience* 28.8, pp. 1816–1823.
- Van Gerven, Marcel, Jason Farquhar, Rebecca Schaefer, Rutger Vlek, Jeroen Geuze, Anton Nijholt, Nick Ramsey, Pim Haselager, Louis Vuurpijl, Stan Gielen, and Peter Desain (2009). "The brain–computer interface cycle". In: *Journal of Neural Engineering* 6.4, p. 041001.
- Van Gerven, Marcel and Ole Jensen (2009). "Attention modulations of posterior alpha as a control signal for two-dimensional brain-computer interfaces". In: *Journal of Neuroscience Methods* 179.1, pp. 78–84.
- Vöröslakos, Mihály, Yuichi Takeuchi, Kitti Brinyiczki, Tamás Zombori, Azahara Oliva, Antonio Fernández-Ruiz, Gábor Kozák, Zsigmond Tamás Kincses, Béla Iványi, György Buzsáki, and Antal Berényi (2018). "Direct effects of transcranial electric stimulation on brain circuits in rats and humans". In: *Nature Communications* 9.1, p. 483.
- Vossel, Simone, Christiane M. Thiel, and Gereon R. Fink (2006). "Cue validity modulates the neural correlates of covert endogenous orienting of attention in parietal and frontal cortex". In: *NeuroImage* 32, pp. 1257–1264.
- Vossen, Alexandra, Joachim Gross, and Gregor Thut (2015). "Alpha power increase after transcranial alternating current stimulation at alpha frequency (a-tACS) reflects plastic changes rather than entrainment". In: *Brain Stimulation* 8.3, pp. 499–508.
- Wallois, Fabrice, Mahdi Mahmoudzadeh, Amol Patil, and Reinhard Grebe (2012). "Usefulness of simultaneous EEG–NIRS recording in language studies". In: *Brain and Language* 121.2, pp. 110–123.
- Wang, Chin-An, Susan E. Boehnke, Brian J. White, and Douglas P. Munoz (2012). "Microstimulation of the Monkey Superior Colliculus Induces Pupil Dilation Without Evoking Saccades". In: *Journal of Neuroscience* 32.11, pp. 3629–3636.
- Wang, Li, Xiong Zhang, Xuefei Zhong, and Yu Zhang (2013). "Analysis and classification of speech imagery EEG for BCI". In: *Biomedical Signal Processing and Control* 8.6, pp. 901–908.
- Wang, Yijun, Ruiping Wang, Xiaorong Gao, Bo Hong, and Shangkai Gao (2006). "A Practical VEP-Based Brain–Computer Interface". In: *IEEE Transactions on Neural Systems and Rehabilitation Engineering* 14.2, pp. 234–240.
- Ward, Laura McKernan, Ross Thomas Aitchison, Melisa Tawse, Anita Jane Simmers, and Uma Shahani (2015). "Reduced Haemodynamic Response in the Ageing Visual Cortex Measured by Absolute fNIRS". In: *PLOS ONE* 10.4, e0125012.

Bibliography

- Weiskopf, Nikolaus, Klaus Mathiak, Simon W. Bock, Frank Scharnowski, Ralf Veit, Wolfgang Grodd, Rainer Goebel, and Niels Birbaumer (2004a). "Principles of a brain-computer interface (BCI) based on real-time functional magnetic resonance imaging (fMRI)". In: *IEEE Transactions on Biomedical Engineering* 51.6, pp. 966–970.
- Weiskopf, Nikolaus, Frank Scharnowski, Ralf Veit, Rainer Goebel, Niels Birbaumer, and Klaus Mathiak (2004b). "Self-regulation of local brain activity using real-time functional magnetic resonance imaging (fMRI)". In: *Journal of Physiology-Paris* 98.4-6, pp. 357–373.
- Weiskopf, Nikolaus, Ranganatha Sitaram, Oliver Josephs, Ralf Veit, Frank Scharnowski, Rainer Goebel, Niels Birbaumer, Ralf Deichmann, and Klaus Mathiak (2007). "Real-time functional magnetic resonance imaging: methods and applications". In: *Magnetic Resonance Imaging* 25.6, pp. 989–1003.
- Weyand, Sabine, Kaori Takehara-Nishiuchi, and Tom Chau (2015). "Exploring methodological frameworks for a mental task-based near-infrared spectroscopy brain-computer interface". In: *Journal of Neuroscience Methods* 254, pp. 36–45.
- Wöllmer, Martin, Marc Al-Hames, Florian Eyben, Björn Schuller, and Gerhard Rigoll (2009). "A multidimensional dynamic time warping algorithm for efficient multimodal fusion of asynchronous data streams". In: *Neurocomputing* 73.1-3, pp. 366–380.
- Wolpaw, Jonathan R. (2010). *Brain-Computer Interfaces*. Ed. by Desney S. Tan and Anton Nijholt. Vol. 110. Human-Computer Interaction Series. London: Springer London, pp. 67–74.
- Wolpaw, Jonathan R., Niels Birbaumer, Dennis J. McFarland, Gert Pfurtscheller, and Theresa M. Vaughan (2002). "Brain-computer interfaces for communication and control". In: *Clinical Neurophysiology* 113.6, pp. 767–791.
- Wolpaw, Jonathan R., Dennis J. McFarland, Gregory W. Neat, and Catherine A. Forneris (1991). "An EEG-based brain-computer interface for cursor control". In: *Electroencephalography and Clinical Neurophysiology* 78.3, pp. 252–259.
- Woodman, Geoffrey F. (2010). "A brief introduction to the use of event-related potentials in studies of perception and attention". In: *Attention, Perception & Psychophysics* 72.8, pp. 2031–2046.
- Worden, Michael S., John J. Foxe, Norman Wang, and Gregory V. Simpson (2000). "Anticipatory biasing of visuospatial attention indexed by retinotopically specific alpha-band electroencephalography increases over occipital cortex". In: *The Journal of Neuroscience* 20.6, RC63.
- World Medical Association (2013). "WMA Declaration of Helsinki - Ethical Principles for Medical Research Involving Human Subjects". In: *JAMA* 310, pp. 2191–2194.
- Xu, Ren, Ning Jiang, Aleksandra Vuckovic, Muhammad Hasan, Natalie Mrachacz-Kersting, David Allan, Matthew Fraser, Bahman Nasserroleslami, Bernie Conway, Kim Dremstrup, and Dario Farina (2014). "Movement-related cortical potentials in paraplegic patients: abnormal patterns and considerations for BCI-rehabilitation". In: *Frontiers in Neuroengineering* 7.August, pp. 1–9.

- Yang, Nicole Y. H., Dong Zhou, Raymond C. K. Chung, Cecilia W. P. Li-Tsang, and Kenneth N. K. Fong (2013). "Rehabilitation Interventions for Unilateral Neglect after Stroke: A Systematic Review from 1997 through 2012." In: *Frontiers in human neuroscience* 7.May, p. 187.
- Yin, Xuxian, Baolei Xu, Changhao Jiang, Yunfa Fu, Zhidong Wang, Hongyi Li, and Gang Shi (2015). "A hybrid BCI based on EEG and fNIRS signals improves the performance of decoding motor imagery of both force and speed of hand clenching". In: *Journal of Neural Engineering* 12.3, p. 036004.
- Yoo, Seung-Schik, Ty Fairmeny, Nan-Kuei Chen, Seh-Eun Choo, Lawrence P. Panych, HyunWook Park, Soo-Young Lee, and Ferenc A. Jolesz (2004). "Brain-computer interface using fMRI: spatial navigation by thoughts". In: *NeuroReport* 15.10, pp. 1591–1595.
- Yu, Juanhong, Kai Keng Ang, Cuntai Guan, and Chuanchu Wang (2013). "A multimodal fNIRS and EEG-based BCI study on motor imagery and passive movement". In: *6th International IEEE/EMBS Conference on Neural Engineering (NER)*, pp. 5–8.
- Zaehle, Tino, Stefan Rach, and Christoph S. Herrmann (2010). "Transcranial Alternating Current Stimulation Enhances Individual Alpha Activity in Human EEG". In: *PLoS One* 5.11, pp. 1–7.
- Zaidi, Ali Danish, Matthias H. J. Munk, Andreas Schmidt, Cristina Risueno-Segovia, Rebekka Bernard, Eberhard Fetz, Nikos Logothetis, Niels Birbaumer, and Ranganatha Sitaram (2015). "Simultaneous epidural functional near-infrared spectroscopy and cortical electrophysiology as a tool for studying local neurovascular coupling in primates." In: *NeuroImage* 120, pp. 394–399.
- Zander, Thorsten O. and Christian Kothe (2011). "Towards passive brain-computer interfaces: applying brain-computer interface technology to human-machine systems in general". In: *Journal of Neural Engineering* 8.2, p. 025005.
- Zhao, Huijuan, Yukari Tanikawa, Feng Gao, Yoichi Onodera, Angelo Sassaroli, Kenji Tanaka, and Yukio Yamada (2002). "Maps of optical differential pathlength factor of human adult forehead, somatosensory motor and occipital regions at multi-wavelengths in NIR." In: *Physics in medicine and biology* 47.12, pp. 2075–2093.
- Zich, Catharina, Stefan Debener, Cornelia Kranczioch, Martin G. Bleichner, Ingmar Gutberlet, and Maarten De Vos (2015). "Real-time EEG feedback during simultaneous EEG-fMRI identifies the cortical signature of motor imagery". In: *NeuroImage* 114, pp. 438–447.
- Zimmermann, Raphael, Laura Marchal-Crespo, Janis Edelmann, Olivier Lambercy, Marie Christine Fluet, Robert Riener, Martin Wolf, and Roger Gassert (2013). "Detection of motor execution using a hybrid fNIRS-biosignal BCI: A feasibility study". In: *Journal of NeuroEngineering and Rehabilitation* 10.1, pp. 1–15.
- Zotев, Vadim, Raquel Phillips, Han Yuan, Masaya Misaki, and Jerzy Bodurka (2014). "Self-regulation of human brain activity using simultaneous real-time fMRI and EEG neurofeedback". In: *NeuroImage* 85, pp. 985–995.

CHRISTOPH SCHNEIDER

Neuroscience, Mathematics & Biomedical Engineering

@ christoph_schneider@hotmail.ch
in linkedin.com/in/schneiderchr

Rue de l'Ale 30, 1003 Lausanne Switzerland
orcid.org/0000-0002-5012-1711



EDUCATION

Ph.D. in Neuroscience

A Multifaceted Approach to Covert Attention Brain-Computer Interfaces

EPFL

May 2014 – Nov 2018

Lausanne, Switzerland

- Enhanced decoding of covert visual attention directly from brain dynamics for the use in a brain-computer interface (BCI).
- Developed a multimodal signal integration system (EEG, fNIRS, eye tracker), implemented real-time feedback solutions, and incorporated noninvasive brain stimulation for BCI.
- Worked with quadriplegic BCI users and patients with disorders of consciousness to allow communication.
- Designed and tutored projects in *Data Analysis and Model Classification* and *Brain-Computer Interaction* as well as supervised a Master student.

M.S. in Biomedical Engineering

Online Feature Discriminant Power Monitoring and Selection

TU Wien

Nov 2008 – March 2013

Vienna, Austria

M.S. in Mathematics

Classification of Vigilance using Hidden Markov Models on EOG Data

TU Wien

Oct 2004 – Oct 2012

Vienna, Austria

WORK EXPERIENCE

R&D Engineer

g.tec medical engineering

Oct 2013 – March 2014

Schiedlberg, Austria

- Developed products for intrasurgical brain mapping and BCI-aided stroke rehabilitation.
- Designed EEG signal processing architectures and algorithms for various BCI applications.
- Published an IEEE paper on decoding hand poses from ECoG signals.

Emergency Paramedic

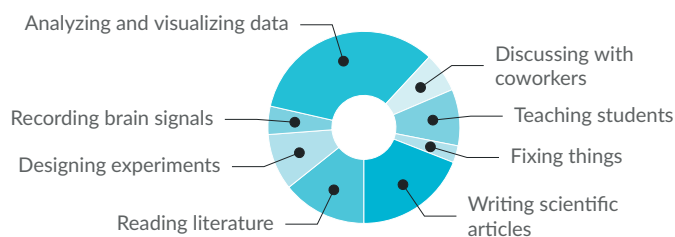
ASB Kärnten & Rotes Kreuz Kärnten

Oct 2004 – March 2014

Villach & Spittal, Austria

- Voluntary paramedic and official first aid instructor.

A DAY IN THE LAB



LIFE PHILOSOPHY

"Go to bed at night a little wiser than you got up in the morning."

MOST PROUD OF



Saving Lives

as a paramedic and improving lives through BCI technology



Winning the Cybathlon

BCI race in 2016 together with the greatest team



Graduating with Honors

in both of my master studies



Winning the Best Delegate

award at an international MUN conference

STRENGTHS

Ambitious Analytic Diligent

Curious Social

BCI EEG fNIRS Data Analysis

Machine Learning Brain Stimulation

Statistics Mathematical Modeling

LANGUAGES

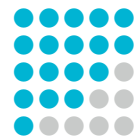
German

English

French

Italian

Persian



PROGRAMMING

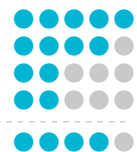
Matlab

Python

C, C++

R

LaTeX



PUBLICATIONS

Journal Articles

- Schneider, Christoph, Michael Pereira, Luca Tonin, and José del R. Millán (2018). "Real-time EEG feedback on alpha power lateralization leads to behavioral improvements in a covert attention task". In: [in preparation].
- Perdikis, Serafeim, Luca Tonin, Sareh Saeedi, Christoph Schneider, and José del R. Millán (2018). "The Cybathlon BCI race: Successful longitudinal mutual learning with two tetraplegic users". In: *PLoS Biology* 16.5, pp. 1–28.

Conference Proceedings

- Schneider, Christoph, Serafeim Perdikis, Marina Silva, Jane Jöhr, Alexander Pincherle, José del R. Millán, and Karin Diserens (2018). "Motor Attempt EEG Paradigm As a Diagnostic Tool for Disorders of Consciousness". In: *Proceedings of the 40th Annual International Conference of the IEEE Engineering in Medicine and Biology Society, Honolulu HI, USA, June 17-21 2018*.
- Schneider, Christoph and José del R. Millán (2016). "Comparing EEG and fNIRS for a covert attention BCI". in: *Proceedings of the 6th International Brain-Computer Interface Meeting, Monterey CA, USA, May 30th - June 3rd 2016*, p. 96.
- Kapeller, Christoph, Christoph Schneider, Kyosuke Kamada, Katsuhiko Ogawa, Naoto Kunii, Rupert Ortner, Robert Prückl, and Christoph Guger (2014). "Single trial detection of hand poses in human ECoG using CSP based feature extraction". In: *Proceedings of the 36th Annual International Conference of the IEEE Engineering in Medicine and Biology Society, Chicago IL, USA, August 26-30 2014*. FL, USA: International Institute of Informatics and Systemics, pp. 4599–4602.

REFEREES

Prof. José del R. Millán

@ jose.millan@epfl.ch

✉ EPFL, STI IBI-STI CNBI
Campus Biotech
Chemin des Mines 9
1202 Geneva, Switzerland

Prof. Frank Rattay

@ rank.rattay@tuwien.ac.at

✉ TU Wien, Institut für Analysis und
Scientific Computing
Wiedner Hauptstraße 8-10
1040 Wien, Austria

Johannes Kropf, PhD

@ johannes.kropf@ait.ac.at

✉ AIT, Biomedical Systems
Viktor Kaplan Straße 2
2700 Wr. Neustadt, Austria

Serafeim Perdikis, PhD

@ serafeim.perdikis@epfl.ch

✉ EPFL, STI IBI-STI CNBI
Campus Biotech
Chemin des Mines 9
1202 Geneva, Switzerland

